© 2014. Published by The Company of Biologists Ltd | Development (2014) 141, 2150-2156 doi:10.1242/dev.107011

RESEARCH ARTICLE

Scaling morphogen gradients during tissue growth by a cell division rule

Inna Averbukh[1,*], Danny Ben-Zvi[2,*], Siddhartha Mishra[3,4,*] and Naama Barkai[1,‡]

ABSTRACT

Morphogen gradients guide the patterning of tissues and organs during the development of multicellular organisms. In many cases, morphogen signaling is also required for tissue growth. The consequences of this interplay between growth and patterning are not well understood. In the *Drosophila* wing imaginal disc, the morphogen Dpp guides patterning and is also required for tissue growth. In particular, it was recently reported that cell division in the disc correlates with the temporal increase in Dpp signaling. Here we mathematically model morphogen gradient formation in a growing tissue, accounting also for morphogen advection and dilution. Our analysis defines a new scaling mechanism, which we term the morphogen-dependent division rule (MDDR): when cell division depends on the temporal increase in morphogen signaling, the morphogen gradient scales with the growing tissue size, tissue growth becomes spatially uniform and the tissue naturally attains a finite size. This model is consistent with many properties of the wing disc. However, we find that the MDDR is not consistent with the phenotype of scaling-defective mutants, supporting the view that temporal increase in Dpp signaling is not the driver of cell division during late phases of disc development. More generally, our results show that local coupling of cell division with morphogen signaling can lead to gradient scaling and uniform growth even in the absence of global feedbacks. The MDDR scaling mechanism might be particularly beneficial during rapid proliferation, when global feedbacks are hard to implement.

KEY WORDS: Dpp, *Drosophila*, Growth, Morphogen, Scaling, Wing disc

INTRODUCTION

Individuals of the same species vary in size due to environmental, genetic and stochastic fluctuations. The body plan remains robust to size variations, in part owing to mechanisms that function at early development to adjust (scale) the pattern of the developing tissue with its size. Scaling entails an effective transmission of global size information to the local setting of each cell. Proposed scaling mechanisms include opposing molecular gradients emanating from opposite poles and dilution of some molecular component defining the morphogen length scale (Wartlick et al., 2011). Most of these theoretical scaling mechanisms assume that tissue pattern is adjusted with tissue size, while size itself is defined independently of the patterning process (Barkai and Ben-Zvi, 2009; Ben-Zvi et al., 2008; Cheung et al., 2011; Gierer and Meinhardt, 1972; Gregor et al., 2008; Houchmandzadeh et al., 2002; Patel and Lall, 2002; Wolpert, 1969). Yet patterning is often concomitant with tissue growth. Furthermore, the same molecules that guide patterning may also be required for tissue proliferation, directly coupling pattern and size (Lanctot et al., 2013; Sato and Kornberg, 2002; Towers et al., 2008). How global tissue properties such as pattern scaling and tissue growth are affected by this local coupling is not well understood.

The *Drosophila* wing imaginal disc provides a central model for studying both pattern scaling and the coordination of patterning and growth. This monolayer epithelium is patterned along the anterior-posterior (AP) axis by a concentration gradient of the Bmp4 homolog Dpp, which is secreted from a line-like source along the AP border and decays gradually away from it (Kicheva et al., 2007). The Dpp concentration gradient was directly visualized and shown to scale with the size of the disc when disc size was perturbed by genetic mutations, and also during the growth of the wild-type disc (Ben-Zvi et al., 2011a; Hamaratoglu et al., 2011; Teleman and Cohen, 2000; Wartlick et al., 2011). Recent results by several groups (including ours) suggest that Dpp gradient scaling depends on expansion-repression (ExR) feedback, in which a diffusible 'expander' molecule that facilitates the spread of the morphogen is repressed by morphogen signaling (Ben-Zvi and Barkai, 2010) (Fig. 1A,B). The secreted molecule Pentagone (Magu – FlyBase) acts as an expander: it is widely diffusible, facilitates the spread of Dpp in a non-cell-autonomous manner and its production is repressed by Dpp signaling (Vuilleumier et al., 2011). Indeed, scaling was lost in third instar wing discs of *pentagone* null mutants, or when its expression was constitutive throughout the disc (Ben-Zvi et al., 2011a, b; Hamaratoglu et al., 2011; Restrepo and Basler, 2011).

In addition to its role as a morphogen patterning the wing disc, Dpp is a growth factor required for the proliferation of cells in the disc (reviewed by Affolter and Basler, 2007; Schwank and Basler, 2010). Interestingly, although Dpp levels decay along the disc, cell proliferation is spatially homogenous (Milan et al., 1996). This spatially uniform growth may be beneficial for reducing mechanical stress (Shraiman, 2005) and for increasing patterning robustness (Schwank and Basler, 2010). Different models were suggested to explain how a graded morphogen profile can direct uniform tissue growth. One proposal is that growth depends on the relative slope of morphogen concentration, which remains position-independent for exponentially decaying gradients (Day and Lawrence, 2000; Rogulja and Irvine, 2005); however, this model cannot explain growth within or at the borders of clones with uniform Dpp signaling (Schwank et al., 2008). Others have proposed that cell division is influenced by mechanical forces that depend on morphogen signaling but spread uniformly along the tissue (Aegerter-Wilmsen et al., 2007; Hufnagel et al., 2007; Shraiman, 2005). Notably, growth of the disc is regulated by additional pathways including Wg and Hippo signaling (Johnston and Sanders, 2003; Rogulja et al., 2008), and by systemic signals such as insulin-like growth factors (Bohni et al., 1999). These signals could

[1]Department of Molecular genetics, Weizmann Institute of Science, Rehovot 76100, Israel. [2]Department of Stem Cell and Regenerative Biology, Harvard University, Cambridge, MA 02138, USA. [3]Center of Mathematics for Applications, University of Oslo, 0316 Oslo, Norway. [4]Seminar for Applied Mathematics ETH, Zurich 8092, Switzerland.
*These authors contributed equally to this work

‡Author for correspondence (naama.barkai@weizmann.ac.il)

Received 11 December 2013; Accepted 26 March 2014

Development (2014) 141, 2150-2156 doi:10.1242/dev.107011

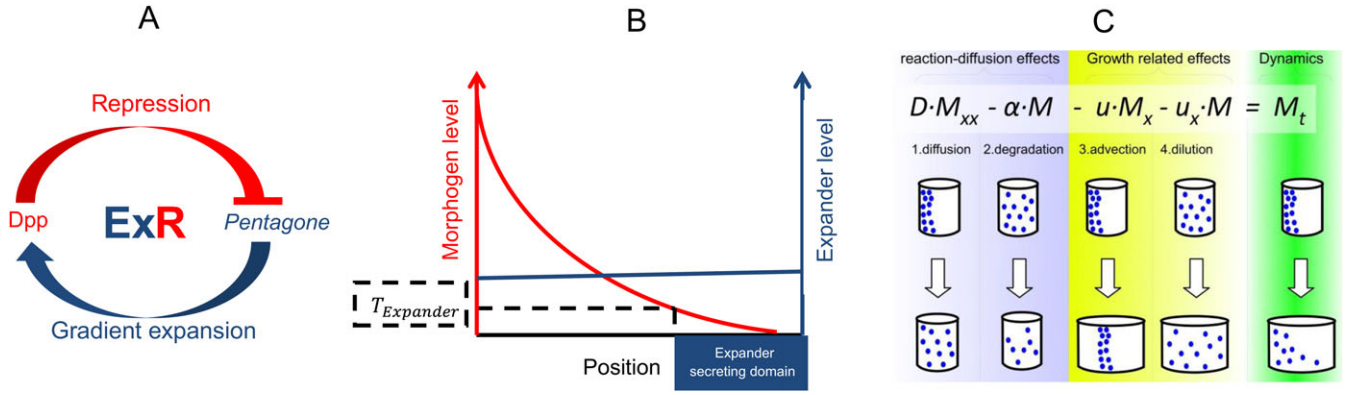

Fig. 1. ExR and coupling growth and patterning by a morphogen. (A) The expansion-repression (ExR) feedback topology. The morphogen represses the secretion of an expander. The expander, which is diffusible and stable, expands the morphogen gradient by enhancing morphogen diffusion and/or decreasing morphogen degradation. (B) Expansion of the morphogen gradient leads to the gradual restriction of the expander secretion domain towards the distal region of the tissue. $T_{Expander}$ is the threshold for expander production repression. The gradient continues to expand until the expander is repressed almost throughout the entire field. The expander accumulates during the expansion of the gradient, such that larger fields will require higher levels of the expander. (C) Morphogen dynamics in a growing tissue. Coupling between growth and patterning by a morphogen gradient. The morphogen gradient profile is determined by morphogen diffusion (1) and its degradation (2). Owing to growth, two other terms shape the distribution: advection of the morphogen (3) and its dilution (4).

compensate for the graded distribution of Dpp to account for uniform growth (Schwank et al., 2011).

Dpp signaling and cell division rates have been quantified *in vivo* in the growing wing disc. The division cycle was shown to strongly correlate with the temporal increase in Dpp signaling, such that cells divided when Dpp signaling increased by ~50% relative to its level at the beginning of the division cycle (Wartlick et al., 2011). This correlation might suggest that cell division is defined by this temporal increase in Dpp signaling. Wartlick et al. noted that such a division rule could lead to spatially uniform growth, provided that the Dpp gradient scales with disc size through some external mechanism.

An emerging idea is, therefore, that the ExR mechanism functions to scale the Dpp gradient with the size of the growing disc, while the Dpp-dependent growth rule described above ensures spatially uniform growth. We examined the consistency of this proposal and were particularly interested in two aspects of this combined dynamics. First, the ExR feedback is effective in scaling morphogen gradients during slow growth, which gives the expander sufficient time to spread in the tissue, but becomes less effective when growth is rapid and the expander does not have time to diffuse and affect the entire tissue. We therefore studied the relation between morphogen gradient and disc size throughout the dynamics of disc growth, including early times when growth is rapid. Second, cells in the lateral domain of the disc receive very little if any Dpp signaling and express Brinker but proliferate at the same rate as medially located cells. Moreover, Brinker-expressing clones in the medial domain proliferate normally (Schwank et al., 2012). These observations led to a debate as to whether the correlation between cell division and the temporal increase in Dpp signaling seen in wild-type discs reflects a causal relationship (Schwank et al., 2012; Wartlick et al., 2012). We were interested in understanding qualitative properties of the proposed Dpp-dependent growth rule to evaluate its consistency with respect to different mutant backgrounds.

To this end, we simulated the ExR feedback in the growing disc using a mathematical framework that accounts for morphogen diffusion, advection and dilution during growth of the tissue. The morphogen-dependent division rule was incorporated into the dynamics, while other contributions to tissue growth were ignored, enabling us to focus exclusively on the properties of this proposed growth mechanism. Surprisingly, scaling and uniform growth were observed throughout the dynamics, also at early times when proliferation was too rapid for the ExR feedback to be effective. Extensive numerical analysis showed that scaling and uniform growth are intertwined at this stage and result solely from the dependence of cell division on the temporal increase in Dpp signaling. Prompted by this observation, we show analytically and numerically that this local MDDR mechanism can result in three global tissue properties: gradient scaling, uniform growth and a final size. We find that MDDR is consistent with many properties of wing disc growth. However, it cannot explain growth of the disc in *pentagone* null discs, in which scaling is lost in third instar, supporting the view that Dpp-independent factors contribute to growth of the disc at that time. More generally, our study demonstrates that local coupling of cell division with morphogen signaling may provide an efficient mechanism for establishing global pattern scaling and tissue growth properties, effective particularly under situations in which global feedbacks are harder to implement.

RESULTS

Model: simulating the ExR feedback in a growing tissue

We consider a one-dimensional growing tissue of size $[0,L(t)]$. The tissue consists of dividing cells whose division times $\tau(x,t)$ depend on time t and cell position x. Since cell division leads to tissue growth, each cell moves with a velocity $u(x,t)$ defined by the cell division rate (see methods in the supplementary material):

$$\frac{du}{dx} \equiv u_x \approx \frac{\ln(2)}{\tau(x,t)}. \quad (1)$$

Here, and in the following, u_x denotes the derivative of u with respect to x. We model a morphogen gradient that is established over the growing tissue. The morphogen with concentration M is secreted from the proximal edge ($x=0$), diffuses with some diffusion coefficient D_M, and degrades linearly at some rate α. To simulate the ExR feedback, we assume that the diffusion and/or degradation of the morphogen depend on some secreted molecule (the expander) with concentration E, the production of which is repressed by morphogen signaling. The expander is widely diffusible and is

Development (2014) 141, 2150-2156 doi:10.1242/dev.107011

degraded slowly. Using the Reynolds transport theorem, we can model the dynamics of the morphogen-expander system using advection-reaction-diffusion equations (Bittig, 2008) (see methods in the supplementary material):

$$M_t = D_M(E)\cdot M_{xx} - \alpha(E)\cdot M - u\cdot M_x - u_x\cdot M, \quad (2a)$$

$$E_t = D_E\cdot E_{xx} - \alpha_E\cdot E - u\cdot E_x - u_x\cdot E + \beta_E\cdot h(M). \quad (2b)$$

The first two terms on the right-hand sides of Eqn 2 describe the change in morphogen or expander concentration due to their respective diffusion and degradation. We assume that both secreted molecules are transported across the field by the movement of the underlying cells, to which they are weakly bound, e.g. through interaction with the extracellular matrix. This movement is described by the third (advection) term. Finally, growth of the tissue dilutes both morphogen and expander, thereby reducing their concentration. This dilution depends on the proliferation rate u_x and is accounted for by the fourth term (Fig. 1C). We assume a constant flux at the proximal boundary: $D_M M_x(L{=}0,t){=}{-}\eta$, zero morphogen flux at the distal boundary, and zero flux at both boundaries of the expander. β_E denotes the rate by which the expander is produced and $h(M){=}(1{+}(M/T_{rep})^n)^{-1}$ describes the morphogen-dependent repression of expander production, which is low at proximal regions where morphogen is high, and high at distal regions where morphogen concentration is low. Note that the region in which the expander is repressed increases as the morphogen expands. We also assume that the expander functions by limiting morphogen degradation, i.e. we set $\alpha(E){=}(\alpha_M/(1{+}E))$ and $D_M(E){=}D_M$ with α_M the morphogen degradation rate without the expander. The analysis is equivalent for assuming modulation of diffusion.

We began by simulating the temporal dynamics of the morphogen-expander distributions in discs growing at different, spatially uniform growth rates (supplementary material Fig. S1) and compared the scaling of the profile in the presence or absence of ExR feedback. As expected, ExR improved scaling at slow growth rates q, but was less effective in faster growing tissues (Ben-Zvi et al., 2011a; Hamaratoglu et al., 2011).

Simulating the Dpp gradient in a growing tissue

We next incorporated the growth rule implied by Wartlick and colleagues, whereby the cell divides when subject to a 50% increase in morphogen signaling (Wartlick et al., 2011). This division rule can be formulated as:

$$\tau(x,t)^{-1} = \theta^{-1}\frac{\dot{M}}{M}, \quad (3)$$

where $\dot{M}$ denotes the full (advective) derivative of M with respect to time, corresponding to the change in morphogen concentration as sensed by the moving cell, and $\theta{=}0.5$ is the fractional change in morphogen signaling required for triggering cell division. Together, Eqns 1-3 describe a closed system in which tissue growth and morphogen gradient formation are coupled.

We simulated this coupled system using parameters measured for the *Drosophila* wing imaginal disc (Fig. 2). The normalized morphogen profile scaled with the size of the growing tissue in accordance with experimental observations (Wartlick et al., 2011) (Fig. 2A,B,F). Growth began rapidly, but gradually slowed down asymptotically at a finite tissue size, comparable to the behavior observed in the wing imaginal disc (Wartlick et al., 2011) (Fig. 2D). Finally, cell division rate was practically independent of cell position along the tissue, consistent with the spatially uniform growth dynamics reported (Milan et al., 1996; Wartlick et al., 2011) (Fig. 2C). Notably, the proliferation rate was much smaller than the Dpp degradation rate throughout the dynamics (Fig. 2E).

We conclude that the coupled dynamics consisting of ExR feedback and MDDR is consistent with growth of the wild-type disc in at least three key aspects: scaling of the Dpp gradient with the size of the growing tissue, spatially uniform tissue growth, and

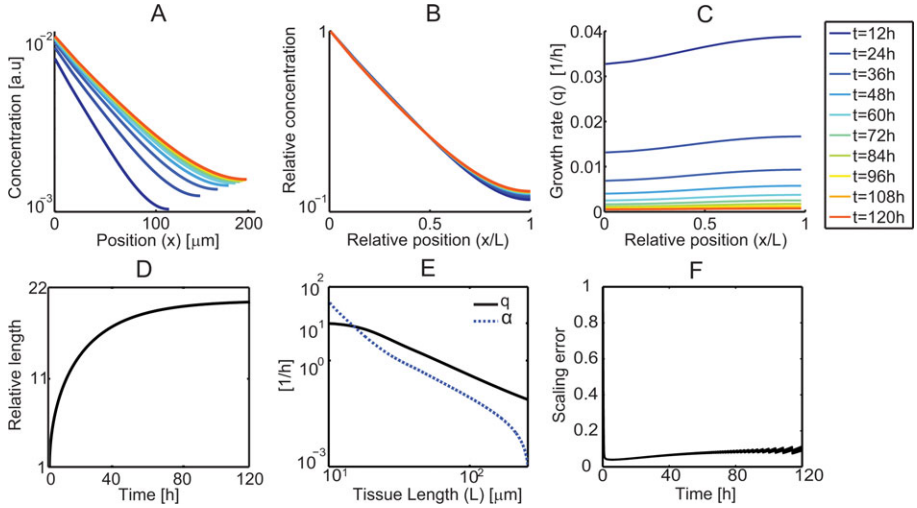

Fig. 2. Numerical simulation results for morphogen gradient dynamics in a tissue growing according to the MDDR with ExR feedback. Parameters correspond to reported measurements of third instar *Drosophila* wing imaginal disc (Wartlick et al., 2011). In all cases, we assume a constant morphogen flux from the source. (A) Morphogen level as a function of position in the tissue at various times. (B) Relative morphogen level as a function of relative position in the tissue. Overlap of the profiles indicates scaling of morphogen gradient with size. (C) Proliferation rate at various times as a function of relative position. Growth is spatially uniform and its rate declines with time. (D) Fold change increase in tissue size as a function of time. (E) Effective morphogen degradation rate α (dotted blue line) and growth rate $q{=}\frac{\dot{L}}{L}$ (black solid line) as functions of tissue length L. Shown on a log log plot. (F) Scaling error defined as: $\left|\frac{\partial\lambda}{\partial L}L\right|$ as a function of time. The scaling error is a dimensionless parameter describing the change in the sharpness of the gradient (λ) relative to the growth of the tissue. Excellent scaling is achieved when $\left|\frac{\partial\lambda}{\partial L}L\right|{<}1$.

Development (2014) 141, 2150-2156 doi:10.1242/dev.107011

Table 1. Scaling and uniform growth percentages

(A) **MDDR with ExR**	
Property	%
Final size	100
Scaling	98.5
Uniform growth	81
Scaling and uniform growth	80.4
(B) **MDDR**	
Property	%
Final size	100
Scaling	75
Uniform growth	100
Scaling and uniform growth	75

growth termination at final time. We verified that all three properties were observed over a wide range of parameters and were also observed for nonlinear morphogen degradation, absorptive boundary conditions and size-dependent Dpp flux (Table 1A; supplementary material Table S1 and Figs S11, S12). Including MDDR increased the robustness of scaling relative to the system in which growth was independent of morphogen signaling: it was now significantly easier to define parameters leading to scaling and uniform growth.

Morphogen-dependent cell division leads to scaling and uniform growth in the absence of an expander

We expected scaling to be established towards late growth, when proliferation slows down. We were therefore surprised to note that scaling and uniform growth were evident very early in the dynamics. In fact, the Dpp gradient scaled even at growth rates that were too rapid to enable efficient compensation by the ExR motif (supplementary material Fig. S2). This is in contrast to the situation of morphogen-independent growth, where scaling was lost in rapidly growing tissues (supplementary material Fig. S1). We therefore asked whether scaling can also be obtained in the absence of ExR feedback.

We simulated the morphogen dynamics in the absence of an expander. Strikingly, although no global feedback was present, this local dynamics was sufficient to reproduce the three global properties described above: scaling of the morphogen gradient with the size of the growing tissue (Fig. 3A,B,F), spatially uniform growth (Fig. 3C) and growth arrest at a finite size (Fig. 3D). While the sharpness of the gradient, as well as the final tissue size, were sensitive to model parameters, all three qualitative properties were observed for a wide range of parameters and were robust also for temporal and spatial noise in the division rule itself (Tables 1, 2; supplementary material Figs S4-S6, S8). In particular, MDDR also provided scaling when the morphogen decay rate was faster than tissue growth, $\alpha_M > q$, as is typical for developing tissues. The effects of the advection and dilution terms are important in the initial phases of growth corresponding to first to early second instar, setting the scaled exponential profile for the entire dynamics consistent with our analytical analysis below. Later during growth, morphogen degradation is dominant over dilution and advection, and the local growth law by itself maintains the scaled gradient (Fig. 3E; supplementary material Figs S13-S15).

Analytical derivation

Our simulation results demonstrated that the local coupling of cell division to morphogen signaling can by itself provide gradient scaling, spatially uniform growth, and a finite size without the ExR

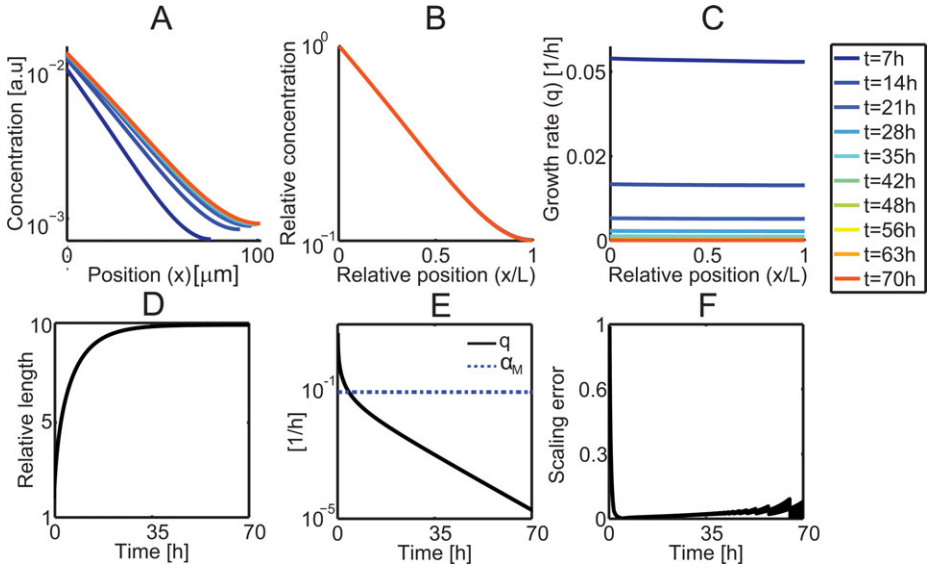

Fig. 3. Numerical simulation results for morphogen gradient dynamics in a tissue growing according to the MDDR without ExR feedback. In all cases, we assume a constant morphogen flux from the source. (A) Morphogen level as a function of position in the tissue at various times. (B) Relative morphogen level as a function of relative position in the tissue. Overlap of the profiles indicates scaling of morphogen gradient with size. (C) Proliferation rate at various times as a function of relative position. Growth is spatially uniform and its rate declines with time. (D) Fold change increase in tissue size as a function of time. (E) Morphogen degradation rate α (dashed blue line) and growth rate $q=\frac{\dot{L}}{L}$ (black solid line). Since there is no expander, morphogen degradation is constant. Note that scaling is achieved during most of the dynamics, when growth rate is much slower than morphogen degradation. (F) Scaling error defined as $\left|\frac{\partial\lambda}{\partial L}L\right|$ as a function of time. The scaling error is a dimensionless parameter describing the change in the sharpness of the gradient relative to the growth of the tissue. Excellent scaling is achieved when $\left|\frac{\partial\lambda}{\partial L}L\right|<1$.

Development (2014) 141, 2150-2156 doi:10.1242/dev.107011

Table 2. Sensitivity to model parameters

Parameter	MDDR	MDDR with ExR
(A) **Final size sensitivity**		
Morphogen diffusion coefficient (D_M)	0.31	0.22
Morphogen degradation rate (α_M)	0.31	0.35
Morphogen incoming flux (η)	0.02	0.01
Growth parameter (θ)	0.7	0.6
Initial tissue length (L_0)	0.3	0.2
(B) **Dynamics duration sensitivity**		
Morphogen diffusion coefficient (D_M)	0.13	0.15
Morphogen degradation rate (α_M)	0.07	0.02
Morphogen incoming flux (η)	0.036	0.035
Growth parameter (θ)	0.48	0.42
Initial tissue length (L_0)	0.31	0.15

mechanism. To better understand the origin of this behavior, we examined analytically the solution of Eqn 1 above, considering the scaled form of the morphogen profile observed numerically:

$$\frac{M(X,t)}{M(0,t)} = \hat{M}\left(\frac{X}{L}\right).$$

Assuming scaling of the gradient, together with the observation that the system converges to some steady state, implies that the resulting profile is exponential throughout the dynamics, following a short transient. This scaled solution further implies that the growth is uniform in space (see methods in the supplementary material for full derivation):

$$u_x = \frac{\dot{L}(t)}{L(t)}, \tag{4}$$

which is consistent with our simulation results. The scaled solution is then of the form (see methods in the supplementary material):

$$M(x,t) = \frac{\eta\lambda L(t)}{D_M}\exp\left(-\frac{1}{\lambda}\frac{x}{L(t)}\right), \tag{5}$$

$$L(t) = \sqrt{L_f^2(1-\exp(-\alpha_M t)) + L_0^2\exp(-\alpha_M t)},$$

$$L_f = \frac{1}{\lambda}\sqrt{\frac{D_M}{\alpha_M}}. \tag{6}$$

Here, λ is a dimensionless constant, defining the morphogen gradient length scale in the relative spatial coordinate $x/L(t)$. It depends on different parameters of the dynamics, including the initial length L_0 and θ (supplementary material Figs S5, S6). The only division rule consistent with this scaled solution is given by:

$$\frac{\dot{M}}{M} \approx \frac{\ln(2)}{\tau(t)} \tag{7}$$

when written in the coordinates of the moving cell. This solution is indeed consistent with the growth rule assumed in our simulations (Eq. 3), with θ=ln(2). As we saw in the simulations, choosing different θ values maintains the same qualitative behavior (Table 1B; see methods in the supplementary material for parameter values, Figs S8 and S10).

Taken together, this analytical result explains our numerical finding that MDDR can provide, by itself, gradient scaling, uniform growth and attainment of a finite size.

ExR feedback prolongs growth, increases tissue size and improves robustness

Next, we returned to the integrated system composed of both ExR and MDDR to examine whether the addition of ExR provides additional advantages. An extensive numerical screen revealed that scaling, uniform growth and finite tissue size are highly robust to the kinetic parameters of the system, both in the presence and absence of ExR feedback (Table 1). Final size and sharpness of the gradient were most sensitive to the growth parameter θ. Sensitivity to most parameters was reduced after introducing ExR (Table 2, Fig. 4A; supplementary material Figs S4 and S5). The percentage of scaled parameter sets increased with the addition of the expander, particularly in cases in which morphogen degradation was significantly faster than the typical cell cycle time (supplementary material Fig. S7).

To obtain analytical insight into the function of the expander in this integrated system, we approximated the ExR dynamics, Eqns 2a and 2b, assuming a flat expander profile. This is justified by previous analysis showing that ExR-dependent scaling requires a highly diffusible expander. Scaling together with a flat expander profile resulted in uniform tissue growth (see methods in the supplementary material). Further, we retrieve the exponential morphogen profile given by Eqn 5 as a solution to the coupled morphogen-expander system, with the temporal dynamics of the tissue length and expander concentration being specified by a system of ordinary differential equations (see methods in the

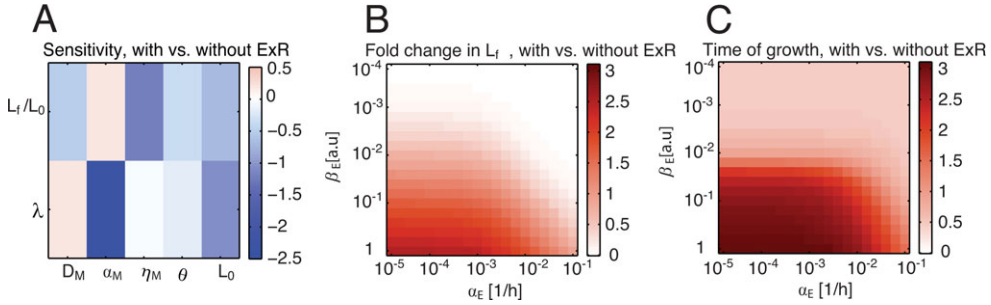

Fig. 4. ExR increases robustness, final size and prolongs growth. (A) Sensitivity log ratio of the final tissue size L_f and the gradient length scale λ, $\log_2\frac{S(p)_{\text{with ExR}}}{S(p)_{\text{No ExR}}}$, to various model parameters with versus without ExR. Sensitivity (S) of a quantity (X) to a parameter (p) is defined as the average over p of $\frac{p}{X}\left|\frac{\partial X}{\partial p}\right|$. In most cases, ExR improves robustness (blue shades). (B) The effect of expander degradation and production rates on $\log_2$ fold change in size: $\log_2\frac{(L_f/L_0)_{\text{with ExR}}}{(L_f/L_0)_{\text{No ExR}}}$. (C) The effect of the expander degradation and production rates on $\log_2$ fold change in growth duration (t_{ss}): $\log_2\frac{(t_{ss})_{\text{with ExR}}}{(t_{ss})_{\text{No ExR}}}$.

Development (2014) 141, 2150-2156 doi:10.1242/dev.107011

supplementary material, Eqs. 62 and 68). The resulting steady-state tissue length and expander concentration are given by:

$$E_f = \frac{c^*\beta_E}{\alpha_E}, \quad L_f = \frac{1}{\lambda}\sqrt{\frac{D_M}{\alpha_M}\left(1+\frac{c^*\beta_E}{\alpha_E}\right)}. \tag{8}$$

Here, c^* denotes the fraction of the tissue where the expander is expressed, which becomes constant following a short initial transient, once scaling commences (supplementary material Fig. S9). The morphogen and expander profiles are consistent with the cell division rule Eqn 7 (see methods in the supplementary material).

Eqn 8 suggests that the expander increases final tissue size. It also extends the time required to reach a steady state by reducing morphogen degradation rate, which is the dominant time scale in this system. This was indeed confirmed by our numerical screen: as predicted by Eqn 8, the fold increase in tissue length and in growth duration due to the addition of an ExR feedback depended on the typical expander level β_E/α_E (Fig. 4B,C). The fold increase in tissue size was also dependent on morphogen length scale at steady state (supplementary material Fig. S3):

$$\lambda_M = \sqrt{\frac{D_M}{\alpha_M}},$$

while the increase in growth duration was proportional to α_M, which is the morphogen degradation rate in the absence of the expander (supplementary material Fig. S3). Thus, removal of the expander from this integrated system is predicted to primarily affect the disc size and growth duration, while having a relatively low impact on the accuracy of scaling. This is in contrast to the experimental results obtained in the wing disc, when removal of *pentagone* resulted in a loss of scaling, but had a relatively minor effect on disc size (Ben-Zvi et al., 2011a, b; Hamaratoglu et al., 2011). This leads us to support the hypothesis that growth in the disc is not driven solely by Dpp signaling, as we discuss below.

DISCUSSION

The main result of the present study is the definition of a theoretical novel scaling mechanism that does not require global feedbacks but depends only on a local division rule, whereby cells divide when subject to some given increase in morphogen signaling. Previous studies have shown that this division rule leads to uniform growth, provided that the gradient scales by some other means (Wartlick et al., 2011). Here we show that, in fact, this division rule by itself can lead to morphogen gradient scaling. The simplicity of this growth rule, which depends only on local feedbacks, together with its robustness to the different parameters including those defining the growth rule itself, suggest that it might be employed during initial stages of tissue development when dynamics and growth are relatively fast and global feedbacks are harder to implement.

We identified the MDDR scaling mechanism while studying growth dynamics in the wing disc, where this morphogen-dependent growth rule was implicated in the context of the Dpp morphogen. We and others have recently shown that scaling of the Dpp morphogen in the wing disc depends on Pentagone, which is likely to function as the expander in the ExR mechanism (Ben-Zvi et al., 2011a; Hamaratoglu et al., 2011). We find that the integrated dynamics composed of both the ExR and the Dpp-dependent MDDR is consistent with many properties of the wing disc. Interestingly, it might also resolve an apparent limitation of the ExR in explaining the independent growth control of the anterior and posterior compartments of the wing disc: inhibition of Dpp signaling in one half of the disc does not substantially affect growth in the other half. This result appears incompatible with global feedback mechanisms, such as those proposed in ExR models. Interestingly, when simulating ExR dynamics combined with an early phase in which the MDDR is active, we find that it can in fact contribute to scaling at the two compartments independently (supplementary material Fig. S10).

In the context of the integrated dynamics, ExR functions primarily in extending the growth duration and increasing tissue size. Removing this feedback is predicted to reduce tissue size but not to alter scaling significantly. This, however, is not consistent with the findings in the wing disc, where removal of *pentagone* abolished scaling but resulted in only a minor reduction (~25%) in length of the AP axis of the disc. Therefore, either our model does not apply to the disc entirely, or it supports the hypothesis that at third instar growth is not entirely driven by the temporal increase in Dpp, and is defined either by absolute Dpp levels or by alternative signals as well (Schwank et al., 2011). If indeed the MDDR model applies to the wing disc, we expect during first and second instars that Dpp levels will correlate with cell division pattern and that scaling will persist in both wild-type and *pentagone* null wing discs. Notably, scaling of the Dpp gradient in wild type would still imply a correlation of cell division with the temporal increase in Dpp signaling (Wartlick et al., 2011), despite the lack of causality as shown by our analytical analysis.

To summarize, we propose that the morphogen-dependent growth rule may complement ExR feedback during wing disc growth, but is unlikely to be instructive for growth at late stages. More generally, our results suggest that a local coupling of cell division with morphogen signaling can establish global pattern scaling and tissue growth properties.

MATERIALS AND METHODS

Parameters

See methods in the supplementary material for full parameter lists.

Numerical method

In order to perform numerical simulations, we transform the morphogen evolution equation by $[x,t]\rightarrow[Y,t]$, with Y being the starting position of a cell at position x and time t. By setting $\bar{M}(Y,t) = M(x,t)$, $\bar{E}(Y,t) = M(x,t)$ the morphogen dynamics equation (Eqn 2) results in:

$$\bar{M}_t = \frac{D_M}{x_Y}\left(\frac{\bar{M}_Y}{x_Y}\right)_Y - \alpha(E)\cdot\bar{M} - \ln(2)\tau^{-1}(Y,t)\cdot\bar{M}, \tag{9}$$

$$\bar{E}_t = \frac{D_E}{x_Y}\left(\frac{\bar{E}_Y}{x_Y}\right)_Y - \alpha_E\cdot\bar{E} - \ln(2)\tau^{-1}(Y,t)\cdot\bar{E} + \beta_E\, h(\bar{M}), \tag{10}$$

$$\frac{dx_Y}{dt} = \ln(2)\tau^{-1}x_Y x_Y(0) = 1. \tag{11}$$

The growth law in Eqn 7 leads to the following equivalent growth law (see methods in the supplementary material for derivation) for the growth parameter θ:

$$\tau^{-1} = \frac{1}{\ln(2)+\theta}\left(\frac{D_M}{x_Y\bar{M}}\left(\frac{\bar{M}_Y}{x_Y}\right)_Y - \alpha(E)\right). \tag{12}$$

The above coupled system is solved numerically using an explicit finite difference scheme (see methods in the supplementary material) and the solutions are re-interpolated to the growing domain. All simulations are

Development (2014) 141, 2150-2156 doi:10.1242/dev.107011

performed using MATLAB (MathWorks). The numerical method is described in detail in methods in the supplementary material.

Acknowledgements
We thank Dr Shlomi Kotler, Dr Dann Huh, Mr Oren Raz, Prof. Benny Shilo and members of our group for fruitful discussions.

Competing interests
The authors declare no competing financial interests.

Author contributions
I.A., D.B.-Z. and S.M. developed the concepts, performed simulations and analytical calculations, analyzed the results and prepared the manuscript prior to submission. N.B. developed the concepts, analyzed the results and prepared the manuscript prior to submission.

Funding
This work was supported by the European Research Council and the Israel Science Foundation. N.B. is the incumbent of the Lorna Greenberg Scherzer Professorial Chair, and the Minerva Foundation. D.B.-Z. is supported by the HFSP long term postdoctoral fellowship and by the Rothschild and Fulbright postdoctoral fellowships. S.M is supported by the European Research Council.

Supplementary material
Supplementary material available online at
http://dev.biologists.org/lookup/suppl/doi:10.1242/dev.107011/-/DC1

References

Aegerter-Wilmsen, T., Aegerter, C. M., Hafen, E. and Basler, K. (2007). Model for the regulation of size in the wing imaginal disc of Drosophila. *Mech. Dev.* **124**, 318-326.
Affolter, M. and Basler, K. (2007). The Decapentaplegic morphogen gradient: from pattern formation to growth regulation. *Nat. Rev. Genet.* **8**, 663-674.
Barkai, N. and Ben-Zvi, D. (2009). 'Big frog, small frog'–maintaining proportions in embryonic development: delivered on 2 July 2008 at the 33rd FEBS Congress in Athens, Greece. *FEBS J.* **276**, 1196-1207.
Ben-Zvi, D. and Barkai, N. (2010). Scaling of morphogen gradients by an expansion-repression integral feedback control. *Proc. Natl. Acad. Sci. U.S.A.* **107**, 6924-6929.
Ben-Zvi, D., Shilo, B.-Z., Fainsod, A. and Barkai, N. (2008). Scaling of the BMP activation gradient in Xenopus embryos. *Nature* **453**, 1205-1211.
Ben-Zvi, D., Pyrowolakis, G., Barkai, N. and Shilo, B.-Z. (2011a). Expansion-repression mechanism for scaling the Dpp activation gradient in Drosophila wing imaginal discs. *Curr. Biol.* **21**, 1391-1396.
Ben-Zvi, D., Shilo, B.-Z. and Barkai, N. (2011b). Scaling of morphogen gradients. *Curr. Opin. Genet. Dev.* **21**, 704-710.
Bittig, T. (2008). *Morphogenetic Signaling in Growing Tissues*. Dresden: Institut für Theoretische Physik Fakultät Mathematik und Naturwissenschaften, Technische Universität.
Böhni, R., Riesgo-Escovar, J., Oldham, S., Brogiolo, W., Stocker, H., Andruss, B. F., Beckingham, K. and Hafen, E. (1999). Autonomous control of cell and organ size by CHICO, a Drosophila homolog of vertebrate IRS1-4. *Cell* **97**, 865-875.
Cheung, D., Miles, C., Kreitman, M. and Ma, J. (2011). Scaling of the Bicoid morphogen gradient by a volume-dependent production rate. *Development* **138**, 2741-2749.
Day, S. J. and Lawrence, P. A. (2000). Measuring dimensions: the regulation of size and shape. *Development* **127**, 2977-2987.
Gierer, A. and Meinhardt, H. (1972). A theory of biological pattern formation. *Kybernetik* **12**, 30-39.
Gregor, T., McGregor, A. P. and Wieschaus, E. F. (2008). Shape and function of the Bicoid morphogen gradient in dipteran species with different sized embryos. *Dev. Biol.* **316**, 350-358.
Hamaratoglu, F., de Lachapelle, A. M., Pyrowolakis, G., Bergmann, S. and Affolter, M. (2011). Dpp signaling activity requires pentagone to scale with tissue size in the growing Drosophila wing imaginal disc. *PLoS Biol.* **9**, e1001182.
Houchmandzadeh, B., Wieschaus, E. and Leibler, S. (2002). Establishment of developmental precision and proportions in the early Drosophila embryo. *Nature* **415**, 798-802.
Hufnagel, L., Teleman, A. A., Rouault, H., Cohen, S. M. and Shraiman, B. I. (2007). On the mechanism of wing size determination in fly development. *Proc. Natl. Acad. Sci. U.S.A.* **104**, 3835-3840.
Johnston, L. A. and Sanders, A. L. (2003). Wingless promotes cell survival but constrains growth during Drosophila wing development. *Nat. Cell Biol.* **5**, 827-833.
Kicheva, A., Pantazis, P., Bollenbach, T., Kalaidzidis, Y., Bittig, T., Julicher, F. and Gonzalez-Gaitan, M. (2007). Kinetics of morphogen gradient formation. *Science* **315**, 521-525.
Lanctot, A. A., Peng, C.-Y., Pawlisz, A. S., Joksimovic, M. and Feng, Y. (2013). Spatially dependent dynamic MAPK modulation by the Nde1-Lis1-Brap complex patterns mammalian CNS. *Dev. Cell* **25**, 241-255.
Milan, M., Campuzano, S. and Garcia-Bellido, A. (1996). Cell cycling and patterned cell proliferation in the Drosophila wing during metamorphosis. *Proc. Natl. Acad. Sci. U.S.A.* **93**, 11687-11692.
Patel, N. H. and Lall, S. (2002). Developmental biology: precision patterning. *Nature* **415**, 748-749.
Restrepo, S. and Basler, K. (2011). Morphogen gradients: expand and repress. *Curr. Biol.* **21**, R815-R817.
Rogulja, D. and Irvine, K. D. (2005). Regulation of cell proliferation by a morphogen gradient. *Cell* **123**, 449-461.
Rogulja, D., Rauskolb, C. and Irvine, K. D. (2008). Morphogen control of wing growth through the Fat signaling pathway. *Dev. Cell* **15**, 309-321.
Sato, M. and Kornberg, T. B. (2002). FGF is an essential mitogen and chemoattractant for the air sacs of the Drosophila Tracheal System. *Dev. Cell* **3**, 195-207.
Schwank, G. and Basler, K. (2010). Regulation of organ growth by morphogen gradients. *Cold Spring Harb. Perspect. Biol.* **2**, a001669.
Schwank, G., Restrepo, S. and Basler, K. (2008). Growth regulation by Dpp: an essential role for Brinker and a non-essential role for graded signaling levels. *Development* **135**, 4003-4013.
Schwank, G., Tauriello, G., Yagi, R., Kranz, E., Koumoutsakos, P. and Basler, K. (2011). Antagonistic growth regulation by Dpp and Fat drives uniform cell proliferation. *Dev. Cell* **20**, 123-130.
Schwank, G., Yang, S.-F., Restrepo, S. and Basler, K. (2012). Comment on "Dynamics of dpp signaling and proliferation control". *Science* **335**, 401.
Shraiman, B. I. (2005). Mechanical feedback as a possible regulator of tissue growth. *Proc. Natl. Acad. Sci. U.S.A.* **102**, 3318-3323.
Teleman, A. A. and Cohen, S. M. (2000). Dpp gradient formation in the Drosophila wing imaginal disc. *Cell* **103**, 971-980.
Towers, M., Mahood, R., Yin, Y. and Tickle, C. (2008). Integration of growth and specification in chick wing digit-patterning. *Nature* **452**, 882-886.
Vuilleumier, R., Affolter, M. and Pyrowolakis, G. (2011). Pentagone: patrolling BMP morphogen signaling. *Fly* **5**, 210-214.
Wartlick, O., Mumcu, P., Kicheva, A., Bittig, T., Seum, C., Julicher, F. and Gonzalez-Gaitan, M. (2011). Dynamics of Dpp signaling and proliferation control. *Science* **331**, 1154-1159.
Wartlick, O., Mumcu, P., Jülicher, F. and Gonzalez-Gaitan, M. (2012). Response to comment on "Dynamics of Dpp signaling and proliferation control". *Science* **335**, 401.
Wolpert, L. (1969). Positional information and the spatial pattern of cellular differentiation. *J. Theor. Biol.* **25**, 1-47.

SCALING MORPHOGEN PATTERN WITH TISSUE SIZE IN THE ABSENCE OF GLOBAL FEEDBACKS (SUPPORTING INFORMATION)

1. Mathematical Framework.

We consider a one-dimensional growing tissue $[0, L(t)]$. The domain growth is modeled with a flow type growth law given by,

$$\begin{aligned} \frac{dx(t)}{dt} &= u(x(t), t), \quad \forall x \in [0, L(t)] \quad t > 0, \\ x(0) &= Y. \end{aligned} \tag{1}$$

Here, u is the (local) flow rate of the growing tissue.

As growth is on account of cell division (we ignore the changes in cell shape and cell movement in this study), the cell proliferation rate (rate at which the cell divides) is given by

$$u_x = \frac{du}{dx}.$$

Now consider any infinitesimal length element $[x_1, x_2]$ with $|x_2 - x_1| << 1$. As (1) holds, we have

$$\begin{aligned} \frac{dx_1(t)}{dt} &= u(x_1, t), \\ x_1(0) &= Y_1, \end{aligned} \tag{2}$$

and

$$\begin{aligned} \frac{dx_2(t)}{dt} &= u(x_2, t), \\ x_2(0) &= Y_2, \end{aligned} \tag{3}$$

Subtracting (2) from (3), we obtain,

$$\begin{aligned} \frac{d(x_2 - x_1)}{dt} &= u(x_2, t) - u(x_1, t), \\ \text{as } |x_2 - x_1| << 1 \quad \Rightarrow \frac{d(x_2 - x_1)}{dt} &\approx u_x(x_1, t)(x_2 - x_1) \\ (x_2 - x_1)(0) &= Y_2 - Y_1, \end{aligned}$$

Solving the above ordinary differential equation leads to an infinitesimal length element that evolves (in time) as,

$$(x_2 - x_1)(t) \approx (Y_2 - Y_1) e^{\int_0^t u_x(x_1, s) ds}. \tag{4}$$

As proliferation is on account of cell division, any infinitesimal tissue element doubles in size within the *cell cycle life time* i.e, the amount it takes for a cell to divide into two. Denoting the cell cycle time as τ, we observe from (4) that the length element $[Y_1, Y_2]$ doubling its size in time τ implies,

$$\begin{aligned} 2(Y_2 - Y_1) &\approx (Y_2 - Y_1)e^{\int_0^\tau u_x(x_1,s)ds} \\ \Rightarrow \ln(2) &\approx \int_0^\tau u_x(x_1, s)ds \approx u_x(x_1, t)\tau \\ \Rightarrow u_x(x_1, t) &\approx \frac{\ln(2)}{\tau(x_1, t)}. \end{aligned}$$

As x_1 is any point in $[0, L]$, we can replace it with x and obtain Eq. 1 in the main text. Note that we have assumed that the proliferation rate u_x does not change (by much) during the cell cycle in the above derivation.

1.1. **Governing equations.** Given the above growth model, the rate of change of morphogen concentration $M(x, t)$ in a growing domain (with expander-dependent degradation) is

$$\frac{d}{dt}\int_{\delta_1(t)}^{\delta_2(t)} M(x,t)dx = \nu(\delta_2(t), t) - \nu(\delta_1(t), t) - \int_{\delta_1(t)}^{\delta_2(t)} \alpha(E)M(x,t)dx,$$

for any infinitesimal length element $(\delta_1(t), \delta_2(t))$. Here $\nu = D_M(E)M_x$ represents the flux on account of diffusion of the morphogen and $\alpha(E)$ is the morphogen degradation. Both the diffusion and the degradation rates can depend on the expander E. Using the Reynolds theorem [1] and the growth condition (1), we obtain the morphogen evolution equation,

$$M_t = D_M(E)M_{xx} - \alpha(E)M - uM_x - u_xM, \quad (x,t) \in [0, L(t)] \times [0, T]. \tag{5}$$

Here, u is the flow rate from (1). The above equation is a advection-reaction-diffusion equation, that has to be supplemented with suitable initial and boundary conditions.

Similarly, the rate of change of expander concentration $E(x, t)$ in a growing domain is given by,

$$\frac{d}{dt}\int_{\delta_1(t)}^{\delta_2(t)} E(x,t)dx = \mu(\delta_2(t), t) - \mu(\delta_1(t), t) - \int_{\delta_1(t)}^{\delta_2(t)} \alpha_E E(x,t)dx + \int_{\delta_1(t)}^{\delta_2(t)} \beta_E h(M(x,t))dx,$$

for any infinitesimal length element $(\delta_1(t), \delta_2(t))$. Here $\mu = D_E E_x$ represents the flux on account of diffusion of the expander. The degradation rate α_E is constant as is the rate of optimal expander concentration β_E and the source (production) function h depends on the Morphogen concentration M. Using the Reynolds theorem [1] and the growth condition (1), we obtain the

morphogen evolution equation,

$$E_t = D_E E_{xx} - \alpha_E E - uE_x - u_x E + \beta_E h(M), \quad (x,t) \in [0, L(t)] \times [0, T]. \tag{6}$$

This establishes the derivation of morphogen and expander evolution equations 2(a) and 2(b) in the text.

For the rest of the paper, we assume that the expander only limits morphogen degradation. Hence, the morphogen diffusion rate $D_M(E) \equiv D_M$ and the expander dependent morphogen degradation rate is

$$\alpha(E) = \frac{\alpha_M}{1 + \frac{E}{E_c}}, \quad E_c \equiv 1.$$

The morphogen dependent expander repression is

$$h(M) = \frac{T_{rep}^n}{T_{rep}^n + M^n},$$

Here, $n >> 1$ is the Hill coefficient. We remark that in the limit of $n \to \infty$, the Hill function converges to the indicator function,

$$h(M) = \mathbb{I}_{\mathcal{P}} = \begin{cases} 1 & \text{if} \quad x \in \mathcal{P}, \\ 0 & \text{otherwise.} \end{cases} \tag{7}$$

with T_{rep} being the threshold of repression of the expander by the morphogen and $\mathcal{P}$ being the expander expression domain:

$$\mathcal{P}(t) = \{x \in [0, L(t)] : M(x,t) \leq T_{rep}\}, \quad P(t) = \text{Length}(\mathcal{P}(t)). \tag{8}$$

For the rest of the analytical results section, we assume that the Hill coefficient $n >> 1$ and use the above approximation for the repression function.

2. Analytical solution properties in the absence of the expander

Motivated by the numerical results presented in the main text (figure 3) that scaling, uniform growth and a finite final tissue size can emerge directly from the coupling of the morphogen patterning to the experimentally observed growth law Eq. 3 of the main text even in the absence of the expander, we analyze the morphogen evolution equation (5) in the absence of the expander E. To do so, we set $E = 0$ in the morphogen evolution equation (5) to obtain:

$$M_t = D_M M_{xx} - \alpha_M M - uM_x - u_x M, \quad (x,t) \in [0, L(t)] \times [0, T]. \tag{9}$$

Our aim is to solve the morphogen evolution equation (9) analytically under biologically reasonable hypothesis. To do so, we first establish a series of desirable properties of the solution.

2.1. **Scaling leads to a finite final tissue size.** The most desirable property that we require of the morphogen profile is that it scales with the growing tissue. For constant morphogen boundary conditions at the edge $x = 0$, the relevant notion of scaling is that the morphogen concentration depends only on the relative cellular position $\xi = \frac{x}{L(t)}$ leading to

$$M(x,t) = M(\xi) = M\left(\frac{x}{L(t)}\right). \tag{10}$$

Similarly, when the morphogen flux is set to constant on the proximal boundary, the relevant notion is normalized scaling i.e,

$$M(x,t) = M(0,t)\widehat{M}(\xi) = M(0,t)\widehat{M}\left(\frac{x}{\omega L(t)}\right), \tag{11}$$

Since we have flux boundary conditions at the proximal boundary, the above equation implies

$$\begin{aligned} D_M M_x(0) &= \eta, \\ \Rightarrow \quad \frac{D_M M(0,t)\hat{M}'(0)}{\omega L(t)} &= \eta. \end{aligned}$$

As $\hat{M}'(0)$ is a constant, the above expression yields,

$$M(0,t) = \frac{C\omega\eta}{D_M}L(t) = \bar{m}L(t), \quad \text{with} \quad \bar{m} = \frac{C\omega\eta}{D_M}. \tag{12}$$

Thus, we require that the morphogen width scales with size but the amplitude of the morphogen can increase linearly with tissue size. In this section, we assume that the (normalized) morphogen profile scales and derive several interesting consequences of this assumption.

First, we show that under the assumption of scaling and other biologically reasonable assumptions, the tissue has to a attain a finite final size. The precise result is stated in the form of the following lemma,

Lemma 2.1. *Let M be a solution of (9) with the following assumptions,*

(i.) *Constant flux boundary conditions on the proximal boundary i.e,*

$$D_M M_x(0,t) = \eta, \quad \eta < 0. \tag{13}$$

(ii.) *The (normalized) morphogen profile scales, i.e it satisfies (11)*

(iii.) *There exists a time $t^* > 0$ such that for all $t > t^*$, there exists a relative position $L^*(t) = CL(t)$ and some (possibly very small) amount of morphogen in a part of the tissue $[0, L^*]$ i.e, there exists an $\epsilon > 0$ (possibly very small) such that*

$$M(x,t) \geq \epsilon, \quad \forall x \in [0, L^*(t)],\ t > t^*. \tag{14}$$

This assumption corresponds to requiring that there is at least a part of the tissue that contains a minimal amount of morphogen after scaling commences at time $t = t^*$.

(iv.) *The tissue growth is always non-negative i.e, $u \geq 0$.*

(v.) *The morphogen concentration forms a gradient i.e,* $\widehat{M}'(\xi) \leq 0$.

Then, the size of the tissue at any time is finite.

Proof. First, we observe that scaling (11) implies

$$M_t = \bar{m} L'(t) \left(\widehat{M} - \widehat{M}'(\xi)\xi \right) \geq 0, \tag{15}$$

as the morphogen concentration and growth are always non-negative, the gradient is non-increasing and relative position $\xi \in [0, 1]$.

Next, for any time $t > t^*$, we integrate the evolution equation (9) over $[0, L^*(t)]$ to obtain using the fundamental theorem of calculus that,

$$\begin{aligned}
\int_0^{L^*(t)} M_t dx &= D_M \int_0^{L^*(t)} M_{xx} dx - \alpha_M \int_0^{L^*(t)} M dx - \int_0^{L^*(t)} (uM)_x dx, \\
&= D_M M_x(L^*(t), t) - D_M M_x(0, t) - \alpha_M \int_0^{L^*(t)} M dx \\
&\quad - u(L(t), t) M(L(t), t) + u(0, t) M(0, t) \\
&\leq -\eta - \alpha_M \int_0^{L^*(t)} M dx - u(L(t), t) M(L(t), t), \\
&\leq -\eta - \alpha_M \int_0^{L^*(t)} M dx
\end{aligned}$$

In the above, we have used boundary conditions (13), the scaling assumption (11) and the non-decreasing gradient assumption v. and the fact that $u(0) = 0$ and growth and morphogen concentration are always non-negative. From the above and (14), we obtain

$$\begin{aligned}
& 0 \leq \int_0^{L^*(t)} M_t dx \leq -\eta - \alpha_M \int_0^{L^*(t)} M dx \\
\Rightarrow \quad & 0 \leq -\eta - \alpha_M L^*(t) \epsilon \\
\Rightarrow \quad & L^*(t) \leq \frac{-\eta}{\alpha_M \epsilon} \\
\Rightarrow \quad & L(t) \leq \frac{-\eta}{C \alpha_M \epsilon}
\end{aligned} \tag{16}$$

Noting that $\eta < 0$, the above equation clearly shows that $L(t)$ is finite for any time t.

Similar results hold for constant morphogen boundary conditions also.

Remark. Given our assumption that cell proliferation drives growth, infinite growth can happen in finite time if the proliferation rate becomes infinite. However, the above argument clearly shows that the cell proliferation rate (defined by our model) remains finite for all time. This is completely consistent with biologically realistic scenarios.

2.2. **Finite final size implies exponentially decay morphogen gradients and uniform growth.** Once the tissue attains a finite final size, clearly $u, u_x \equiv 0$ and the equation will converge to a steady state. The steady solution of (5) with flux boundary conditions is given by,

$$M_{st}(x) = CL_f e^{-\frac{x}{\lambda L_f}}, \tag{17}$$

for some constant C (determined from the boundary conditions) and for some λ that needs to be determined. Here, L_f is the final tissue size (also to be determined). As the solution scales throughout the dynamics (at least after an initial transient), it is reasonable to assume from the shape of the solution at steady state (19) that the unsteady solution is also a exponentially decaying morphogen profile:

$$M(x,t) = \bar{m}L(t)e^{-\frac{x}{\lambda L(t)}}, \tag{18}$$

with the same C, λ as in (19) and with $L(t)$ being the length of the tissue at time t. The solution for constant morphogen boundary conditions can be determined analogously.

Given the solution (18), we plug it in (5) to obtain,

$$\frac{L'(t)}{L(t)} + \frac{xL'}{\lambda L^2} = D_M \left(\frac{1}{\lambda L}\right)^2 - \alpha_M - u_x + u\frac{1}{\lambda L}. \tag{19}$$

Differentiating the above equation by x we get

$$u_{xx} = \frac{1}{\lambda L}u_x - \frac{1}{\lambda L}\frac{L'}{L} \tag{20}$$

The general solution for the above equation is ,

$$u_x = a(t)e^{\frac{x}{\lambda L}} + \frac{\dot{L}}{L} \tag{21}$$

Integrating again over x we get

$$u = a(t)\lambda L e^{\frac{x}{\lambda L}} + x\frac{L'}{L} + b(t) \tag{22}$$

From the definition of u (1), we obtain the boundary conditions are $u(x = 0) = 0$, $u(x = L) = L'(t)$. Substituting, we get that $a(t) = 0$, and therefore $u_{xx} = 0$ and u_x is independent of space, i.e. growth is uniform. Note that the above argument employs a general solution of the equation (20) and this solution cannot be uniquely determined due to the presence of time-dependent coefficients a, b. However, the assertion that growth is uniform is still valid as the coefficients in (20) are independent of the space variable.

2.3. **Explicit solutions for scaled morphogen profiles.** We have shown that scaling can imply uniform growth. Consequently,

$$x(t) = Yg(t). \tag{23}$$

Here, $g(t)$ is the time dependent uniform growth rate. From (1), we observe that for uniform growth,

$$\begin{aligned}\frac{dx(t)}{dt} &= Y\dot{g}(t),\\ &= x(t)\frac{\dot{g}(t)}{g(t)} = x(t)\frac{\dot{L}(t)}{L(t)}, \quad \text{as } L(t) = L_0 g(t)\\ g(0) &= 1.\end{aligned}$$

Hence,

$$u(x,t) = \frac{x\dot{L}(t)}{L(t)}. \tag{24}$$

Substituting the above form of the flow rate u into the evolution equation (9), we obtain the morphogen evolution (in growing coordinates) for a uniformly growing tissue:

$$M_t + x\frac{\dot{L}(t)}{L(t)}M_x = D_M M_{xx} - \alpha_M M - \frac{\dot{L}(t)}{L(t)}M, \tag{25}$$

If we assume normalized scaling (11), we show above that we obtain uniform growth (23). Consequently,

$$\begin{aligned}M_t + \frac{x\dot{L}}{L}M_x &= \frac{\dot{L}}{L}M - \frac{x\dot{L}}{L^2}\widehat{M}'(\xi) + \frac{x\dot{L}}{L^2}\widehat{M}'(\xi)\\ &= \frac{\dot{L}}{L}M,\end{aligned} \tag{26}$$

Substituting the above into the morphogen evolution equation (25), we obtain

$$\frac{\widehat{M}''(\xi)}{\widehat{M}(\xi)} = \frac{\omega^2}{D_M}\left(2L(t)\dot{L}(t) + \alpha_M L(t)^2\right). \tag{27}$$

The left hand side of the above equation (27) depends only on the relative position ξ and the right hand side depends only on the time variable. The equality of these terms implies that both the left and right hand sides have to be equal for all values i.e, for some constant $\overline{\lambda}$, we have

$$\frac{\widehat{M}''(\xi)}{\widehat{M}(\xi)} = \frac{1}{\overline{\lambda}^2}, \tag{28}$$

and

$$\frac{\omega^2}{D_M}\left(2L(t)\dot{L}(t) + \alpha_M L(t)^2\right) = \frac{1}{\overline{\lambda}^2}. \tag{29}$$

By setting $\lambda = \omega\overline{\lambda}$, we can solve the ODEs (28) and (29) explicitly and obtain the analytical solutions

$$\begin{aligned} M(x,t) &= \overline{m} L(t) e^{\frac{-x}{\lambda L(t)}} \\ L(t) &= \sqrt{L_f^2\left(1 - e^{-\alpha_M t}\right) + L_0^2 e^{-\alpha_M t}}, \\ L_f &= \frac{1}{\lambda}\sqrt{\frac{D_M}{\alpha_M}}, \end{aligned} \tag{30}$$

Thus recovering the explicit solution Eq.5, Eq.6 in the main text. Note that L_f is the final tissue size in this case.

Remark. An alternative derivation of the solution formulas (30) can be performed by using the scaled exponential ansatz (18) into (19). However, this derivation requires an a priori assumption of an exponentially decaying gradient. On the other hand, our derivation, as presented above, only requires the assumptions of scaling and uniform growth and derives an exponentially decaying gradient as a consequence of these assumptions.

For the case of point boundary conditions i.e, when the level of morphogen at the proximal boundary is kept constant, we substitute the perfectly scaled solution profile (10) into (58), and obtain

$$\frac{M''(\xi)}{M(\xi)} = \frac{\omega^2}{D_M}\left(L(t)\dot{L}(t) + \alpha_M L(t)^2\right). \tag{31}$$

The left hand side of the above equation (31) depends only on the relative position ξ and the right hand side depends only on the time variable. The equality of these terms implies that both the left and right hand sides have to be equal for all values i.e, for some constant $\overline{\lambda}$, we have

$$\frac{M''(\xi)}{M(\xi)} = \frac{1}{\overline{\lambda}^2}, \tag{32}$$

and

$$\frac{\omega^2}{D_M}\left(L(t)\dot{L}(t) + \alpha L(t)^2\right) = \frac{1}{\overline{\lambda}^2} \tag{33}$$

We can solve the ODEs (32) and (33) explicitly and obtain the analytical solutions

$$\begin{aligned} M(x,t) &= M_0 e^{\frac{-x}{\lambda L(t)}} \\ L(t) &= \sqrt{L_f^2\left(1 - e^{-2\alpha t}\right) + L_0^2 e^{-2\alpha t}}, \\ L_f &= \frac{1}{\lambda}\sqrt{\frac{D_M}{\alpha_M}}, \end{aligned} \tag{34}$$

Remark. In both sets of explicit solutions, (30) for constant flux boundary conditions and (34) for constant morphogen (level) boundary conditions, we observe that the scaled morphogen profiles are only consistent with exponentially decaying initial morphogen gradients. This fact is easy to realize by setting $t = 0$ in both explicit solution formulas. Therefore, when the initial data is not an exponentially decaying profile, we expect that there is an initial transient $0 \leq t \leq T_*$, during which the morphogen profile dynamically evolves into a scaled solution profile of the form

$$M(x,t) = M_0 e^{\frac{-x}{\lambda L(t)}}, \quad \forall x \in [0, L(t)], \quad \forall t > T_*.$$

This onset time T_* is necessary for the solution to start scaling. Further discussion about the onset time and the initial transient is provided in the section on numerical experiments. In the presence of an initial transient i.e if $T_* > 0$, the above theory still holds for $t \geq T_*$ and all the expressions derived above can be readily modified to accommodate this onset time.

2.4. **Derivation of simplified consistent growth laws.** In the case of flux boundary conditions, we see that the explicit morphogen profile (30) satisfies,

$$\begin{aligned} \dot{M} &= M_t + uM_x, \\ \Rightarrow \frac{\dot{M}}{M} &= \frac{M_t}{M} + \frac{x\dot{L}}{L}\frac{M_x}{M}, \\ &= \frac{\dot{L}}{L} + \frac{x\dot{L}}{L^2} - \frac{x\dot{L}}{L^2}, \\ &= \frac{\dot{L}}{L} = \frac{\ln 2}{\tau} \end{aligned}$$

Thus, deriving Eq. 7 in the main text.

Similarly, for the explicit solutions (34) for constant morphogen levels at the source (proximal) boundary conditions, a direct calculation shows

$$\begin{aligned} \dot{M} &= M_t + uM_x, \\ \Rightarrow \frac{\dot{M}}{M} &= \frac{M_t}{M} + \frac{x\dot{L}}{L}\frac{M_x}{M}, \\ &= \frac{x\dot{L}}{L^2} - \frac{x\dot{L}}{L^2}, \\ &\equiv 0. \end{aligned} \tag{35}$$

This establishes that for point boundary conditions, $\dot{M} \equiv 0$, i.e, in other words, the cells divide to maintain homeostasis.

2.5. **Homeostatic growth law as a limit case of growth law Eq. 3 (main text).** The simplified growth law (Eq. 3 in the main text) is

$$\frac{1}{\tau} = \frac{1}{\theta}\frac{\dot{M}}{M}. \tag{36}$$

Clearly, setting $\theta = \ln(2)$ recovers Eq. 7 (the case of constant flux boundary conditions).

It is reasonable to assume that the cell division time $\tau > 0$ i.e, the cell cycle cannot be infinitely fast. We have the following calculation,

$$\begin{aligned} \frac{\theta}{\tau} &= \frac{\dot{M}}{M}, \\ \text{hence,} \quad \lim_{\theta\to 0}\frac{\theta}{\tau} = 0 &\Rightarrow \lim_{\theta\to 0}\frac{\dot{M}}{M} = 0, \\ &\Rightarrow \lim_{\theta\to 0}\dot{M} = 0. \end{aligned}$$

The above follows from the fact that the morphogen $M > 0$ i.e, there is some basal (very small) morphogen signalling. Thus, the limit case of the growth law Eq. 3 of the main text, when $\theta \to 0$ leads recovers the homeostasis $\dot{M} = 0$, which is consistent with constant morphogen levels at source boundary conditions.

2.6. **Noise in the growth parameter θ.** As indicated in the main text, the global properties of scaled morphogen profile, uniform tissue growth and attainment of a finite final size are quite robust to the various biochemical parameters of the system when the morphogen evolution equation (9) is simulated together with the growth law, Eq. 3 in the main text. A crucial role is played by the growth parameter θ as it determines when exactly the cell divides. It is reasonable to suppose that an universal value of the parameter θ (i.e, the same value of θ for all cells in the tissue) is probably unrealistic in real biological scenarios. A more plausible assumption is to introduce some noise in θ. Will the global properties be robust with respect to this intrinsic noise ? To answer this question, we simulated the morphogen equation (9) with growth law Eq. 3 in the main text, with a noisy $\theta = \ln(2) + 0.2\mathcal{N}$ with $\mathcal{N}$ denoting the standard normal. The resulting mean morphogen profile as function of relative concentration and mean proliferation rate as a function of relative tissue position are shown in figure S8. The results clearly show that the properties of scaled morphogen profiles and uniform tissue growth were robust to the noise in the growth parameter. Both properties are obtained with a standard deviation which is less than 1 percent of the mean (calculated over 500 samples).

3. Analytical results in the presence of the expander

The above analytical results and the numerical results presented in the main text show that scaling and uniform growth can result directly from local cell division rule, even in the absence of the expander. The analytical

results presented below explain the role that the expander plays in this paradigm.

3.1. **Scaled morphogen profiles lead to a finite final tissue size, even in the presence of the expander.** First, we show that under the assumption of normalized scaling of the morphogen (11) and other biologically reasonable assumptions, the tissue has to a attain a finite final size. The precise result is stated in the form of the following lemma,

Lemma 3.1. *Let M be a solution of (5) with the following assumptions,*

(i.) *Constant flux boundary conditions on the proximal boundary i.e,*

$$DM_x(0,t) = \eta, \quad \eta < 0. \tag{37}$$

(ii.) *The (normalized) morphogen profile scales, i.e it satisfies (11)*

(iii.) *There exists a time $t^* > 0$ such that for all $t > t^*$, there exists a relative position $L^*(t) = CL(t)$ and some (possibly very small) amount of morphogen in a part of the tissue $[0, L^*]$ i.e, there exists an $\epsilon > 0$ (possibly very small) such that*

$$M(x,t) \geq \epsilon, \quad \forall x \in [0, L^*(t)], \ t > t^*. \tag{38}$$

This assumption corresponds to requiring that there is at least a part of the tissue that contains a minimal amount of morphogen after scaling commences at time $t = t^*$.

(iv.) *The tissue growth is always non-negative i.e, $u \geq 0$.*

(v.) *The morphogen concentration forms a gradient i.e, $\widehat{M}'(\xi) \leq 0$.*

(vi.) *The expander concentration is bounded (finite) for all time, i.e, there exists a constant K such that $\forall t > 0$,*

$$E(x,t) \leq K, \quad \forall x \in [0, L(t)].$$

Then, the size of the tissue at any time is finite.

Proof. First, we observe that scaling (11) implies

$$M_t = \bar{m} L'(t) \left(\widehat{M} - \widehat{M}'(\xi)\xi \right) \geq 0, \tag{39}$$

as the morphogen concentration and growth are always non-negative, the gradient is non-increasing and relative position $\xi \in [0, 1]$.

Next, we integrate the evolution equation (13) over $[0, L^*(t)]$ to obtain using the fundamental theorem of calculus that,

$$\begin{aligned}\int_0^{L^*(t)} M_t dx &= D_M \int_0^{L^*(t)} M_{xx} dx - \alpha_M \int_0^{L^*(t)} \frac{M}{1+E} dx - \int_0^{L^*(t)} (uM)_x dx,\\ &= D_M M_x(L(t),t) - D_M M_x(0,t) - \alpha_M \int_0^{L^*(t)} \frac{M}{1+E} dx\\ &\quad - u(L(t),t)M(L(t),t) + u(0,t)M(0,t)\\ &\leq -\eta - \alpha_M \int_0^{L^*(t)} \frac{M}{1+E} dx - u(L(t),t)M(L(t),t),\\ &\leq -\eta - \alpha_M \int_0^{L^*(t)} \frac{M}{1+E} dx\end{aligned}$$

In the above, we have used boundary conditions (37), the scaling assumption (11) and the non-decreasing gradient assumption v. and the fact that $u(0) = 0$ and growth and morphogen concentration are always non-negative.

From the above, the assumption [vi.] on the expander and (38), we obtain

$$\begin{aligned} & 0 \leq \int_0^{L^*(t)} M_t dx \leq -\eta - \alpha \int_0^{L^*(t)} \frac{M}{1+E} dx \\ \Rightarrow \quad & 0 \leq -\eta - \alpha_M L^*(t)\epsilon \\ \Rightarrow \quad & L^*(t) \leq \frac{-\eta}{\alpha_M \epsilon} \\ \Rightarrow \quad & L(t) \leq \frac{-\eta}{C\alpha_M \epsilon} \end{aligned} \tag{40}$$

with $\epsilon = \frac{\bar{\epsilon}}{1+K}$. The above equation clearly shows that $L(t)$ is finite for any time t.

3.2. **Finite final tissue size and flat expander profile implies exponentially decaying morphogen gradients and uniform growth.** Henceforth, we will assume that the expander profile is flat i.e,

$$E(x,t) = E(t), \quad \forall x \in [0, L(t)]. \tag{41}$$

This assumption is reasonable, particularly for highly diffusible expanders i.e, when $D_E >> 1$, see [2] for motivation of why using a flat expander profile is biologically realistic.

Once the tissue attains a finite final size, clearly $u, u_x \equiv 0$ and the equations will converge to a steady state. As the expander profile is assumed to flat (spatially uniform), the steady solution of (5) with flux boundary conditions and a constant (in space) steady state morphogen concentration M_{st}, is given by,

$$M_{st}(x) = \bar{m} L_f e^{-\frac{x}{\lambda L_f}}, \tag{42}$$

for some decay length λ that needs to be determined. Here, L_f is the final tissue size (also to be determined). As the solution scales throughout the

dynamics (after a possible initial transient stage), it is reasonable to assume from the shape of the solution at steady state (19) that the unsteady solution is also a exponentially decaying morphogen profile:

$$M(x,t) = \overline{m} L(t) e^{-\frac{x}{\lambda L(t)}}, \tag{43}$$

with the same C, λ as in (42) and with $L(t)$ being the length of the tissue at time t. The solution for constant morphogen boundary conditions can be determined analogously.

Given the solution (43), we plug it in (5) to obtain,

$$\frac{L'(t)}{L(t)} + \frac{xL'}{\lambda L^2} = D_M \left(\frac{1}{\lambda L}\right)^2 - \frac{\alpha_M}{1+E(t)} - u_x + u\frac{1}{\lambda L}. \tag{44}$$

Using the fact that the expander profile is flat in space (41) and differentiating the above equation by x we get

$$u_{xx} = \frac{1}{\lambda L} u_x - \frac{1}{\lambda L}\frac{L'}{L} \tag{45}$$

The general solution for the above equation is ,

$$u_x = a(t) e^{\frac{x}{\lambda L}} + \frac{\dot{L}}{L} \tag{46}$$

Integrating again over x we get

$$u = a(t)\lambda L e^{\frac{x}{\lambda L}} + x\frac{L'}{L} + b(t) \tag{47}$$

From the definition of u (1), we obtain the boundray conditions are $u(x = 0) = 0$, $u(x = L) = L'(t)$. Substituting, we get that $a(t) = 0$, and therefore $u_{xx} = 0$ and u_x is independent of space, i.e. growth is uniform.

3.3. **Effective evolution equation for a flat expander profile in an uniformly growing tissue.** Under the assumptions that the expander profile is flat and the expander is assumed to very diffusive, i.e., $D_E >> 1$, we can (formally) derive an effective equation for the expander dynamics. We do so using an operator splitting approach.

Observing the expander evolution equation (6) reveals that three different effects (operators) contribute to the dynamics:

1. *Production* characterized by the term $\beta_E \mathbb{I}_{\mathcal{P}}$ i.e, the expander is produced in an expression domain (part of the tissue) at a constant rate, with $\mathbb{I}$ being the indicator function defined in (7).
2. *Diffusion* characterized by the term $D_E E_{xx}$.
3. *Dilution* modeled by the terms $\alpha_E E$ (expander degradation), $u_X E$ (dilution due to growth) and uE_x (transport due to growth).

Our strategy would be to analyze the expander evolution equation at any given time t, by factoring the total evolution over a given very small time step Δt into three parts. Given a spatially uniform expander profile $E(t)$ at time t, first, we will produce the expander assuming that it does not diffuse or

dilute (due to the very small time step), then we diffuse it without producing or diluting it and finally, we dilute it without producing or diffusing it. The process is iterated over each small time step to obtain the global (in time and space) dynamics of the expander. We formalize the above heuristics below:

Let $\mathcal{S}_t$ be the evolution operator for E from the evolution equation (6). In other words,

$$\mathcal{S}_t : E(x,0) \mapsto E(x,t), \quad E(x,t) = \mathcal{S}_t E(x,0). \tag{48}$$

For a small time step Δt, the operator can be split (factorized) into three constituent operators i,e,

$$E(x,t+\Delta t) := \mathcal{S}_{\Delta t} E(x,t) = \mathcal{S}^3_{\Delta t}\mathcal{S}^2_{\Delta t}\mathcal{S}^1_{\Delta t} E(x,t). \tag{49}$$

Here, $\mathcal{S}^1_t$ is the solution operator associated with the production equation:

$$E_t = \beta_E \mathbb{I}_{\mathcal{P}(t)}. \tag{50}$$

Similarly, $\mathcal{S}^2_t$ is the solution operator associated with the diffusion equation:

$$E_t = D_E E_{xx}, \tag{51}$$

and $\mathcal{S}^3_t$ is the solution operator associated with the transport-dilution equation:

$$E_t + uE_x + u_x E = -\alpha_E E, \tag{52}$$

Note that the global evolution can be obtained by iteration of the above procedure over k time steps with $k\Delta t = t$ i,e,

Assuming a flat initial expander profile (41) for a given time, we can explicitly solve the equation (50) for a small time step Δt to obtain,

$$\mathcal{S}^1_{\Delta t} E(x,t) = E(t) + \Delta t \beta_E \mathbb{I}_{\mathcal{P}(t)}. \tag{53}$$

Thus, the expander concentration that we obtain after the production step is a jump discontinuity between $E(t)$ and $E(t) + \beta_E \Delta t$.

Now, we consider the diffusion step i.e, solve the diffusion equation (51) with initial data $\mathcal{S}^1_{\Delta t}$ as calculated above. As the diffusion is fast, i.e, $D_E >> 1$, this jump discontinuity very rapidly diffuses to a constant:

$$\mathcal{S}^2_{\Delta t}\mathcal{S}^1_{\Delta t} E(x,t) = E^{av}(t+\Delta t). \tag{54}$$

Note that integrating the diffusion equation (51) over the length of tissue $[0.L(t)]$ and using the zero flux boundary conditions for the expander we

obtain that

$$\int_0^{L(t)} E_t(x,t)dx = D_E \int_0^{L(t)} E_{xx}(x,t)dx,$$

$$\Rightarrow \quad \frac{d}{dt}\int_0^{L(t)} E(x,t)dx = D_E(E_x(L(t),t) - E_x(0,t)) \quad \text{integration by parts,}$$

$$\equiv 0.$$

$$\Rightarrow \int_0^{L(t)} E(x,t+\Delta t)dx \equiv \int_0^{L(t)} E(x,t)dx, \quad \forall \Delta t.$$

The last equation above is a statement of the conservation of total expander concentration in the whole domain when there is no flux across its boundaries and when it is only diffusing inside the domain.

Using the above mass conservation and the formula (53), we can calculate the constant (in space) E^{av} in (54) as

$$\begin{aligned} LE^{av}(t) &= \int_0^{L(t)} \mathcal{S}^2_{\Delta t}\mathcal{S}^1_{\Delta t}E(t)dx \\ &= \int_0^{L(t)} \mathcal{S}^1_{\Delta t}E(t)dx \\ &= (L-P)E(t) + P(E(t)+\beta_E\Delta t) \\ &= LE(t) + P\beta_E\Delta t. \\ \Rightarrow \quad E^{av}(t) &= E(t) + \frac{P(t)}{L(t)}\beta_E\Delta t. \end{aligned}$$

In the final step, we solve the transport-dilution equation (52) with the above initial data. As the data is a constant, the transport has no effect and the data is just diluted by the (uniform in space) degradation terms, i.e,

$$\mathcal{S}^3_{\Delta t}E^{av}(t) = E^{av}(t) - \Delta t(\alpha_E + u_x)E^{av}(t). \tag{55}$$

Therefore, combining each of the above three steps, the evolution of the expander for the short time Δt is given by,

$$\begin{aligned} E(x,t+\Delta t) &:= \mathcal{S}^3_{\Delta t}\mathcal{S}^2_{\Delta t}\mathcal{S}^1_{\Delta t}E(x,0), \\ &= E(t) + \frac{P(t)}{L(t)}\beta_E\Delta t - \alpha_E E(t)\Delta t - u_x E\Delta + \mathcal{O}((\Delta t)^2). \end{aligned} \tag{56}$$

Hence,

$$\begin{aligned} E_t &= \lim_{\Delta t \to 0} \frac{E(t+\Delta t) - E(t)}{\Delta t} \\ &= \lim_{\Delta t \to 0} \left(\frac{P(t)}{L(t)} \beta_E - \alpha_E E(t) - u_x E(t) + \mathcal{O}(\Delta t) \right), \\ &= \frac{P(t)}{L(t)} \beta_E - \alpha_E E(t) - u_x E(t). \end{aligned}$$

Therefore, the effective expander evolution equation for highly diffusible expander is given by

$$\dot{E} = \frac{P(t)}{L(t)} \beta_E - (\alpha_E + u_x) E. \tag{57}$$

3.4. **Explicit solutions for scaled morphogen profiles.** We have shown that scaling and a flat expander profile imply that the tissue grows uniformly. Therefore, the morphogen evolution equation (5) takes the form:

$$M_t + x \frac{\dot{L}(t)}{L(t)} M_x = D_M M_{xx} - \alpha_M \frac{M}{1+E} - \frac{\dot{L}(t)}{L(t)} M, \tag{58}$$

If we assume normalized scaling (11), we obtain from (58) that

$$\begin{aligned} M_t + \frac{x\dot{L}}{L} M_x &= \frac{\dot{L}}{L} M - \frac{x\dot{L}}{L^2} \widehat{M}'(\xi) + \frac{x\dot{L}}{L^2} \widehat{M}'(\xi) \\ &= \frac{\dot{L}}{L} M, \end{aligned} \tag{59}$$

Substituting the above into the morphogen evolution equation (58), we obtain

$$\frac{\widehat{M}''(\xi)}{\widehat{M}(\xi)} = \frac{\omega^2}{D_M} \left(2L(t)\dot{L}(t) + \alpha_M \frac{L(t)^2}{1+E} \right). \tag{60}$$

The left hand side of the above equation (60) depends only on the relative position ξ and the right hand side depends only on the time variable. The equality of these terms implies that both the left and right hand sides have to be equal for all values i.e, for some constant $\bar{\lambda}$, we have

$$\frac{\widehat{M}''(\xi)}{\widehat{M}(\xi)} = \frac{1}{\bar{\lambda}^2}. \tag{61}$$

By setting $\lambda = \omega\bar{\lambda}$, the general solution of the above ODE is given by,

$$M(x,t) = \bar{m} L(t) e^{\frac{-x}{\lambda L(t)}} \tag{62}$$

which is precisely Eqn 4 in the main text. Note that the presence of a flat expander results in exactly the same scaled profile as the absence of the expander

Similarly, the right hand side of (60) results in the ODE,

$$\frac{\dot{L}}{L} = \frac{D_M \lambda^2}{2L^2} - \frac{\alpha_M}{2(1+E)}. \tag{63}$$

This, together with the effective expander evolution equation (57),

$$\dot{E} = \frac{P}{L}\beta_E - \alpha_E E - \frac{\dot{L}}{L}E., \tag{64}$$

together constitutes a coupled system whose solution determines the tissue length and the expander concentration in time.

3.5. **Explicit expression of the expander production domain.** In order to complete the system (57) and (63), we need to specify the expander expression domain $\mathcal{P}$. To this end, we use the explicit morphogen profile (62) and calculate $\mathcal{P}$ (8) directly below.

As M is monotonically decreasing in space, we have two possible cases:

- *Case 1:* For any given t, $M(0,t) < T_{rep}$. In this case, the morphogen has not accumulated enough to repress the expander anywhere through the tissue length. Hence,

$$\mathcal{P}(t) = [0, L(t)], \quad P(t) = L(t),$$

- *Case 2:* There exists a $x^* \in [0, L(t)]$ such that

$$\begin{aligned} M(x^*, t) &= T_{rep} \\ \Rightarrow \quad \bar{m} L(t) e^{\frac{-x^*}{\lambda L(t)}} &= T_{rep} \\ \Rightarrow \quad x^* = \lambda L \ln(L) - \lambda L \ln\left(\frac{T_{rep}}{\bar{m}}\right). & \end{aligned}$$

Therefore,

$$\mathcal{P}(t) = [x^*(t), L(t)], \quad P(t) = L - x^* = L - \lambda L \ln(L) + \lambda L \ln\left(\frac{T_{rep}}{\bar{m}}\right) \tag{65}$$

Hence, in this case,

$$\frac{P}{L} = 1 - \lambda \ln(L) + \lambda \ln\left(\frac{T_{rep}}{\bar{m}}\right). \tag{66}$$

We can make a further approximation in the case of relatively large tissues i.e if $L >> 1$, the $L\ln(L) \approx L$ and the length of the expander domain (65) simplifies as

$$P(t) = (1-\lambda)L + \lambda L \ln\left(\frac{T_{rep}}{\bar{m}}\right) \tag{67}$$

and

$$\frac{P(t)}{L(t)} = 1 - \lambda + \lambda \ln\left(\frac{T_{rep}}{\bar{m}}\right) = c^*. \tag{68}$$

Thus, in both cases (at least for relatively long tissues), the expander is expressed in a domain which is a constant fraction of the tissue length and grows linearly with the tissue length. Henceforth, we will assume that Case 2 holds as this is indeed true for the long time asymptotics of the system as in a biological relevant system, enough morphogen eventually accumulates to suppress the expander at least in some part of the tissue.

Hence, the effective equation for the evolution evolution is

$$\dot{E} = c^*\beta_E - \alpha_E E - \frac{\dot{L}}{L}E. \tag{69}$$

Combining (63) and (69), we derive the equations that govern the dynamics of coupled tissue length-expander concentration system.

We have not been able to obtain explicit solution formulas for (63) and (69), one can easily show that the right hand side of the ODE is Lipschitz continuous when $L > 0$. Hence, by the classical Cauchy-Lipschitz theorem, unique solutions of the ODE system exist for all time. Furthermore, extensive numerical simulations show that the ODE system converges (in a finite time) to the steady state of the form,

$$E^{st} = \frac{c^*\beta_E}{\alpha_E}, \qquad L^{st} = \frac{1}{\lambda}\sqrt{\frac{D}{\alpha}\left(1 + \frac{c^*\beta_E}{\alpha_E}\right)}. \tag{70}$$

Thus, we derive Eq. 8 in the main text. An example of a simulation of the ODE system (63) and (69) is shown in figure S9. The example clearly shows convergence to the predicted steady states in finite time.

Remark. The case of absence of expander can be easily recovered from the above analysis by setting $E \equiv 0$ in (5). We obtain the explicit solutions (30) for the flux boundary conditions. Note that ODE (63) is decoupled and can be readily solved.

3.6. **Point boundary conditions.** The above analysis for scaled solutions and flat expander profiles can also be carried analogously in the case where the absolute concentration of morphogen, rather than its flux, is fixed at the proximal boundary i.e,

$$M(0,t) \equiv M_0, \quad \forall t.$$

In this case, we can require for the morphogen profile to be scaled i.e, the morphogen concentration depends only on the relative cellular position $\xi = \frac{x}{L(t)}$ leading to

$$M(x,t) = M(\xi) = M\left(\frac{x}{L(t)}\right). \tag{71}$$

By carrying out the steps in the derivation, as in the case of flux boundary conditions, one can show that the scaled morphogen profile is of the form,

$$M(x,t) = M_0 e^{\frac{-x}{\lambda L(t)}}$$

Also, the tissue length and expander concentration are related by the ODE system,

$$\begin{aligned} \frac{\dot{L}}{L} &= \frac{D\omega^2}{L^2} - \frac{\alpha}{1+E}, \\ \dot{E} &= c^*\beta_E - \alpha_E E - \frac{\dot{L}}{L}E. \end{aligned} \tag{72}$$

3.7. **Derivation of consistent growth laws.** In the case of flux boundary conditions, we see from the morphogen evolution equation (58) that scaled solutions (11) satisfy,

$$\begin{aligned} \dot{M} &= M_t + uM_x, \\ \Rightarrow \frac{\dot{M}}{M} &= \frac{M_t}{M} + \frac{x\dot{L}}{L}\frac{M_x}{M}, \\ &= \frac{\dot{L}}{L} + \frac{x\dot{L}}{L^2} - \frac{x\dot{L}}{L^2}, \\ &= \frac{\dot{L}}{L} = \frac{\ln 2}{\tau} \end{aligned}$$

Thus, deriving Eq. 7 in the main text.

4. Numerical schemes

As stated in the main text, our aim is to systematically investigate the solutions of the coupled growth-patterning system Eqs, 1,2 (main text) with growth law Eq. 9 (main text) and to show that the resulting morphogen profile scales, the resulting tissue grows uniformly and attains a finite final size. We carry out this investigation over a very large range of the parameter space with extensive numerical simulations.

The numerical simulation of Eqs. 1,2,9 of main text is challenging on account of the fact that we are trying to approximate a nonlinear system of advection-reaction-diffusion equations on a growing domain and with nonlinear coupling between the growth law and the morphogen evolution. The main idea behind an efficient numerical simulation is to transform the morphogen and expander evolution equations in growing coordinates to the fixed coordinates.

4.1. **Governing equation in fixed coordinates.** For the numerical simulation of the system (5), we need to transform the morphogen evolution equation on a growing domain into a fixed coordinate system. We do so by transforming (5) to the fixed initial domain $[0, L_0]$ by using the coordinate transformation:

$$\overline{M}(Y,t) = M(x,t), \qquad \overline{E}(Y,t) = E(x,t). \tag{73}$$

Here the relation between the position $x = x(t)$ and the fixed coordinate Y is established through (1) i.e, $x(t)$ is the position at time t of the cell that was located at position Y at time $t = 0$.

Differentiating (1) with respect to Y, we obtain the flow equation,

$$\begin{aligned} \frac{d}{dt}x_Y &= u_Y, \\ x_Y(0) &= 1. \end{aligned} \tag{74}$$

Similarly differentiating (73) with respect to time on both sides, we obtain,

$$\begin{aligned} \overline{M}_Y Y_t + \overline{M}_t &= M_t + M_x x_t, \\ \Rightarrow \overline{M}_t &= M_t + uM_x. \end{aligned}$$

Note that in the above derivation, we use $Y_t \equiv 0$ (as the initial condition Y remains fixed in time) and also the flow type growth law (1). Similar computation results in

$$\overline{E}_t = E_t + uE_x.$$

Using the above relations, we transform the advection-diffusion-reaction morphogen and expander evolution equations (5) and (6) to fixed coordinates resulting in

$$\begin{aligned} \overline{M}_t &= \frac{D_M}{x_Y}\left(\frac{\overline{M}_Y}{x_Y}\right)_Y - \alpha(\overline{E})\overline{M} - \frac{u_Y}{x_Y}\overline{M}, \quad \forall (Y,t) \in [0,L_0]\times[0,T], \\ \overline{E}_t &= \frac{D_E}{x_Y}\left(\frac{\overline{E}_Y}{x_Y}\right)_Y - \alpha_E\overline{E} - \frac{u_Y}{x_Y}\overline{E} + \beta_E h(\overline{M}). \end{aligned} \tag{75}$$

The only input required to complete the evolution equations (75) and (74) is the *cell proliferation rate*: $\frac{u_Y}{x_Y}$ as,

$$\frac{d}{dt}x_Y = u_Y = \frac{u_Y}{x_Y}x_Y = \frac{\ln(2)}{\tau}x_Y \tag{76}$$

This establishes Eqs. 9 and 10 in the main text.

From the growth law Eq. 3 of the main text , the above expression reduces to,

$$\begin{aligned} \frac{1}{\tau} &= \frac{1}{\theta}\left(\frac{D_M}{x_Y\overline{M}}\left(\frac{\overline{M}_Y}{x_Y}\right)_Y - \alpha(E) - \frac{\ln(2)}{\tau}\right) \\ \Rightarrow\ (\theta+\ln(2))\frac{1}{\tau} &= \frac{D_M}{x_Y\overline{M}}\left(\frac{\overline{M}_Y}{x_Y}\right)_Y - \alpha(E), \\ \Rightarrow\ \frac{1}{\tau} &= \frac{1}{\theta+\ln(2)}\left(\frac{D}{x_Y\overline{M}}\left(\frac{\overline{M}_Y}{x_Y}\right)_Y - \alpha(E)\right), \end{aligned}$$

Thus, deriving Eq. 11 in the main text.

From (76), we define,

$$K = u_x = \frac{u_Y}{x_Y} = \frac{\ln(2)}{\ln(2)+\theta}\left(\left(\frac{D}{X_Y M}\left(\frac{\overline{M}_Y}{X_Y}\right)_Y - \alpha(E)\right)\right), \tag{77}$$

and obtain the accompanying growth law.

We numerically approximate the coupled system (75), (76) with growth law (77) with the following finite difference scheme: the fixed domain $[0, L_0]$

is discretized into $N+1$ equally spaced points $Y_j = j\Delta y$, with $\Delta y = L_0/N$ being the mesh size. The time interval of simulation $[0,T]$ is discretized with $\overline{N}$ intervals $t^n = n\Delta t$. The approximate solutions are denoted as

$$\overline{M}_j^n \approx \overline{M}(Y_j, t^n), \quad \overline{E}_j^n \approx \overline{E}(Y_j, t^n),$$

We use a standard (forward Euler) finite difference of the form,

$$\begin{aligned}
\overline{M}_j^{n+1} - \overline{M}_j^n &= \frac{2D\sigma}{(X_Y)_j^n}\left(\frac{\overline{M}_{j+1}^n - \overline{M}_j^n}{(X_Y)_j^n + (X_Y)_{j+1}^n}\right) \\
&\quad - \frac{2D\sigma}{(X_Y)_j^n}\left(\frac{\overline{M}_j^n - \overline{M}_{j-1}^n}{(X_Y)_j^n + (X_Y)_{j-1}^{n+1}}\right) \\
&\quad - \Delta t\alpha(\overline{E}_j^n)\overline{M}_j^n - \Delta t K_j^n \overline{M}_j^n, \\
\overline{E}_j^{n+1} - \overline{E}_j^n &= \frac{2D\sigma}{(X_Y)_j^n}\left(\frac{\overline{E}_{j+1}^n - \overline{E}_j^n}{(X_Y)_j^n + (X_Y)_{j+1}^n}\right) \\
&\quad - \frac{2D\sigma}{(X_Y)_j^n}\left(\frac{\overline{E}_j^n - \overline{E}_{j-1}^n}{(X_Y)_j^n + (X_Y)_{j-1}^{n+1}}\right) \\
&\quad - \Delta t\alpha_E \overline{E}_j^n - \Delta t K_j^n \overline{E}_j^n + \Delta t\beta_E h(\overline{M}_j^n),
\end{aligned} \tag{78}$$

with $\sigma = \frac{\Delta t}{(\Delta y)^2}$.

Furthermore, we use a backward Euler discretization of the ODE (74):

$$(X_Y)_j^{n+1} = \frac{(X_Y)_j^n}{(1 - \Delta t K_j^n)}, \tag{79}$$

with the growth law being set by,

$$\begin{aligned}
K_j^n &= \frac{\ln(2)}{\ln(2)+\theta}\left(\frac{2D_M\sigma}{(X_Y)_j^n\overline{M}_j^n}\left(\frac{\overline{M}_{j+1}^n - \overline{M}_j^n}{(X_Y)_j^n + (X_Y)_{j+1}^n}\right)\right) \\
&\quad - \frac{\ln(2)}{\ln(2)+\theta}\left(\frac{2D_M\sigma}{(X_Y)_j^n\overline{M}_j^n}\left(\frac{\overline{M}_{j+1}^n - \overline{M}_j^n}{(X_Y)_j^n + (X_Y)_{j+1}^n}\right)\right) \\
&\quad - \frac{\ln(2)\alpha(\overline{E}_j^n)}{\ln(2)+\theta}.
\end{aligned} \tag{80}$$

We implement point boundary conditions by fixing morphogen concentration at source:

$$\overline{M}(0,t) = M_0,$$

and flux boundary conditions by specifying the morphogen flux at the source:

$$\frac{D\overline{M}_Y}{X_Y}(0,t) = \eta.$$

The boundary conditions at the lateral boundary are set to be non-reflecting Neumann type boundary conditions:

$$\frac{D\overline{M}_Y}{X_Y}(L_0, t) = 0.$$

Similarly, we use zero-flux boundary conditions for the expander at both the proximal and distal boundaries:

$$\overline{E}_Y(0, t) = \overline{E}_Y(L_0, t) \equiv 0.$$

4.2. **Scaling and uniform growth scores.** In our simulations, we need to decide whether a system has a scaled morphogen gradient or not. For any given time t, we fit an exponential of the form (18) to the computed morphogen profile. Then, we calculate the time t_{ss} at which growth has reached steady state. The steady state for growth is reached when

$$100\frac{L_{t+\Delta t} - L_t}{L_t} < 0.001, \tag{81}$$

i.e, steady state is reached when the relative increase in L between consecutive time points is below 0.001%.

The time t_λ of the onset of scaling is reached when

$$100\frac{\lambda_{t+\Delta t} - \lambda_t}{\lambda_t} < 0.006. \tag{82}$$

In other words, scaling is attainted once the relative increase in λ between consecutive time points is below 0.006%. The tissue is declared to be scaled if the morphogen gradient scales to the growing tissue for at least 50% of the duration of growth:

$$\frac{t_{ss} - t_\lambda}{t_{ss}} > 0.5 \tag{83}$$

In order to decide whether the system grows uniformly or not, we adopt the following criteria. At any given time, we track the proportion that lineage of the first 10% and third 20% of cells occupy in the growing tissue. As in the case of specifying the scaling score, a tissue is considered to grow uniformly, if for at least 50% of the time before t_{ss} the relative increase in the part of the tissue of the first 10% or the third 20% between consecutive time points is below 6.5%

The fine tuning of the numerical thresholds mentioned above was done empirically by observing simulations. Observe that both the scaling criteria and uniform growth criteria take into account the fact that there is an initial phase of development during which the morphogen may not scale and the tissue may not grow uniformly. We remark that the scaling score and the uniform growth score have been used in generating table 1 in the main text (results).

4.3. **Scaling error.** The scaling error is a dimensionless parameter describing the change in the sharpness of the gradient in relative coordinates (λ_{rel}), relative to the growth of the tissue. Since this is a dimensionless quantity which is ideally zero, excellent scaling is achieved when $\left|\frac{\partial\lambda}{L}\right| \ll 1$. Scaling is reasonable when $\left|\frac{\partial\lambda}{L}\right| \approx 1$.

In order to compare scaling quality as a function of proliferation rate (q) between simulations with decreasing q and simulations with constant q, we have used this scaling error. In the constant q case, the scaling error converges during a simulation to a certain value and remains stable until a very large size is reached (for constant q tissue length increases exponentially). Then, the morphogen level is almost zero everywhere except the proximal end rendering the simulation biologically invalid. This behavior was observed in numerous simulations. Therefore, in the constant q case the scaling error is taken as this stable value.

4.4. **Simulation scenarios and parameter values.**

4.4.1. *Figure 2.* We simulated a tissue with a morphogen dependent growth law and ExR with following parameters consistent with experimental measurements for the wing disc:

$D_M[\mu m^2 sec^{-1}]$	400
$\alpha_M[h^{-1}]$	10
$\eta[a.u.]$	100
$D_E[\mu m^2 sec^{-1}]$	400
$\alpha_E[h^{-1}]$	0.05
$\beta_E[a.u.]$	10
$T_{Expander}[a.u.]$	0.01
θ	0.5
$L_0[\mu m]$	10

4.4.2. *Figure 3.* A tissue with a morphogen dependent growth law, no ExR:

$D_M[\mu m^2 sec^{-1}]$	100
$\alpha_M[h^{-1}]$	0.1
$\eta[a.u.]$	10
θ	0.5
$L_0[\mu m]$	10

4.4.3. *Figure 4.* Sensitivity $S_X(p)$ of a quantity X to a parameter p is defined as the average over p of $\frac{p}{X}\left|\frac{\partial X}{\partial p}\right|$.

In plot (a) we tested the Sensitivity ratio of the final tissue size and the gradient length scale (in relative coordinates), $log_2 \frac{S(p) with\, ExR}{S(p) No\, ExR}$, to various model parameters. For this test we used a basic parameter set:

$D_M[\mu m^2 sec^{-1}]$	10
$\alpha_M[h^{-1}]$	0.1
$\eta[a.u.]$	1
$D_E[\mu m^2 sec^{-1}]$	100
$\alpha_E[h^{-1}]$	10^{-2}
$\beta_E[a.u.]$	0.25
$T_{Expander}[a.u.]$	0.01
θ	1
$L_0[\mu m]$	10

In order to calculate each $S_X(p)$ for every p_0 we simulated this parameter set 10 times when only the value of p_0 varies between simulations. We then calculated $S_X(p_0)$ for $X = L_f$ and $X = \lambda$ (relative coordinates), using the formula

$$S_X(p_0) = mean_{p_0}\left(\frac{p_o}{X}\left|\frac{\partial X}{\partial p_0}\right|\right)$$

, averaging over the 10 runs. We did this twice for each $S_X(p_0)$ - once with ExR and once without. We then calculated for each P and X,

$$log_2 \frac{S(p) with\, ExR}{S(p) No\, ExR}$$

, which is the quantity plotted in the figure 4a. The value ranges used for each p was,

$D_M[\mu m^2 sec^{-1}] \in$	[1,100]
$\alpha_M[h^{-1}] \in$	[0.01,1]
$\eta[a.u.] \in$	[0.1,10]
$D_E[\mu m^2 sec^{-1}]$	100
$\alpha_E[h^{-1}]$	10^{-2}
$\beta_E[a.u.]$	0.25 or 0
$T_{Expander}[a.u.]$	0.01
$\theta \in$	[0.4,2]
$L_0[\mu m] \in$	[5,50]

In plots 4b and 4c, the basic parameter set is the one used in 4a. In 4b and 4c, we varied the values of α_E and β_E. For each combination (α_E, β_E) we compared the result (L_f in 4b and relative λ in 4c) with ExR to the result without ExR. The range of values of α_E and β_E used can be seen in figures 4b and 4c.

4.4.4. *Table 1.* Valid runs are runs in which the tissue grew at least 2 fold. Only valid runs were taken into account for percentages of scaling and uniform growth. The parameter ranges are shown below. In both table 1a and 1b all possible parameter combinations were simulated.

Table 1a:

$D_M[\mu m^2 sec^{-1}]$	10,100
$\alpha_M[h^{-1}]$	1,10
$\eta[a.u.]$	1,10,100
$D_E[\mu m^2 sec^{-1}]$	10,100
$\alpha_E[h^{-1}]$	$10^{-2}, 10^{-3}, 10^{-5}$
$\beta_E[a.u.]$	0.1,1,10
$T_{Expander}[a.u.]$	0.01
θ	0.5
$L_0[\mu m]$	10,40
# runs	864
# valid runs	663

Table 1b:

$D_M[\mu m^2 sec^{-1}]$	1,10,50,100,150
$\alpha_M[h^{-1}]$	0.1,0.5,1,5,10
$\eta[a.u.]$	0.1,1,10,70,100
θ	0.5,0.8,1.2
$L_0[\mu m]$	5,10,20
# runs	3375
# valid runs	2010

4.4.5. *Table 2.* See figure 4a

4.4.6. *Figure S1.* The following parameter set was simulated for several values of the proliferation rate q:

$D_M[\mu m^2 sec^{-1}]$	100
$\alpha_M[h^{-1}]$	100
$\eta[a.u.]$	100
$D_E[\mu m^2 sec^{-1}]$	100
$\alpha_E[h^{-1}]$	10^{-3}
$\beta_E[a.u.]$	10
$T_{Expander}[a.u.]$	0.1
$q \in$	[0.001,1]
$L_0[\mu m]$	10

4.4.7. *Figure S2.* Morphogen dependent growth law and ExR: same parameters as figure S1, with $\theta = 1.2$. ExR alone: same parameters as figure S1

4.4.8. *Figure S3.* We simulated the following parameter set (morphogen dependent growth law with ExR) varying for each run D_M and α_M:

$D_M[\mu m^2 sec^{-1}] \in$	[1,100]
$\alpha_M[h^{-1}] \in$	[0.01,1]
$\eta[a.u.]$	1
$D_E[\mu m^2 sec^{-1}]$	100
$\alpha_E[h^{-1}]$	10^{-2}
$\beta_E[a.u.]$	0.25
$T_{Expander}[a.u.]$	0.01
θ	1
$L_0[\mu m]$	10

20 different values for D_M and 20 different values for α_M were chosen and all possible (D_M, α_M) combinations were simulated. The total number of simulations used for this plot is 400, the values of (D_M, α_M) chosen were logarithmically spaced 20 element vectors in the above specified ranges.

4.4.9. *Figure S4-S5.* See figure 4a.

4.4.10. *Figure S6.* Similarly to figures S4, S5 the same basic parameter set was used. Here, $S_X(p)$ are plotted when X are ExR only parameters. For every X, 10 equally spaced values were simulated. The values used were

$D_M[\mu m^2 sec^{-1}]$	10
$\alpha_M[h^{-1}]$	0.1
$\eta[a.u.]$	1
$D_E[\mu m^2 sec^{-1}] \in$	[10,1000]
$\alpha_E[h^{-1}] \in$	$[0.002, 0.2]$
$\beta_E[a.u.] \in$	[0.025,2.5]
$T_{Expander}[a.u.] \in$	[0.004,0.4]
θ	0.5
$L_0[\mu m]$	10

4.4.11. *Figure S7.* **Plots a-d:**

$D_M[\mu m^2 sec^{-1}]$	100
$\alpha_M[h^{-1}]$	1
$\eta[a.u.]$	1
θ	1
$L_0[\mu m]$	10

Plots e-h:

$D_M[\mu m^2 sec^{-1}]$	100
$\alpha_M[h^{-1}]$	1
$\eta[a.u.]$	1
$D_E[\mu m^2 sec^{-1}]$	100
$\alpha_E[h^{-1}]$	10^{-2}
$\beta_E[a.u.]$	1
$T_{Expander}[a.u.]$	0.01
θ	1
$L_0[\mu m]$	10

Plot i:

$D_M[\mu m^2 sec^{-1}]$	10
$\alpha_M[h^{-1}]$	1
$\eta[a.u.]$	1
$D_E[\mu m^2 sec^{-1}]$	100
$\alpha_E[h^{-1}]$	10^{-2}
$\beta_E[a.u.]$	1
$T_{Expander}[a.u.]$	0.01
q	0.1
$L_0[\mu m]$	10

4.4.12. *Figure S10.* **Plots a-c:** (**Right compartment**)

$D_M[\mu m^2 sec^{-1}]$	400
$\alpha_M[h^{-1}]$	10
$\eta[a.u.]$	100
$D_E[\mu m^2 sec^{-1}]$	400
$\alpha_E[h^{-1}]$	0.05
$\beta_E[a.u.]$	10
$T_{Expander}[a.u.]$	0.01
θ	0.5
$L_0[\mu m]$	10

Plots a-c: (**Left compartment**)

$D_M[\mu m^2 sec^{-1}]$	400
$\alpha_M[h^{-1}]$	10
$\eta[a.u.]$	100
$D_E[\mu m^2 sec^{-1}]$	400
$\alpha_E[h^{-1}]$	0.05
$\beta_E[a.u.]$	0
$T_{Expander}[a.u.]$	0.01
θ	0.5
$L_0[\mu m]$	10

Plots d-f: (**Right compartment**)

$D_M[\mu m^2 sec^{-1}]$	400
$\alpha_M[h^{-1}]$	10
$\eta[a.u.]$	100
$D_E[\mu m^2 sec^{-1}]$	400
$\alpha_E[h^{-1}]$	0.05
$\beta_E[a.u.]$	10
$T_{Expander}[a.u.]$	0.01
θ	0.5
$L_0[\mu m]$	10

Plots d-f: (**Left compartment**)

$D_M[\mu m^2 sec^{-1}]$	400
$\alpha_M[h^{-1}]$	10
$\eta[a.u.]$	100
$D_E[\mu m^2 sec^{-1}]$	400
$\alpha_E[h^{-1}]$	0.05
$\beta_E[a.u.]$	0
$T_{Expander}[a.u.]$	0.01
θ	0.8
$L_0[\mu m]$	10

Plots g-i: (**Right compartment**)

$D_M[\mu m^2 sec^{-1}]$	400
$\alpha_M[h^{-1}]$	10
$\eta[a.u.]$	100
$D_E[\mu m^2 sec^{-1}]$	400
$\alpha_E[h^{-1}]$	0.05
$\beta_E[a.u.]$	10
$T_{Expander}[a.u.]$	0.01
θ	0.5
$L_0[\mu m]$	10

Plots g-i: (**Left compartment**)

$D_M[\mu m^2 sec^{-1}]$	400
$\alpha_M[h^{-1}]$	10
$\eta[a.u.]$	100
$D_E[\mu m^2 sec^{-1}]$	400
$\alpha_E[h^{-1}]$	0.05
$\beta_E[a.u.]$	0
$T_{Expander}[a.u.]$	0.01
θ	0.8
$L_0[\mu m]$	10

4.5. **Figures S11,S12. 1.** The morphogen flux is taken to be increasing in time ,i.e,

$$\eta(t) := 0.1\eta_0 L(t).$$

Figures S11 a,b: (**MDDR + ExR:**)

$D_M[\mu m^2 sec^{-1}]$	100
$\alpha_M[h^{-1}]$	10
$\eta_0[a.u.]$	10
$D_E[\mu m^2 sec^{-1}]$	100
$\alpha_E[h^{-1}]$	0.01
$\beta_E[a.u.]$	10
$T_{Expander}[a.u.]$	0.01
θ	0.5
$L_0[\mu m]$	10

Figures S12 a,b: (**MDDR alone:**)

$D_M[\mu m^2 sec^{-1}]$	100
$\alpha_M[h^{-1}]$	0.1
$\eta_0[a.u.]$	10
θ	0.5
$L_0[\mu m]$	10

2. Absorbing boundary conditions for the morphogen M on the edge distant from the morphogen source (distal boundary):
Figure S11 c,d (MDDR + ExR)

$D_M[\mu m^2 sec^{-1}]$	100
$\alpha_M[h^{-1}]$	1
$\eta[a.u.]$	1
$D_E[\mu m^2 sec^{-1}]$	10
$\alpha_E[h^{-1}]$	0.01
$\beta_E[a.u.]$	10
$T_{Expander}[a.u.]$	0.01
θ	0.5
$L_0[\mu m]$	10

Figures S12 c,d: (**MDDR alone:**)

$D_M[\mu m^2 sec^{-1}]$	100
$\alpha_M[h^{-1}]$	0.1
$\eta[a.u.]$	10
θ	0.5
$L_0[\mu m]$	10

3. Nonlinear degradation of M with degradation term,

$$\alpha(M) := -\alpha(E)M - nl(E)M^2, \qquad nl(E) := (nl)_M(1+E)^{p1}.$$

Figure S11 e,f (MDDR + ExR)

$D_M[\mu m^2 sec^{-1}]$	100
$\alpha_M[h^{-1}]$	0
$(nl)_M$	1
$\eta[a.u.]$	1
$D_E[\mu m^2 sec^{-1}]$	10
$\alpha_E[h^{-1}]$	0.05
$\beta_E[a.u.]$	10
$T_{Expander}[a.u.]$	0.01
θ	0.5
$L_0[\mu m]$	10

Figures S12 e,f: (**MDDR alone:**)

$D_M[\mu m^2 sec^{-1}]$	100
$\alpha_M[h^{-1}]$	0
$(nl)_M$	1
$\eta[a.u.]$	10
θ	0.5
$L_0[\mu m]$	10

4: Nonlinear degradation of E with $(nl)_E$, being the coefficient of quadratic degradation:

$$\alpha(E) := -\alpha_E E - nl_E E^2.$$

Figure S11 g,h (MDDR + ExR)

$D_M[\mu m^2 sec^{-1}]$	100
$\alpha_M[h^{-1}]$	1
$\eta[a.u.]$	10
$D_E[\mu m^2 sec^{-1}]$	100
$\alpha_E[h^{-1}]$	0
$(nl)_E$	0.01
$\beta_E[a.u.]$	10
$T_{Expander}[a.u.]$	0.01
θ	0.5
$L_0[\mu m]$	10

5. Different $h(M)$ and $\alpha(E)$. As in the previous two tables,

$$h(M) := \frac{1}{1+\left(\frac{M}{T_{rep}}\right)^{hl}}, \qquad \alpha(E) := \alpha_E(1+E)^{p1}.$$

Table S11 i,j: (MDDR + ExR)

$D_M[\mu m^2 sec^{-1}]$	10
$\alpha_M[h^{-1}]$	1
$\eta[a.u.]$	1
$D_E[\mu m^2 sec^{-1}]$	10
$\alpha_E[h^{-1}]$	0.05
$\beta_E[a.u.]$	10
$T_{Expander}[a.u.]$	0.01
θ	0.5
$L_0[\mu m]$	10
hl	1
$p1$	-2

4.6. **Table S1.** In this table, valid runs are those runs where the tissue grew two fold. Only valid runs were taken into account for calculating percentages for scaling and uniform growth. The parameter ranges are shown below. In all the tables below, all possible parameter combinations were simulated.

4.6.1. *Case. 1:* The morphogen flux is taken to be increasing in time ,i.e,

$$\eta(t) := 0.1\eta_0 L(t).$$

Table S1a: (MDDR + ExR)

$D_M[\mu m^2 sec^{-1}]$	10,100
$\alpha_M[h^{-1}]$	1,10
$\eta_0[a.u.]$	1,10,
$D_E[\mu m^2 sec^{-1}]$	10,100
$\alpha_E[h^{-1}]$	$0.05, 0.01$
$\beta_E[a.u.]$	1,10
$T_{Expander}[a.u.]$	0.01
θ	0.5
$L_0[\mu m]$	10
# runs	64
# valid runs	63

Table S1b: (MDDR alone)

$D_M[\mu m^2 sec^{-1}]$	10,100
$\alpha_M[h^{-1}]$	1,10
$\eta[a.u.]$	1,10
θ	0.5,0.8
$L_0[\mu m]$	10,20
# runs	32
# valid runs	8

4.6.2. *Case 2:* Absorbing boundary conditions for the morphogen M on the edge distant from the morphogen source (distal boundary): **Table S1c: (MDDR + ExR)**

$D_M[\mu m^2 sec^{-1}]$	10,100
$\alpha_M[h^{-1}]$	1,10
$\eta[a.u.]$	1,10
$D_E[\mu m^2 sec^{-1}]$	10,100
$\alpha_E[h^{-1}]$	$0.05, 0.01$
$\beta_E[a.u.]$	1,10
$T_{Expander}[a.u.]$	0.01
θ	0.5
$L_0[\mu m]$	10
# runs	64
# valid runs	38

Table S1d: (MDDR alone)

$D_M[\mu m^2 sec^{-1}]$	10,100
$\alpha_M[h^{-1}]$	1,10
$\eta[a.u.]$	1, 10
θ	0.5,0.8
$L_0[\mu m]$	10,20
# runs	32
# valid runs	6

4.6.3. *Case 3:* Nonlinear degradation of M with degradation term,

$$\alpha(M) := -\alpha(E)M - nl(E)M^2, \qquad nl(E) := (nl)_M(1+E)^{p1}.$$

Table S1e: (MDDR + ExR)

$D_M[\mu m^2 sec^{-1}]$	10,100
$\alpha_M[h^{-1}]$	1,10
$(nl)_M$	1, 10
$\eta[a.u.]$	1,10
$D_E[\mu m^2 sec^{-1}]$	10,100
$\alpha_E[h^{-1}]$	0.05
$\beta_E[a.u.]$	10
$T_{Expander}[a.u.]$	0.01
θ	0.5
$L_0[\mu m]$	10
# runs	48
# valid runs	48

Table S1f: (MDDR alone)

$D_M[\mu m^2 sec^{-1}]$	10,100
$\alpha_M[h^{-1}]$	1,10
$\eta[a.u.]$	1, 10
$(nl)_M$	1, 10
θ	0.5,0.8
$L_0[\mu m]$	10,20
# runs	48
# valid runs	32

4.6.4. *Case 4:* Nonlinear degradation of E with $(nl)_E$, being the coefficient of quadratic degradation:

$$\alpha(E) := -\alpha_E E - nl_E E^2.$$

Table S1g: (MDDR + ExR)

$D_M[\mu m^2 sec^{-1}]$	10,100
$\alpha_M[h^{-1}]$	1,10
$\eta[a.u.]$	1,10
$D_E[\mu m^2 sec^{-1}]$	10,100
$\alpha_E[h^{-1}]$	$0, 0.05$
$(nl)_E$	$0.01, 0.05$
$\beta_E[a.u.]$	10
$T_{Expander}[a.u.]$	0.01
θ	0.5
$L_0[\mu m]$	10
# runs	64
# valid runs	50

4.6.5. *Case 5:* Different $h(M)$ and $\alpha(E)$. As in the previous two tables,

$$h(M) := \frac{1}{1 + \left(\frac{M}{T_{rep}}\right)^{hl}}, \qquad \alpha(E) := \alpha_E (1+E)^{p1}.$$

In the previous two tables, we set $hl = 4,\ p1 = -1$. In the following table, we vary these coefficients in order to test different functional forms of these functions.

Table S1h: (MDDR + ExR)

$D_M[\mu m^2 sec^{-1}]$	10,100
$\alpha_M[h^{-1}]$	1,10
$\eta[a.u.]$	1,10
$D_E[\mu m^2 sec^{-1}]$	10,100
$\alpha_E[h^{-1}]$	0.05
$(nl)_E$	$0.01, 0.05$
$\beta_E[a.u.]$	10
$T_{Expander}[a.u.]$	0.01
θ	0.5
$L_0[\mu m]$	10
hl	1,2
$p1$	-2,-5
# runs	64
# valid runs	63

4.7. **Final tissue length prediction.**

4.7.1. *Without ExR.* The predicted final size in this case is given by formula (30):

$$L_f^{Predicted} = \frac{1}{\lambda}\sqrt{\frac{D_M}{\alpha_M}}.$$

In order to calculate this value for a certain parameter set, we ran the simulation until final size was reached and then took the relative gradient length scale achieved as λ for the calculation. We then compared the final length the tissue reached in the simulation, L_f, to the prediction by calculating the ratio: $\frac{L_f}{L_f^{Predicted}}$. We calculated this ratio for all valid parameter sets used for table 1b (2010 sets) and by averaging over all 2010 sets obtained the following result:

$$\frac{L_f}{L_f^{Predicted}} = 1.15 \pm 0.06$$

.

4.7.2. *With ExR.* In this case, the final sizes are predicted by (70) to be

$$L_f^{Predicted} = \frac{1}{\lambda}\sqrt{\frac{D_M}{\alpha_M}\left(1 + c^*\frac{\beta_E}{\alpha_E}\right)}$$

with

$$c^* = E^{st}\frac{\alpha_E}{\beta_E},$$

resulting in

$$L_f^{Predicted} = \frac{1}{\lambda}\sqrt{\frac{D_M}{\alpha_M}(1 + E^{st})}.$$

This prediction is valid in cases of flat expander profile. In order to test this prediction we took 72 parameter sets which had flat expander profile and ran each simulation until final size was reached. We took the relative gradient length scale achieved as λ for the calculation and the spatial average of expander level achieved as E^{st}. We then compared the final length the tissue reached in the simulation, L_f, to the prediction by calculating the ratio: $\frac{L_f}{L_f^{Predicted}}$. We calculated this ratio for all parameter sets and by averaging over all sets obtained the following result:

$$\frac{L_f}{L_f^{Predicted}} = 1.3 \pm 0.03.$$

The parameter sets tested are all possible combinations of the following values:

$D_M[\mu m^2 sec^{-1}]$	80,100,150
$\alpha_M[h^{-1}]$	5,10,20
$\eta[a.u.]$	1
$D_E[\mu m^2 sec^{-1}]$	10,100
$\alpha_E[h^{-1}]$	0.008,0.01
$\beta_E[a.u.]$	1,2
$T_{Expander}[a.u.]$	0.01
θ	0.5
$L_0[\mu m]$	10
# runs	72
# valid runs	72

4.8. **The role of advection and dilution in MDDR dynamics.** In the absence of the expander, the morphogen evolution equation (5) consists of four different terms,

- Morphogen diffusion, modeled by $D_M M_{xx}$.
- Morphogen degradation, modeled by $\alpha_M M$.
- Advection, modeled by uM_x, for flow rate u and
- Dilution on account of growth, modeled by $u_x M$.

In order to compare the relative contributions of each of the above terms (and the underlying physical effects) to the global dynamics, we calculate the amplitudes (as a function of the tissue domain) of each term and plot these amplitude at different time snapshots in SI Figure 13. The amplitudes are calculated from the morphogen concentration M and flow rate u using simple finite differences. The parameter set used to generate SI Figure 13 is exactly the same as the parameter set used to generate Figure 3, i.e, Table 4.4.2.

From SI figure 13, it is clear that initially and for a short period of time (about T=5), the advection and dilution terms are indeed comparable to the morphogen degradation. However, after this short initial transient, the growth rate slows and the advection and dilution terms rapidly decay in amplitude as compared to the morphogen degradation. As shown in Figure 3, the morphogen gradient continues to scale with tissue size and the tissue continues to grow. In fact, the tissue grows about two to three fold during this time window. In this case, the initially comparable dilution and advection were enough to yield scaling and uniform growth, through the MDDR mechanism.

To further test the role of advection and dilution in the global dynamics, we performed the following simulations:

4.8.1. *SI Figure 14.* First, we simulated tissues that do not grow. In such tissues, the morphogen is secreted at the source and diffuses through the length of the tissue, while being subject to degradation. To do so, we set the flow rate $u \equiv 0$ in the morphogen evolution equation (5) and use the

following parameters:

$D_M[\mu m^2 sec^{-1}]$	10
$\alpha_M[h^{-1}]$	0.1
$\eta[a.u.]$	1
$L_0[\mu m]$	10, 20, 40

The results are shown in SI Figure 14 (a,b,c,d). In SI Figure 14 (a,b), we consider the spread of morphogen (via diffusion) for three different tissue lengths. The corresponding steady state morphogen concentration in both absolute and relative coordinates is plotted. As seen from SI Figure 14 (b), the morphogen gradient does not scale as the normalized morphogen concentration depends on the absolute position in the tissue. Thus, pure diffusion and degradation are not enough to provide scaling.

In SI figure 14 (c,d), we plot the temporal dynamics of a non-growing tissue of tissue length $L = 20$. The other parameters are the same as in the previous table. As seen from SI Figure 14 (c,d), the morphogen gradient diffuses into the tissue and reaches a steady state when the diffusion balances the degradation. But as expected (see [2]), the gradient does not scale in any sense as the concentration depends on the absolute position.

In contrast to this case, we consider the situation of a tissue that grows with the MDDR mechanism. The corresponding parameters are reported in the following table:

$D_M[\mu m^2 sec^{-1}]$	10
$\alpha_M[h^{-1}]$	0.1
$\eta[a.u.]$	1
θ	1
$L_0[\mu m]$	10, 20, 40

The parameters for diffusion, degradation, initial tissue length and morphogen flux are exactly the same as in previous of non-growing tissue. The results for this simulation are plotted in SI Figure 14 (e,f). As seen before in Figure 3, the morphogen gradient scales with the growing tissue in this case (see SI Figure 14 f). Thus, the role of advection and dilution is essential in producing scaling of the morphogen gradient through the MDDR growth mechanism.

This role can be further explained with the following observation. Once the tissue grows, advection and dilution are inevitable consequences of growth. These terms will be small for most of the dynamics as growth rate is exponentially decaying (see SI figure 13 and also the analytical formula (30)) but they will not be negligible initially. We start from zero (or constant) morphogen initial condition and have morphogen flux coming into the tissue. As our growth law calculates the temporal relative change in concentration, the growth rate has to be high and non-negligible in comparison to degradation

initially (as morphogen starts coming in). Growth rate then decreases, as we observe analytically and in all the simulations.

Again from the simulations, we observe that the dynamics starts with an initial (very short) transient phase that is due to the growth law being based on relative change. During this transient, the morphogen gradient is formed and it is not yet scaled. The scaling happens once this transient is over and the gradient can be described in terms of the formula (30) for some final tissue length L_f and gradient decay length λ. Then, the tissue continues growing and the gradient continues to scale until steady state is reached at a time scale of $\frac{1}{\alpha_M}$. During this rather long phase, advection and dilution terms are negligible in comparison to degradation (see SI figure 13). The contribution of advection and dilution is to determine the scaled form the gradient that will take on at steady state i.e, determining the morphogen decay length λ in (30).

4.8.2. *SI figure 15.* To further emphasize the role of the dilution and advection, we simulated a system which grows according to MDDR, but without a dilution term in the morphogen evolution equation, on multiple parameter sets and compared the results with the same system with a dilution term. The results are presented in SI figure 15 which is generated with the following parameters:
For SI figure 15, a-h, we use,

$D_M[\mu m^2 sec^{-1}]$	100
$\alpha_M[h^{-1}]$	0.1
$\eta[a.u.]$	10
θ	0.5
$L_0[\mu m]$	10

For SI figure 15, i-p, we use,

$D_M[\mu m^2 sec^{-1}]$	100
$\alpha_M[h^{-1}]$	0.1
$\eta[a.u.]$	1
θ	0.5
$L_0[\mu m]$	10

For SI figure 15, q-x, we use,

$D_M[\mu m^2 sec^{-1}]$	100
$\alpha_M[h^{-1}]$	0.1
$\eta[a.u.]$	1
θ	1.2
$L_0[\mu m]$	10

The results of this study (eliminating dilution in the morphogen evolution) can be divided into these 4 cases:

- Discarding the dilution term results in: larger final size, yet poorer scaling and lack of uniform growth.

- Discarding the dilution term results in: smaller final size, yet reasonably good scaling but without uniform growth.
- Discarding the dilution term results in: smaller final size, non-uniform growth and bad scaling.
- Discarding the dilution term results in a non-biological morphogen profile (too shallow) or non-biological growth (step function like growth)

As we predicted, in all simulations removing the dilution term resulted in different λ'. Scaling was still retained in most cases while uniform growth was more sensitive to the removal of dilution. At times, the profiles obtained were non biological: too shallow due to not enough morphogen degradation in the absence of dilution or step like growth. These results are consistent with our understanding of the role of dilution and advection as described above. Since the advection term is always smaller or similar in amplitude to dilution, we expect similar results when eliminating it from the morphogen equation.

Summarizing the above discussion, we would like to point out that advection and dilution play an essential role in the MDDR mechanism, particularly for the initial period of growth. In the absence of these terms or when the terms are negligible compared to degradation for the whole growth period, MDDR may not suffice for scaling and additional mechanisms, such as expansion-repression, might be needed. Moreover, advection and dilution decay rapidly in amplitude with time and are negligible compared to degradation (SI Figure 13) for most of the growth window. Hence, our simulation results are consistent with experimental findings of slow growth (with negligible advection and dilution) in the third instar.

References

[1] L. D. Landau and E. M. Lipschitz. Fluid Mechanics, 2nd edition, *Butterworth Heinemann,* 1987, 532 pp.

[2] D. Ben-Zvi., and N. Barkai, Scaling of morphogen gradients by an expansion-repression integral feedback control. *Proc Natl Acad Sci U S A* 2010, 107, 6924-6929.

Figure S1. ExR improves scaling and becomes more effective as growth rate q decreases.

In plots (a)-(i) Morphogen or expander level as a function of position in the tissue is shown for 10 evenly spaced time points throughout the dynamics, from earliest time point in blue to latest time point in red. In all plots the same parameter set is simulated for various values of the growth rate q, with and without ExR.

(a,d,g): Morphogen relative level (normalized to the level at the source) as a function of relative position (x/L) in the tissue at various times **without ExR:** For q=1 [1/h] in plot (a), for q=0.1 [1/h] in plot (d) and for q=0.001 [1/h] in plot (g).

(b,e,h): Morphogen relative level (normalized to the level at the source) as a function of relative position (x/L) in the tissue at various times **with ExR:** For q=1 [1/h] in plot (b), for q=0.1 [1/h] in plot (e) and for q=0.001 [1/h] in plot (h).

(c,f,i): Expander level as a function of position in the tissue at various times: for q=1 [1/h] in plot (c), for q=0.1 [1/h] in plot (f) and for q=0.001 [1/h] in plot (i).

(j) Scaling error defined as: $\left|\frac{\partial\lambda}{\partial L}L\right|$ as a function of q, with ExR. With constant q, the scaling error in the simulation converges to a constant after a certain time T, that constant is shown in the plot.

Figure S2. With MDDR and ExR scaling is achieved even for rapid growth rates.

Scaling error defined as $\left|\frac{\partial\lambda}{\partial L}L\right|$ as a function of growth rate $q=\frac{\dot{L}}{L}$ for a particular parameter set. In the blue solid line for MDDR and ExR feedback and in the black dashed line for the same parameter set only with a constant q growth function and ExR feedback. With constant q, the scaling error in the simulation converges to a constant after a certain time T, that constant is shown in the plot.

Figure S3. The effect of ExR on tissue growth and duration of growth.

a) The effect of ExR on fold change in tissue length:$\log_2\frac{(L_f/L_0)_{with\ ExR}}{(L_f/L_0)_{NO\ ExR}}$ for various $\lambda_M=\sqrt{\frac{D_M}{\alpha_M}}$ and α_M. Final size is increased by ExR for a large variety of parameter sets. This increase depends on $\lambda_M=\sqrt{\frac{D_M}{\alpha_M}}$ which is the length scale of the morphogen.

b) The effect of ExR on growth duration: $\log_2\frac{(t_{ss})_{\text{with ExR}}}{(t_{ss})_{\text{NO ExR}}}$ for various $\lambda_M=\sqrt{\frac{D_M}{\alpha_M}}$ and α_M. ExR significantly prolongs dynamics which allows for further growth and a larger final size. The expander's effect mainly depends on α_M, which is the quantity modulated by the expander.

Figure S4. Sensitivity of fold change in size to model parameters, with vs. without ExR.

Dependence of fold change of the final tissue size compared with initial tissue size on the morphogen diffusion coefficient (a,f), morphogen degradation rate (b,g), morphogen flux (c,h), growth parameter (d,i) and initial size (e,i). (a-e) describe a system with a morphogen dependent growth law and an expander, (f-j) describe the same system without an expander. Sensitivity, S, of final size L_f to a parameter p was determined by simulating the parameter set with different values of p and calculating the average over 10 values p of $\frac{p}{L_f}\left|\frac{\partial L_f}{\partial p}\right|$.

Figure S5. Sensitivity of morphogen gradient length scale to model parameters, with vs. without ExR.

The gradient scales, and is well described by an exponential with a length scale of λ in the relative coordinates. Sensitivity of λ to a parameter p was determined by simulating the wild type parameter set with different values of p and calculating the average over 10 values p of $\frac{p}{\lambda}\left|\frac{\partial\lambda}{\partial p}\right|$. (a-e) describe a system with a morphogen dependent growth law and an expander, (f-j) describe the same system without an expander.

Figure S6. Sensitivity of fold change in size and morphogen gradient length scale to ExR parameters.

Sensitivity S (defined as in figure S4,S5) of final tissue size relative to initial size (a-d) and the morphogen gradient relative length scale (e-h) to variations of expander parameters: expander diffusion coefficient (a,e), expander degradation rate (b,f), expander production rate (c,g), morphogen threshold concentration above which expander production is repressed (d,h).

Figure S7. For parameter sets which did not scale under the $\alpha_M \gg q$ regime, adding ExR improves scaling and uniform growth.

a-d morphogen dependent growth only.

a) growth rate q and morphogen degradation rate α_M as a function of time; b) the tissue grows less, and growth takes less time; c) the gradient fails to scale, x-axis in relative coordinates; d) scaling error remains high throughout the growth.

(e-h) Adding ExR to the system with the same parameters affects the dynamics dramatically.

e) Growth rate q and morphogen degradation rate α_M as a function of time. Note that α_M decreases as a result of expander activity; f) growth is longer and the tissue grows extensively;

g) The tissue shows very good scaling, x-axis in relative coordinates; h) scaling error is very low in most of the dynamics.

i) The same system with ExR only and spatially uniform external growth with q=0.01. The simulation was run until the tissue grew 2 fold, ExR alone resulted in poor scaling.

Figure S8. Simulation of Eq.7 (SI) with a noisy θ.

a) Distribution of θ.
b) Mean relative morphogen concentration (Y-axis) vs. relative position (X-axis) for several time points T[h] shows scaling.
c) Mean proliferation rate (Y-axis) [1/h] vs. relative position (X-axis) for several time points T[h]shows uniform growth. All statistics were computed with 500 samples.

Figure S9. Numerical solution of the ODE system 61 and 67 (SI) using ODE45 in MATLAB.

The figure clearly shows that the expander concentration and the tissue length converge to steady state values given by 68 (SI) for this parameter set. The same convergence holds for all tested parameter sets (approximately 1000).

The parameter values are: E(t=0) =1[a.u];L(t=0) = 1.66[μm]; c* = 0.5; β_E = 2[a.u]; α_E = 0.1[1/h];D_M = 2[μm^2/h]; α_M= 0.1[1/h]

Figure S10. Simulating the two compartments of the wing disc with different conditions in each compartment.

a-c:

The left compartment which is at $-1 \leq x \leq 0$, was simulated with no expander production. The right compartment which is at $0 \leq x \leq 1$, was simulated with the same parameters as the left but with expander production (Fig 2 parameters, matching measured wing disc quantities). In both compartments, growth was according to MDDR.

a) Fold change increase in tissue size as a function of time.
b) Relative morphogen level as a function of relative position in the tissue.
c) Expander level as function of relative position in the tissue at various times.

d-f:

The left compartment ($-1 \leq x \leq 0$) and the right compartment ($0 \leq x \leq 1$) were simulated with the same parameters (Fig 2 parameters, matching measured wing disc quantities) except for the growth parameter θ which was 0.5 in the right compartment and 0.8 in the left. In both compartments, growth was according to MDDR.

d) Fold change increase in tissue size as a function of time.
e) Relative morphogen level as a function of relative position in the tissue.
f) Expander level as function of relative position in the tissue at various times.

g-i:

The left compartment ($-1 \leq x \leq 0$) and the right compartment ($0 \leq x \leq 1$) were simulated with the same parameters (Fig 2 parameters, matching measured wing disc quantities) except for the growth parameter θ which was 0.5 in the right compartment and 0.8 in the left. In both compartments, growth was according to MDDR for $t \leq t_0$. For the rest of the simulation, $t_0 \leq t \leq T$, growth was determined by an external input. The t_0 chosen was $0.5\,T$.

g) Fold change increase in tissue size as a function of time.
h) Relative morphogen level as a function of relative position in the tissue.
i) Expander level as function of relative position in the tissue at various times.

Figure S11. Simulating MDDR with ExR for different conditions.

a-b: Increasing morphogen flux

a) Relative morphogen level as a function of relative position in the tissue.
b) Growth rate as a function of relative position in the tissue at various times.

c-d: Absorbing B.C for the morphogen on the distal edge of the tissue

c) Relative morphogen level as a function of relative position in the tissue.
d) Growth rate as a function of relative position in the tissue at various times.

e-f: Nonlinear morphogen degradation

e) Relative morphogen level as a function of relative position in the tissue.
f) Growth rate as a function of relative position in the tissue at various times.

g-h: Nonlinear expander degradation

g) Relative morphogen level as a function of relative position in the tissue.
h) Growth rate as a function of relative position in the tissue at various times.

i-j: Different forms of h(M) and α(E)

i) Relative morphogen level as a function of relative position in the tissue.
j) Growth rate as a function of relative position in the tissue at various times.

Figure S12. Simulating MDDR alone for different conditions.

a-b: Increasing morphogen flux

a) Relative morphogen level as a function of relative position in the tissue.
b) Growth rate as a function of relative position in the tissue at various times.

c-d: Absorbing B.C for the morphogen on the distal edge of the tissue

c) Relative morphogen level as a function of relative position in the tissue.
d) Growth rate as a function of relative position in the tissue at various times.

e-f: Nonlinear morphogen degradation

e) Relative morphogen level as a function of relative position in the tissue.
f) Growth rate as a function of relative position in the tissue at various times.

Figure S13. Comparing the amplitude of the 4 terms of eq. 2a for several time points.

The amplitude of the 4 terms of eq. 2a for an MDDR alone system:

$$\text{Diffusion: } D_M \cdot M_{xx}$$

$$\text{Degradation: } \alpha_M \cdot M$$

$$\text{Advection: } u \cdot M_x$$

$$\text{Dilution: } u_x \cdot M$$

For consecutive time points as stated in the title of each plot.

Figure S14. Comparing morphogen dynamics with vs. without growth.

a-b: System without growth, the steady state of the morphogen gradient is plotted for several tissue lengths. In the absence of growth, the gradient doesn't scale with tissue length.

a) Absolute morphogen level as a function of absolute position in the tissue.
b) Relative morphogen level as a function of relative position in the tissue.

c-d: System without growth simulated for a fixed tissue length. Temporal dynamics of the gradient is shown for several time points (see legend).

c) Absolute morphogen level as a function of absolute position in the tissue.
d) Relative morphogen level as a function of relative position in the tissue.

e-f: System with growth according to MDDR. Temporal dynamics of the gradient is shown for several time points (see legend).

e) Absolute morphogen level as a function of absolute position in the tissue.
f) Relative morphogen level as a function of relative position in the tissue.

All simulations were done with the same parameters (see SI for values).Comparing the 2 bottom rows shows morphogen dynamics is different with Vs. without growth.

Figure S15. Comparing morphogen dynamics with and without dilution.

In all simulation growth was according to MDDR without an expander. The morphogen evolution equation did or did not include a dilution term (see legend).

a-h: Discarding dilution results in: larger final size, lesser scaling and uniform growth.

a-d: Morphogen evolution equation with dilution
e-h: Morphogen evolution equation without dilution

i-p: Discarding dilution results in: smaller final size, lesser scaling and uniform growth.

i-l: Morphogen evolution equation with dilution
m-p: Morphogen evolution equation without dilution

q-x: Discarding dilution results in: smaller final size, less uniform growth and bad scaling.

q-t: Morphogen evolution equation with dilution
u-x: Morphogen evolution equation without dilution

Fig. S1

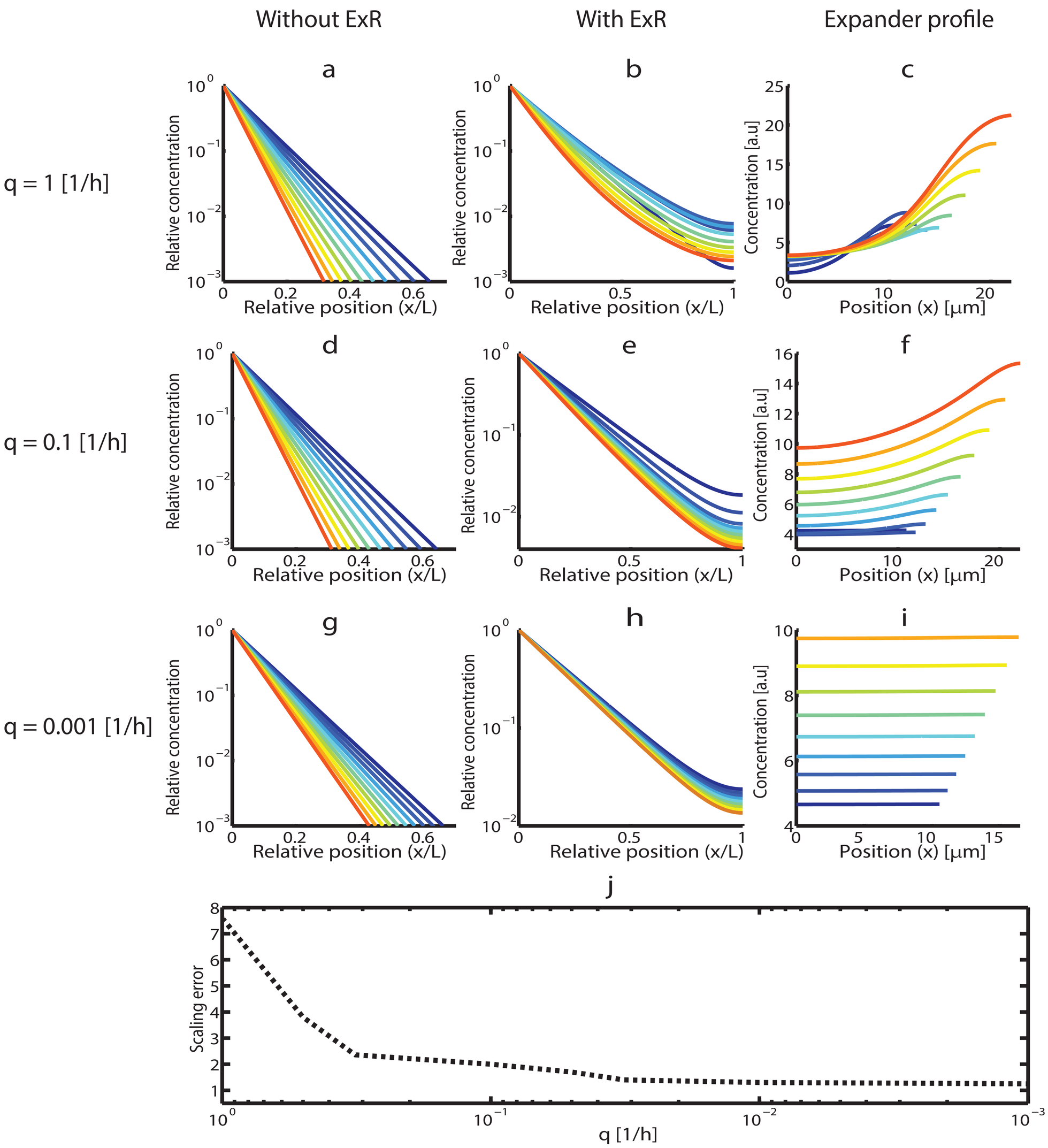
Without ExR
With ExR
Expander profile
a
b
c
d
e
f
g
h
i
j
q = 1 [1/h]
q = 0.1 [1/h]
q = 0.001 [1/h]
Relative concentration
Relative position (x/L)
Concentration [a.u]
Position (x) [μm]
Scaling error
q [1/h]

Fig. S2

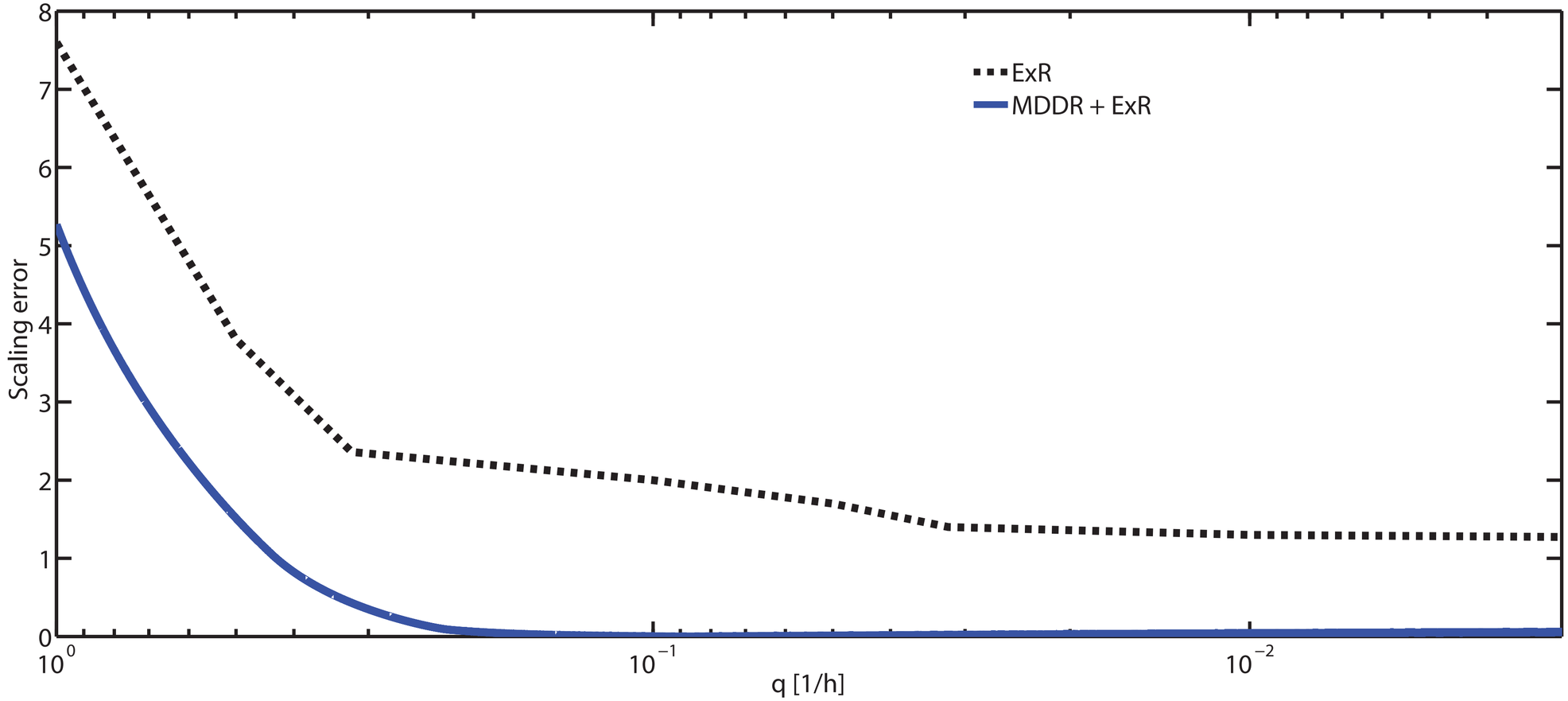

Fig. S3

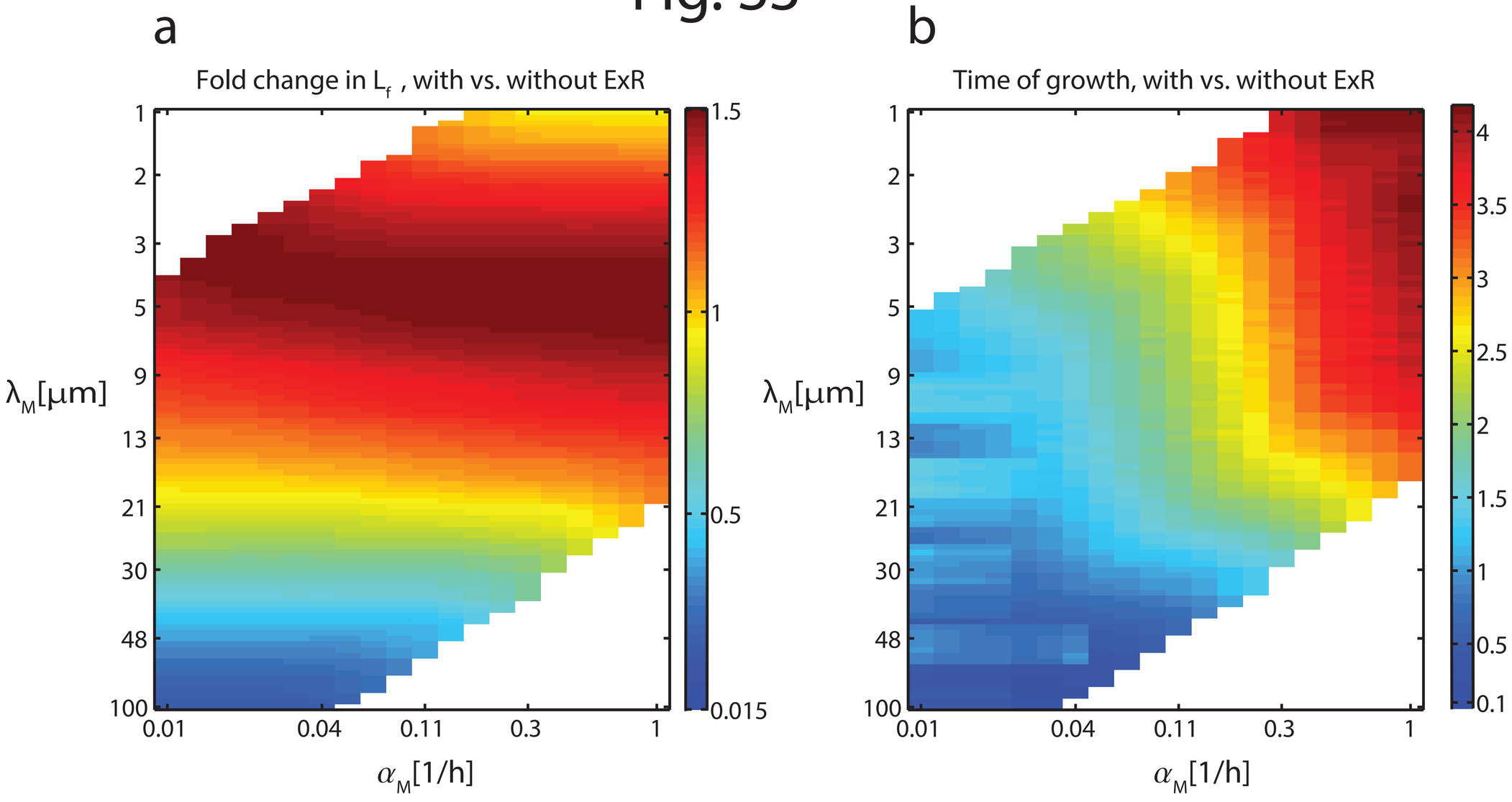
a
Fold change in L_f , with vs. without ExR
λ_M[μm]
1
2
3
5
9
13
21
30
48
100
0.01
0.04
0.11
0.3
1
α_M[1/h]
1.5
1
0.5
0.015
b
Time of growth, with vs. without ExR
λ_M[μm]
1
2
3
5
9
13
21
30
48
100
0.01
0.04
0.11
0.3
1
α_M[1/h]
4
3.5
3
2.5
2
1.5
1
0.5
0.1

Fig. S4

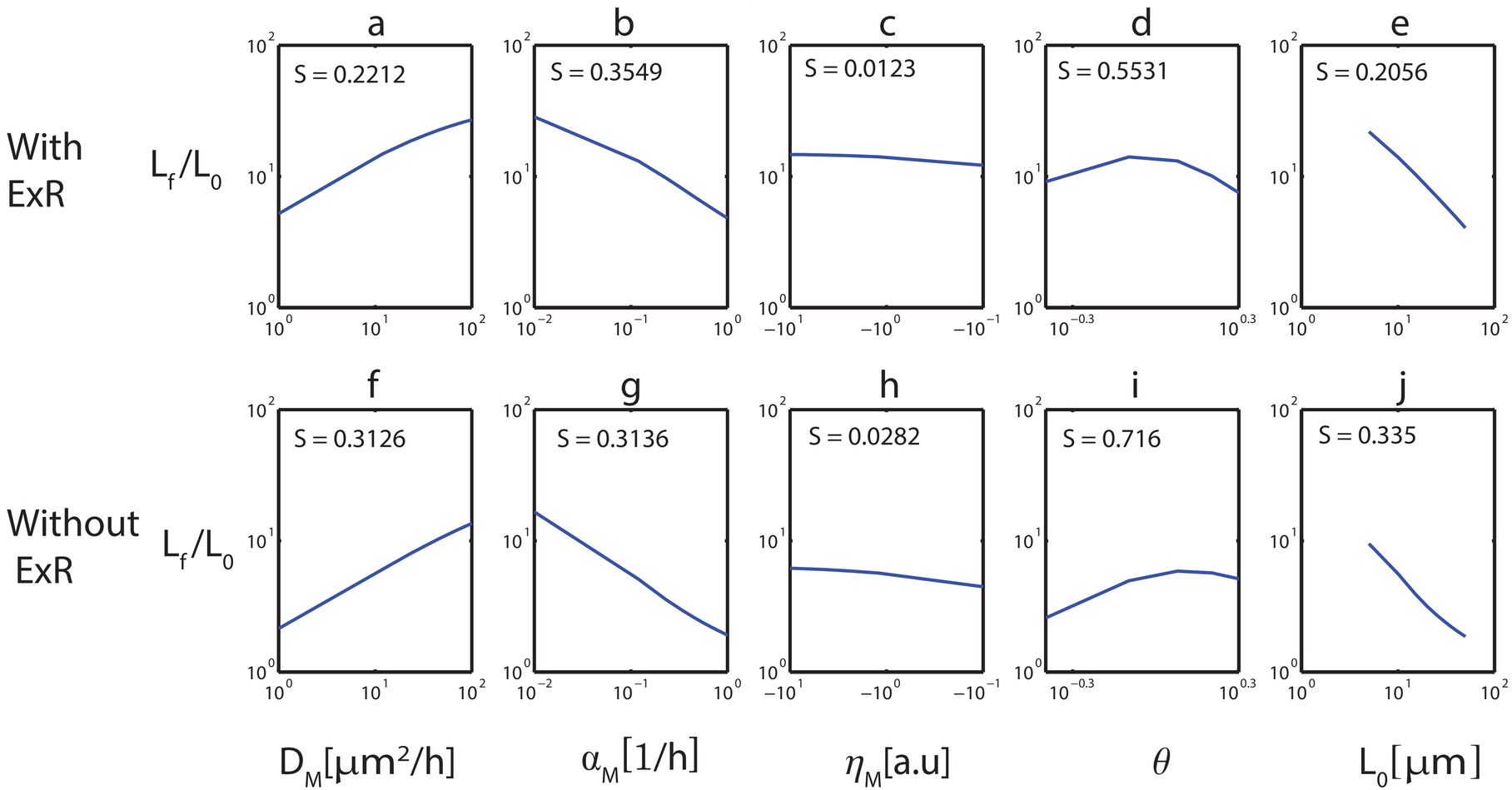
With ExR
Without ExR
L_f/L_0
a
b
c
d
e
f
g
h
i
j
S = 0.2212
S = 0.3549
S = 0.0123
S = 0.5531
S = 0.2056
S = 0.3126
S = 0.3136
S = 0.0282
S = 0.716
S = 0.335
$D_M[\mu m^2/h]$
$\alpha_M[1/h]$
η_M[a.u]
θ
$L_0[\mu m]$

Fig. S5

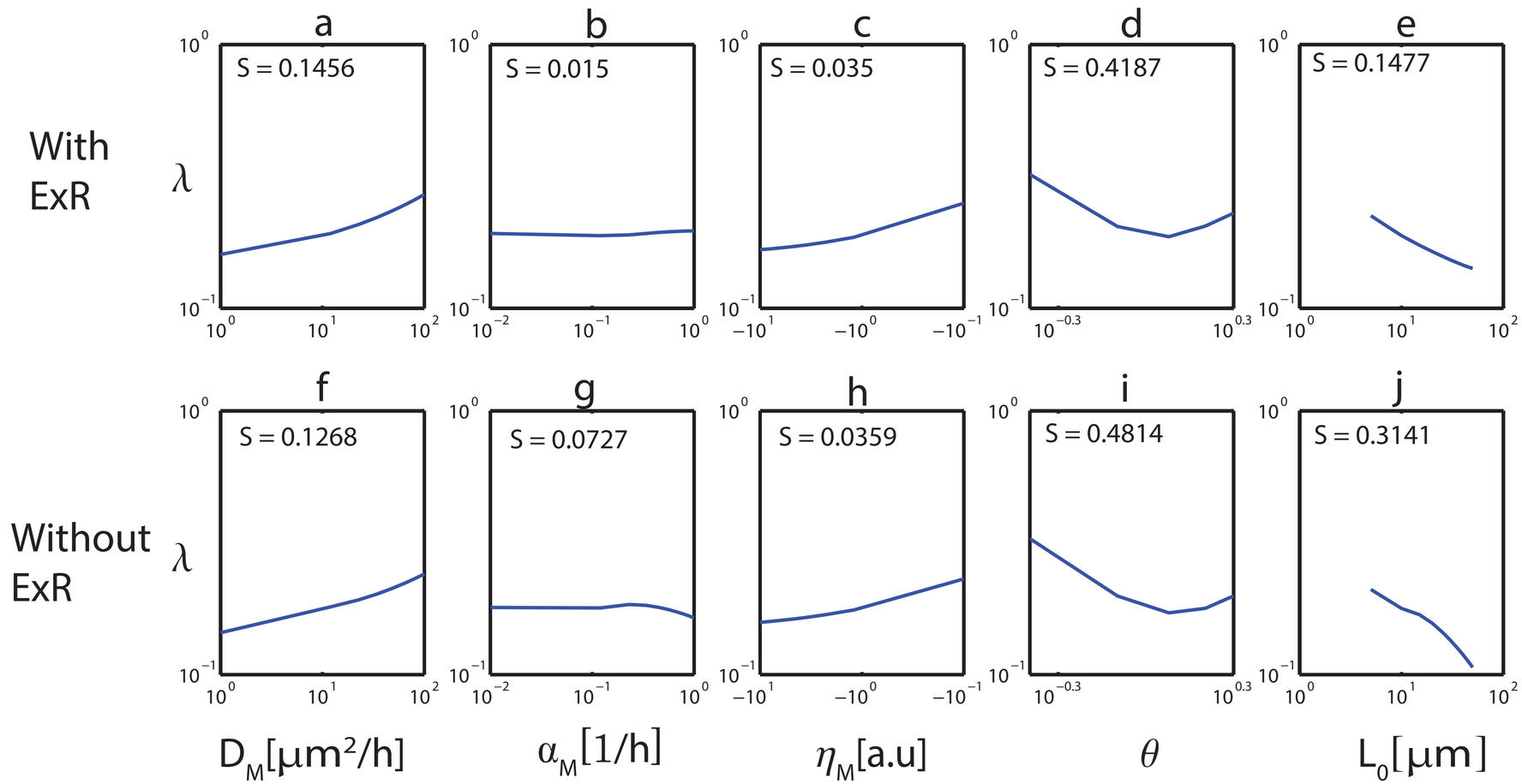
With ExR
Without ExR
λ
a
b
c
d
e
f
g
h
i
j
S = 0.1456
S = 0.015
S = 0.035
S = 0.4187
S = 0.1477
S = 0.1268
S = 0.0727
S = 0.0359
S = 0.4814
S = 0.3141
$D_M[\mu m^2/h]$
$\alpha_M[1/h]$
η_M[a.u]
θ
$L_0[\mu m]$

Fig. S6

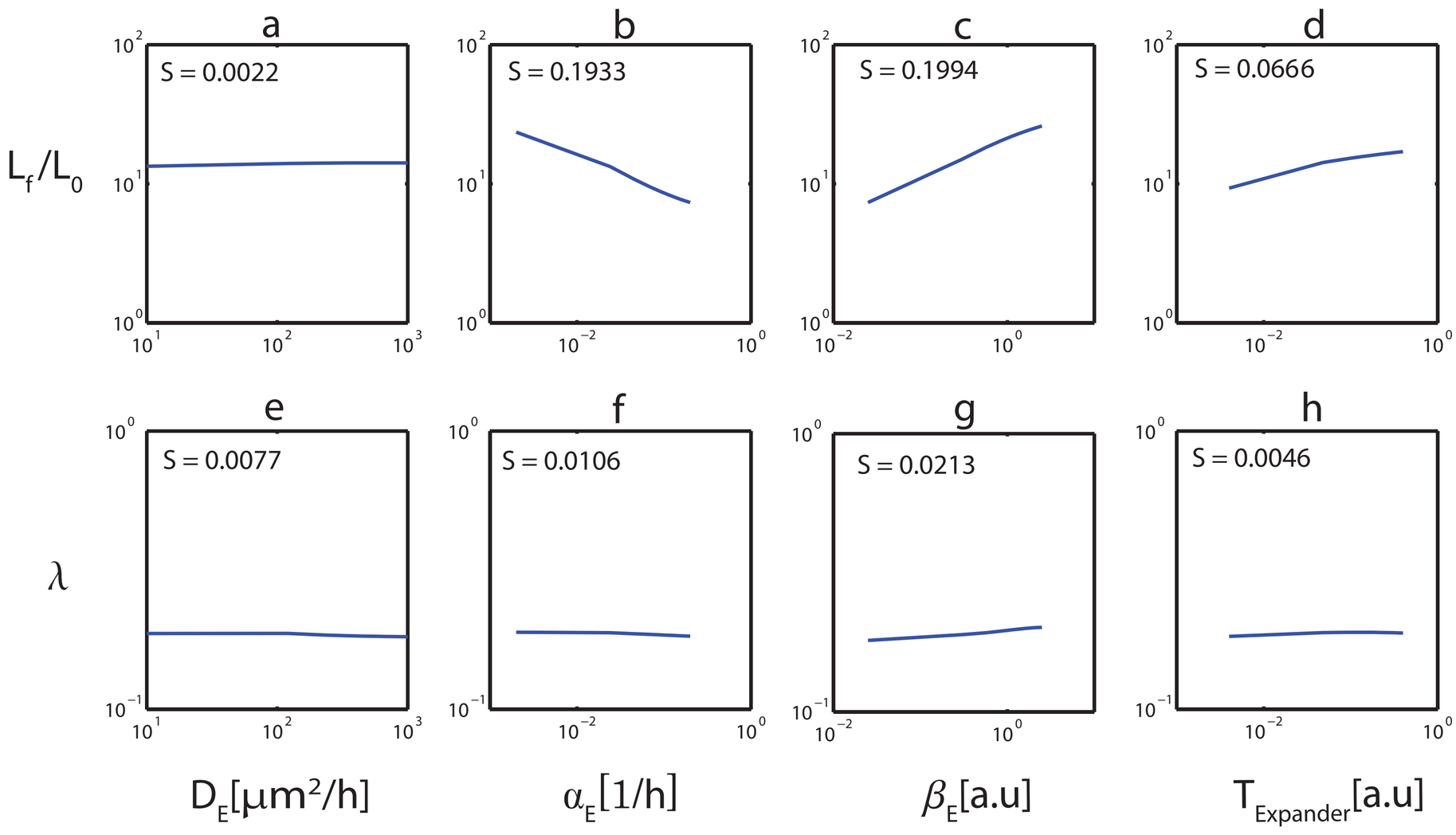
a
b
c
d
S = 0.0022
S = 0.1933
S = 0.1994
S = 0.0666
L_f/L_0
e
f
g
h
S = 0.0077
S = 0.0106
S = 0.0213
S = 0.0046
λ
$D_E[\mu m^2/h]$
$\alpha_E[1/h]$
β_E[a.u]
$T_{Expander}$[a.u]

Fig. S7

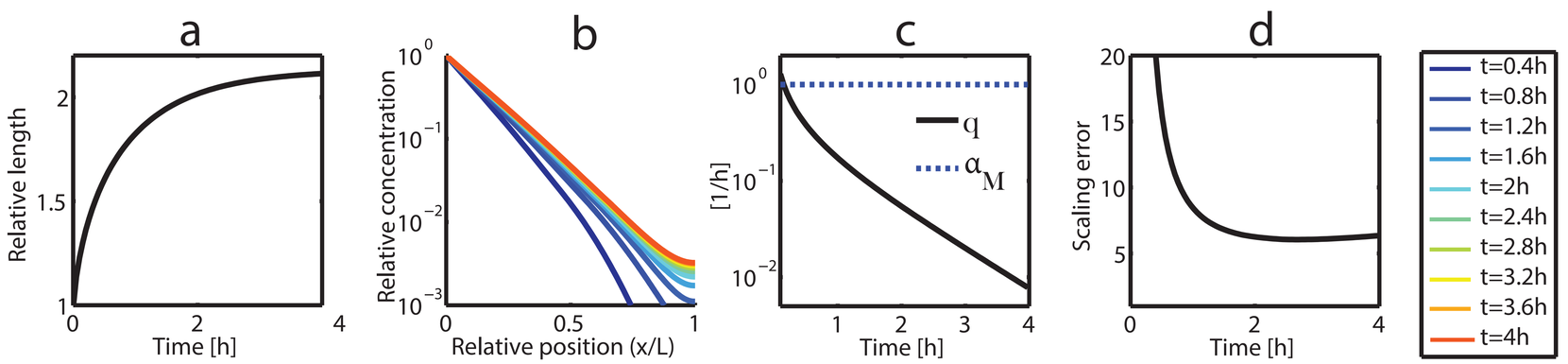
a
Relative length
Time [h]
b
Relative concentration
Relative position (x/L)
c
[1/h]
q
α M
Time [h]
d
Scaling error
Time [h]
t=0.4h
t=0.8h
t=1.2h
t=1.6h
t=2h
t=2.4h
t=2.8h
t=3.2h
t=3.6h
t=4h
e
Relative length
Time [h]
f
Relative concentration
Relative position (x/L)
g
[1/h]
q
α
Time [h]
h
Scaling error
Time [h]
t=50h
t=100h
t=150h
t=200h
t=250h
t=300h
t=350h
t=400h
t=450h
t=500h
i
Scaling error
Time [h]

Fig. S8

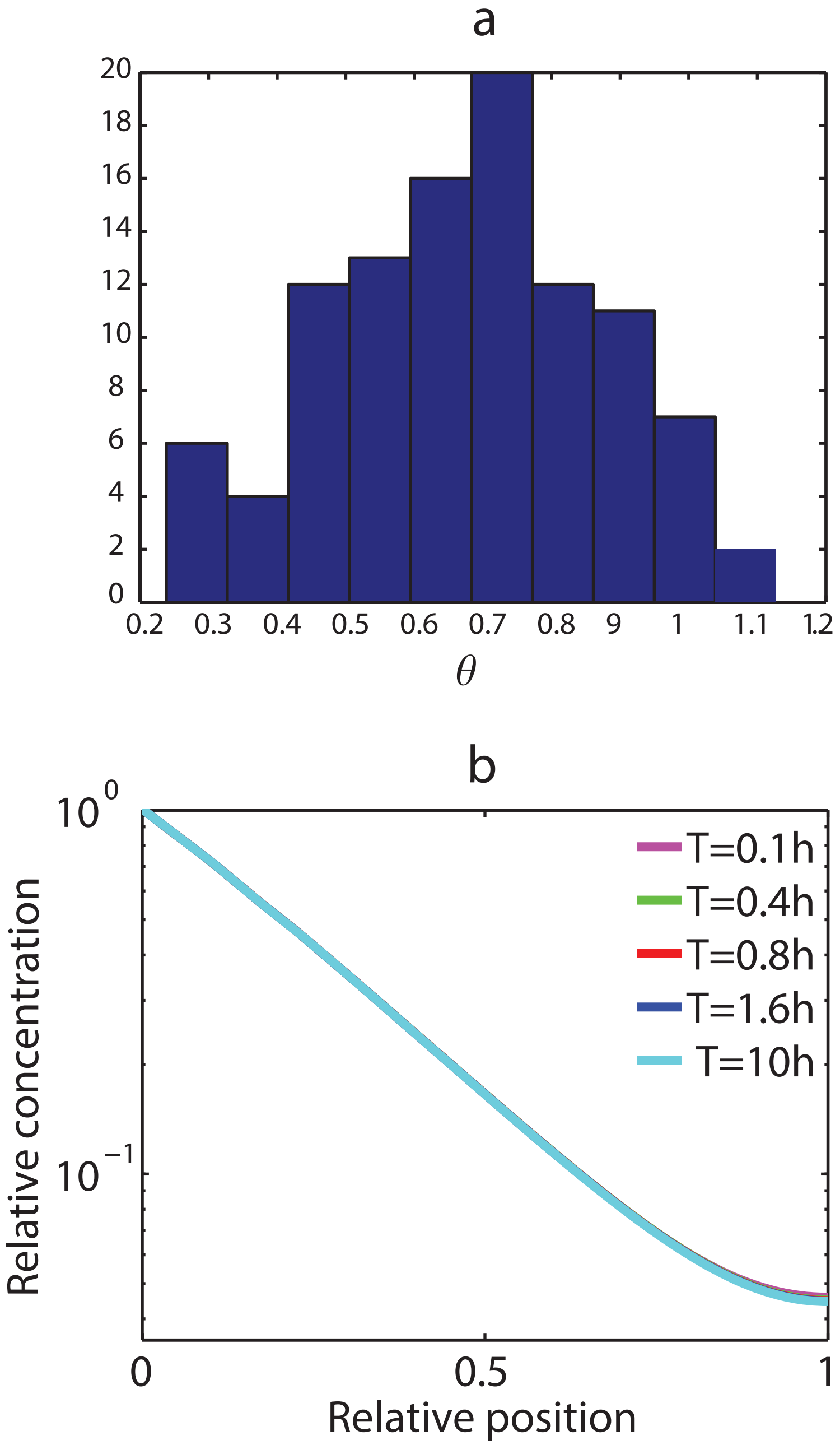
a
20
18
16
14
12
10
8
6
4
2
0
0.2
0.3
0.4
0.5
0.6
0.7
0.8
9
1
1.1
1.2
θ
b
10^0
10^−1
Relative concentration
T=0.1h
T=0.4h
T=0.8h
T=1.6h
T=10h
0
0.5
1
Relative position
c
10^0
10^-1
10^-2
10^-3
10^-4
Proliferation rate [1/h]
T=0.1h
T=0.4h
T=0.8h
T=1.6h
T=10h
0
0.5
1
Relative position

Fig. S9

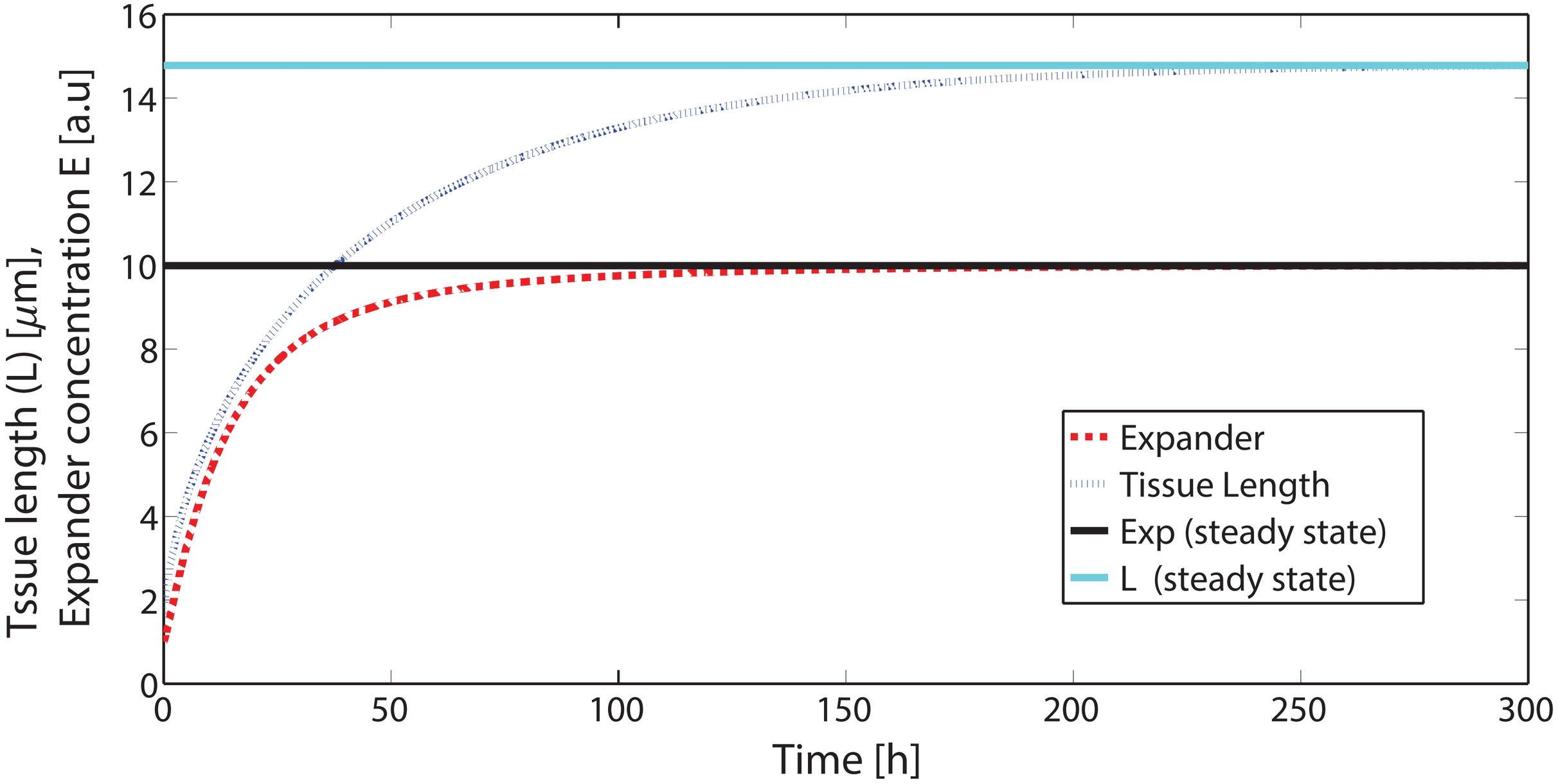
Tssue length (L) [μm],
Expander concentration E [a.u]
Time [h]
0
2
4
6
8
10
12
14
16
0
50
100
150
200
250
300
Expander
Tissue Length
Exp (steady state)
L (steady state)

Fig. S10

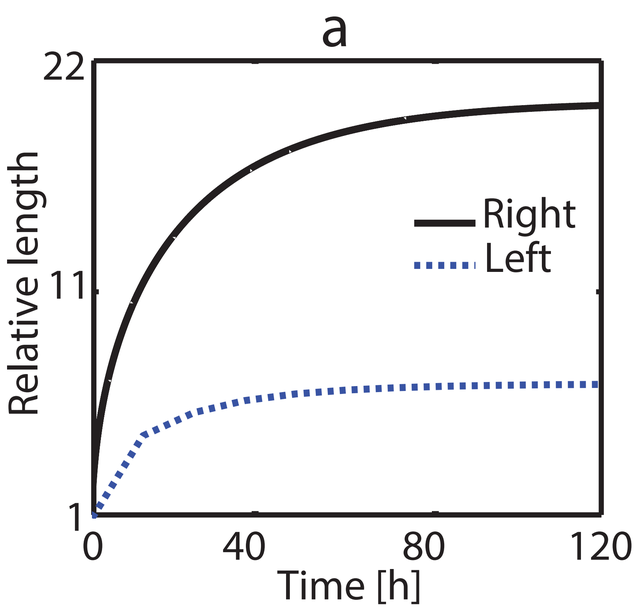
a
Relative length
Time [h]
Right
Left
22
11
1
0
40
80
120

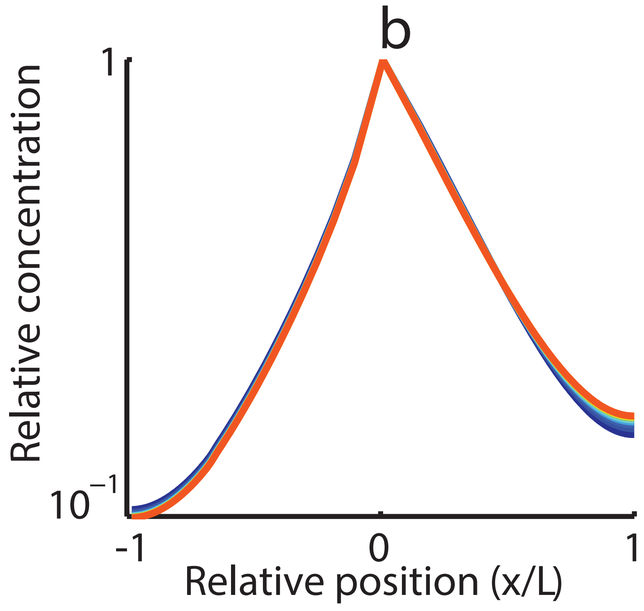
b
Relative concentration
Relative position (x/L)
1
10^{-1}
-1
0
1

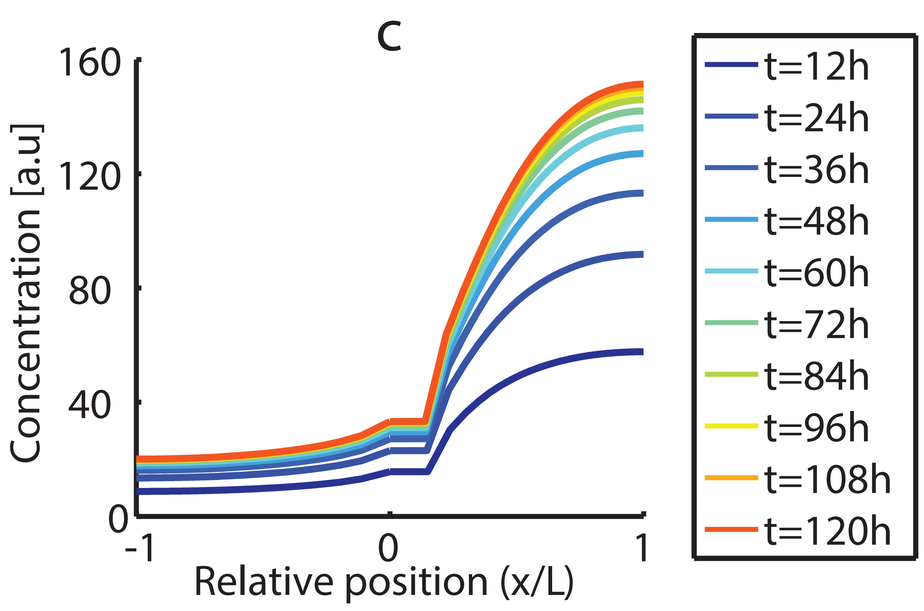
c
Concentration [a.u]
Relative position (x/L)
160
120
80
40
0
-1
0
1
t=12h
t=24h
t=36h
t=48h
t=60h
t=72h
t=84h
t=96h
t=108h
t=120h

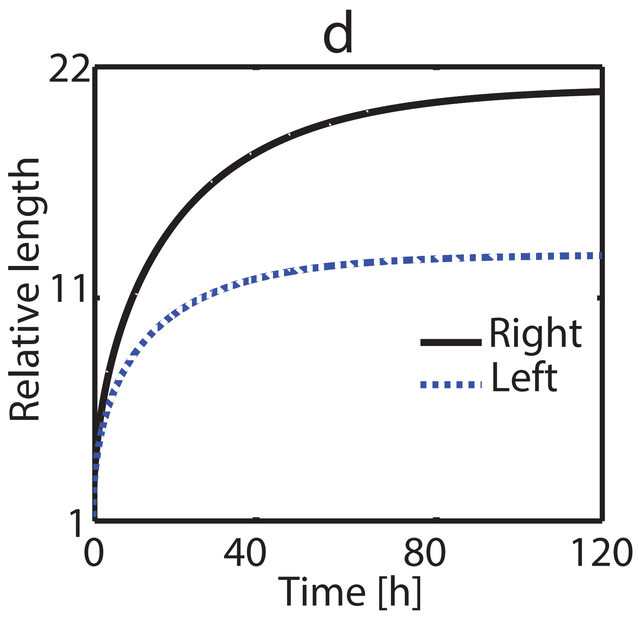
d
Relative length
Time [h]
Right
Left
22
11
1
0
40
80
120

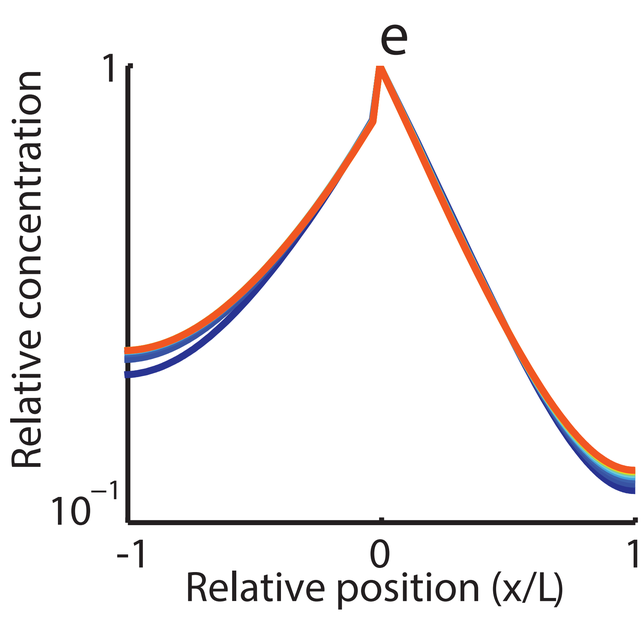
e
Relative concentration
Relative position (x/L)
1
10^{-1}
-1
0
1

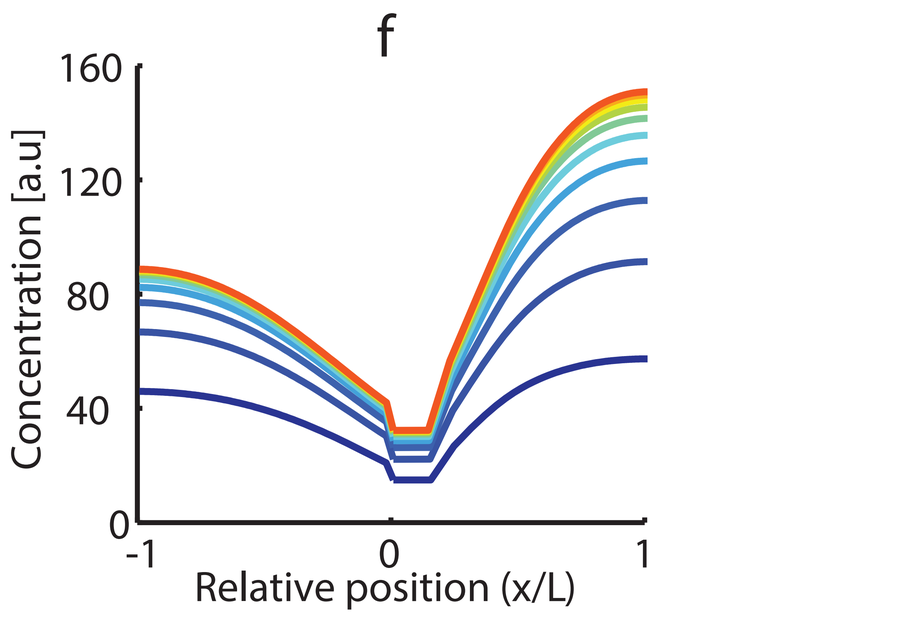
f
Concentration [a.u]
Relative position (x/L)
160
120
80
40
0
-1
0
1

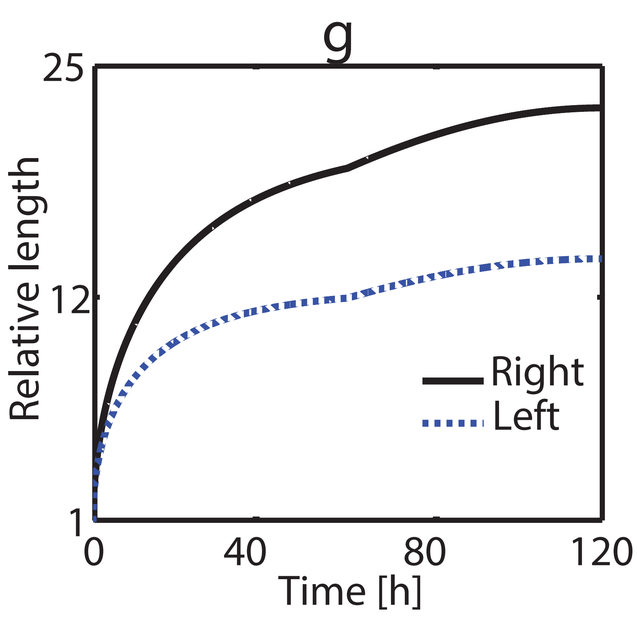
g
Relative length
Time [h]
Right
Left
25
12
1
0
40
80
120

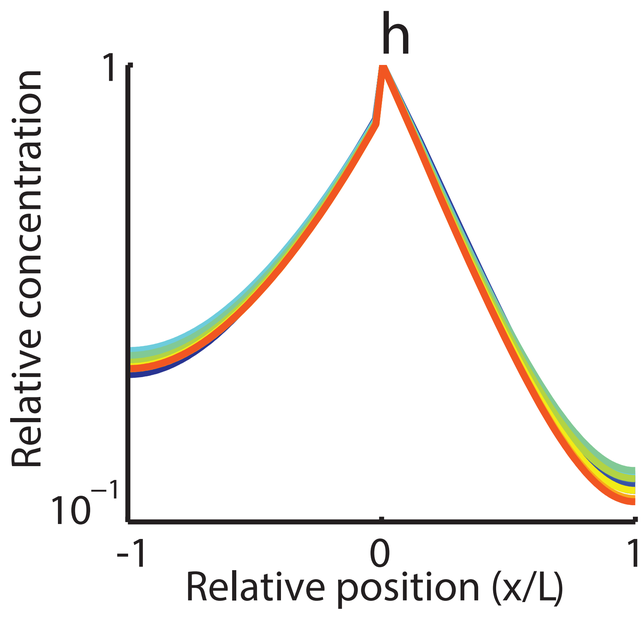
h
Relative concentration
Relative position (x/L)
1
10^{-1}
-1
0
1

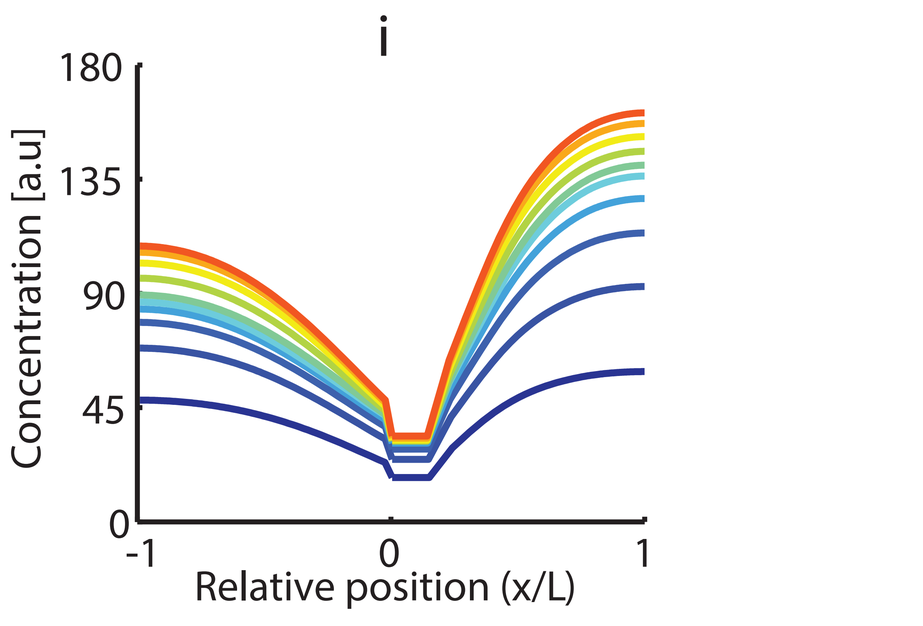
i
Concentration [a.u]
Relative position (x/L)
180
135
90
45
0
-1
0
1

Fig. S11

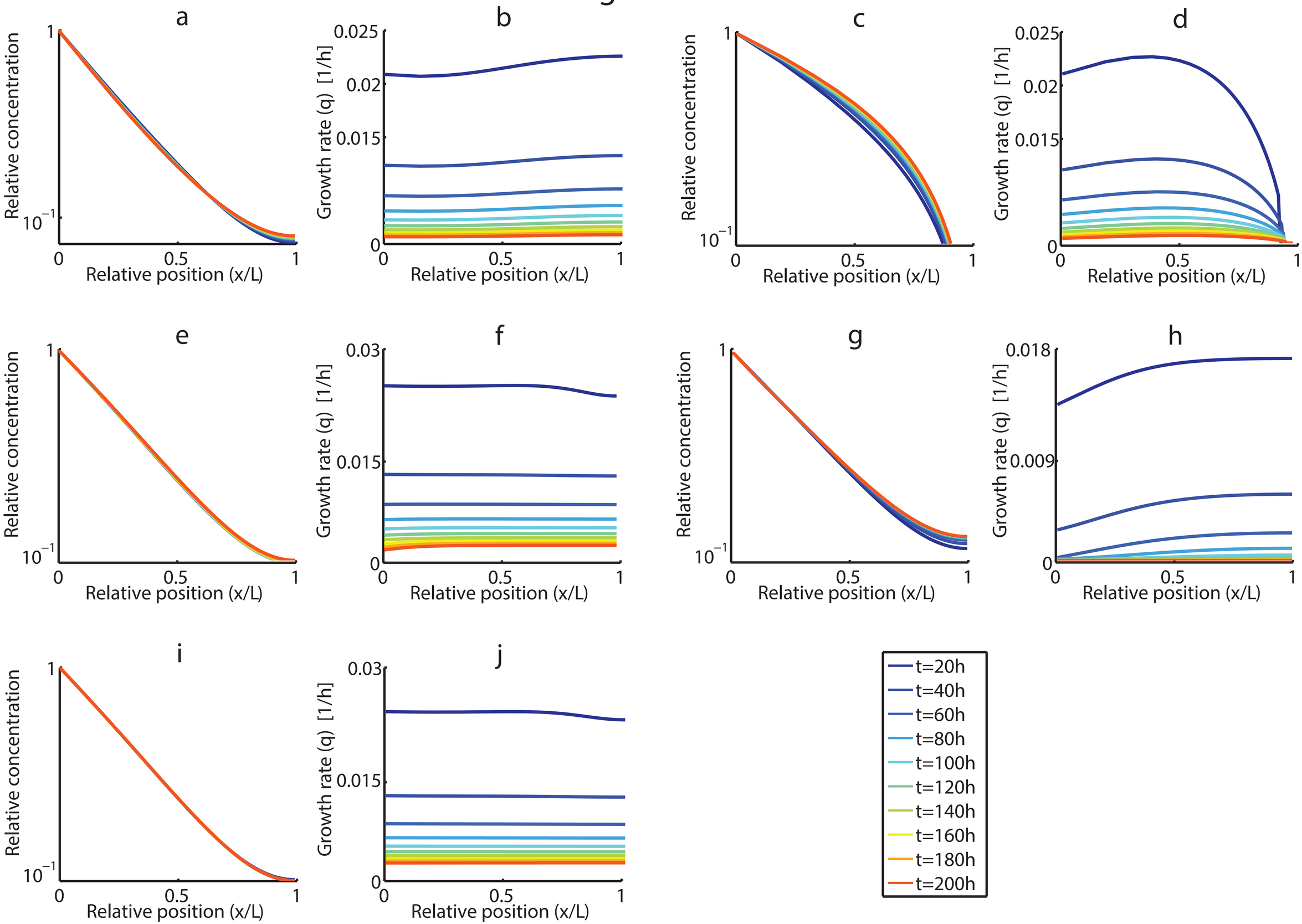
a
b
c
d
e
f
g
h
i
j
Relative concentration
Growth rate (q) [1/h]
Relative position (x/L)
t=20h
t=40h
t=60h
t=80h
t=100h
t=120h
t=140h
t=160h
t=180h
t=200h

Fig. S12

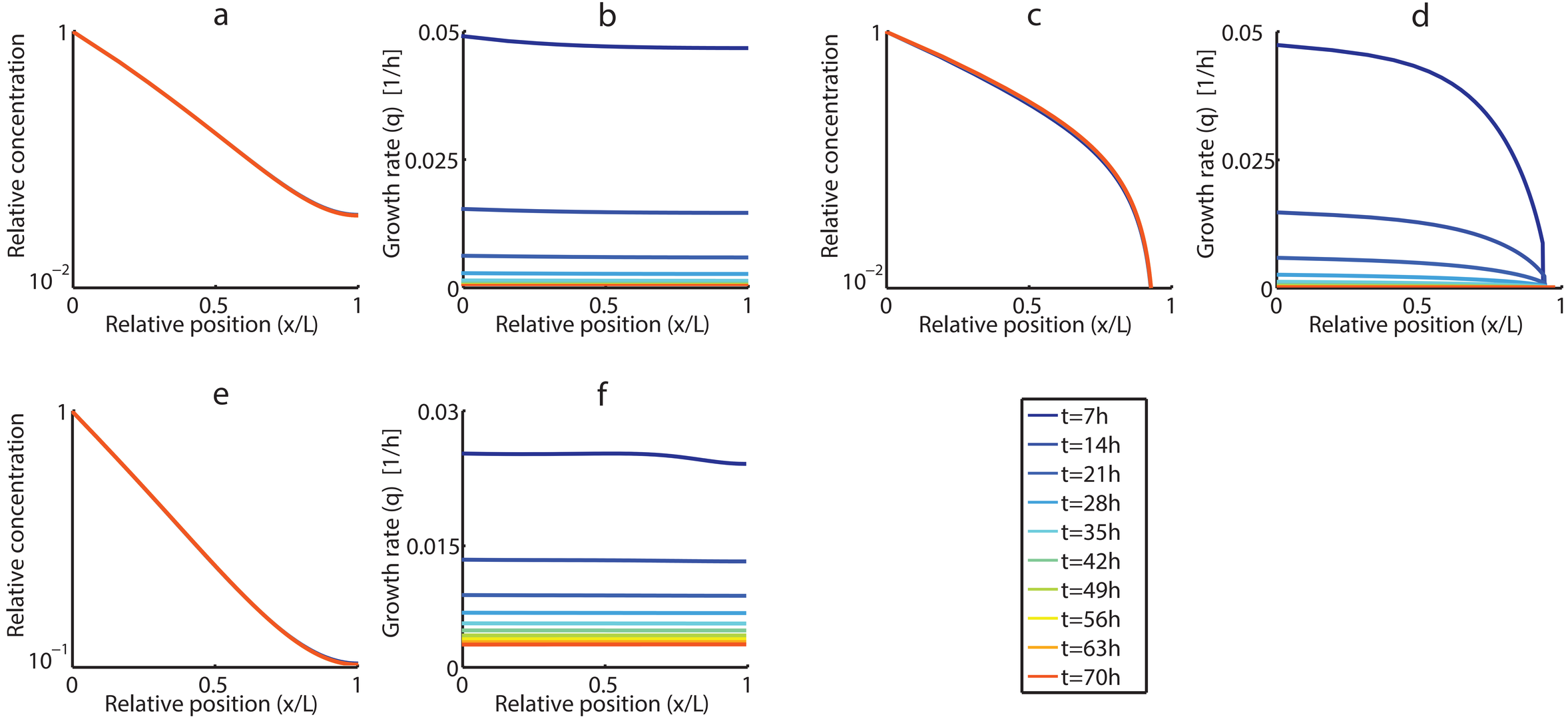
a
b
c
d
e
f
Relative concentration
Growth rate (q) [1/h]
Relative position (x/L)
1
10^{-2}
10^{-1}
0
0.5
0.05
0.025
0.03
0.015
t=7h
t=14h
t=21h
t=28h
t=35h
t=42h
t=49h
t=56h
t=63h
t=70h

Fig S13

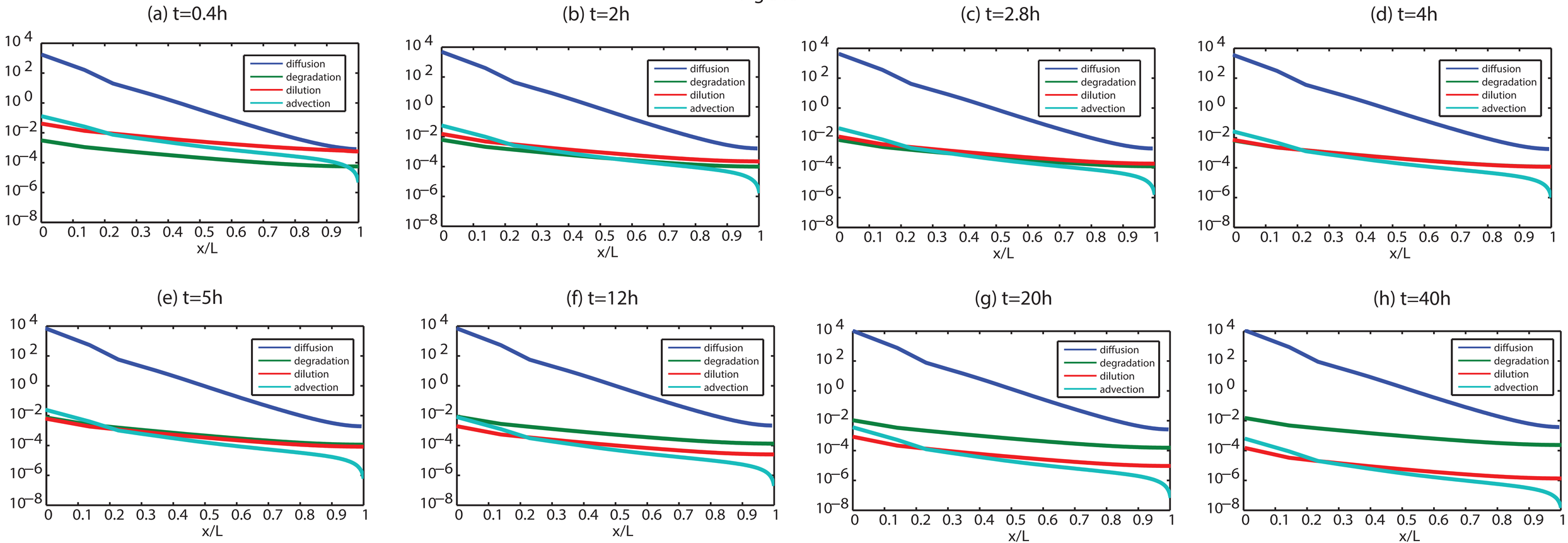
(a) t=0.4h
(b) t=2h
(c) t=2.8h
(d) t=4h
(e) t=5h
(f) t=12h
(g) t=20h
(h) t=40h
diffusion
degradation
dilution
advection
x/L

Fig. S14

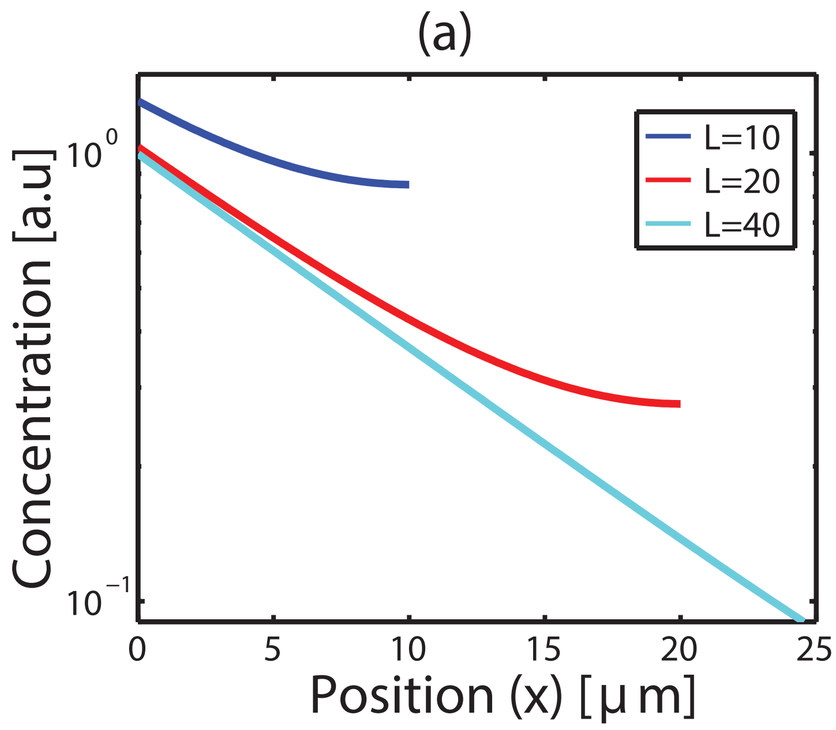
(a)
Concentration [a.u]
10^0
10^{-1}
L=10
L=20
L=40
0
5
10
15
20
25
Position (x) [μm]

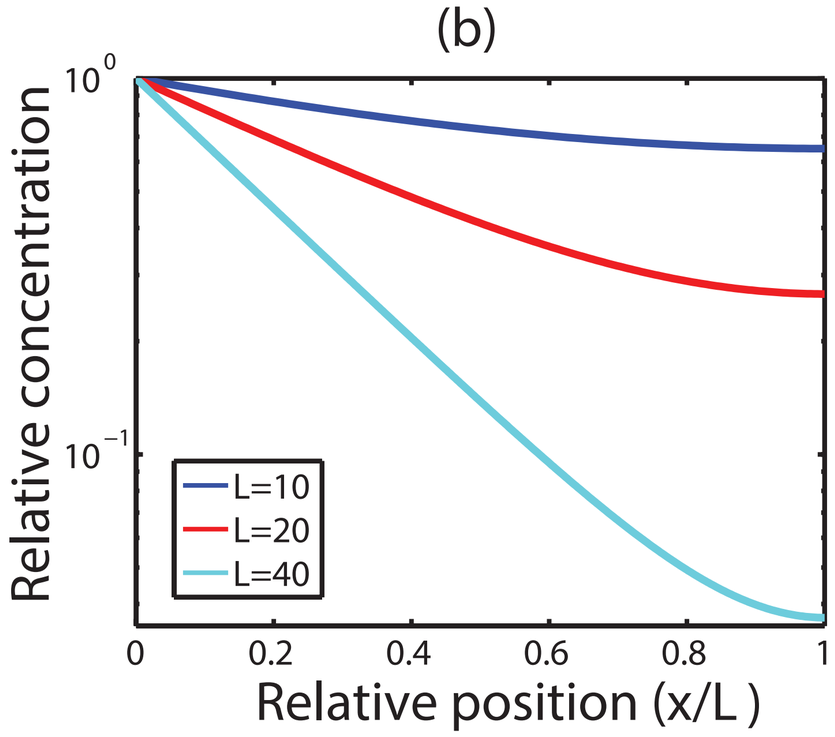
(b)
Relative concentration
10^0
10^{-1}
L=10
L=20
L=40
0
0.2
0.4
0.6
0.8
1
Relative position (x/L)

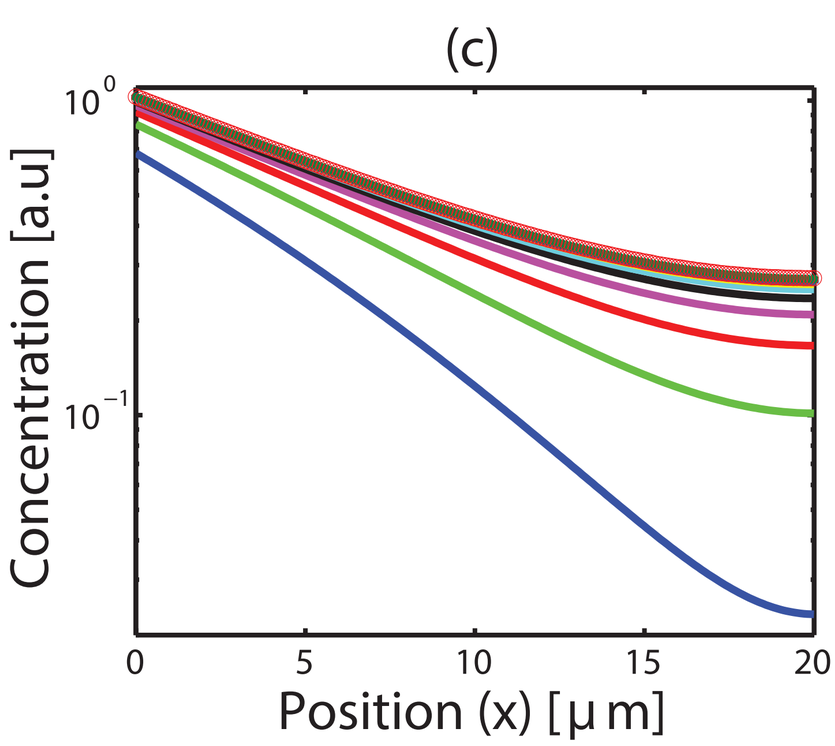
(c)
Concentration [a.u]
10^0
10^{-1}
0
5
10
15
20
Position (x) [μm]

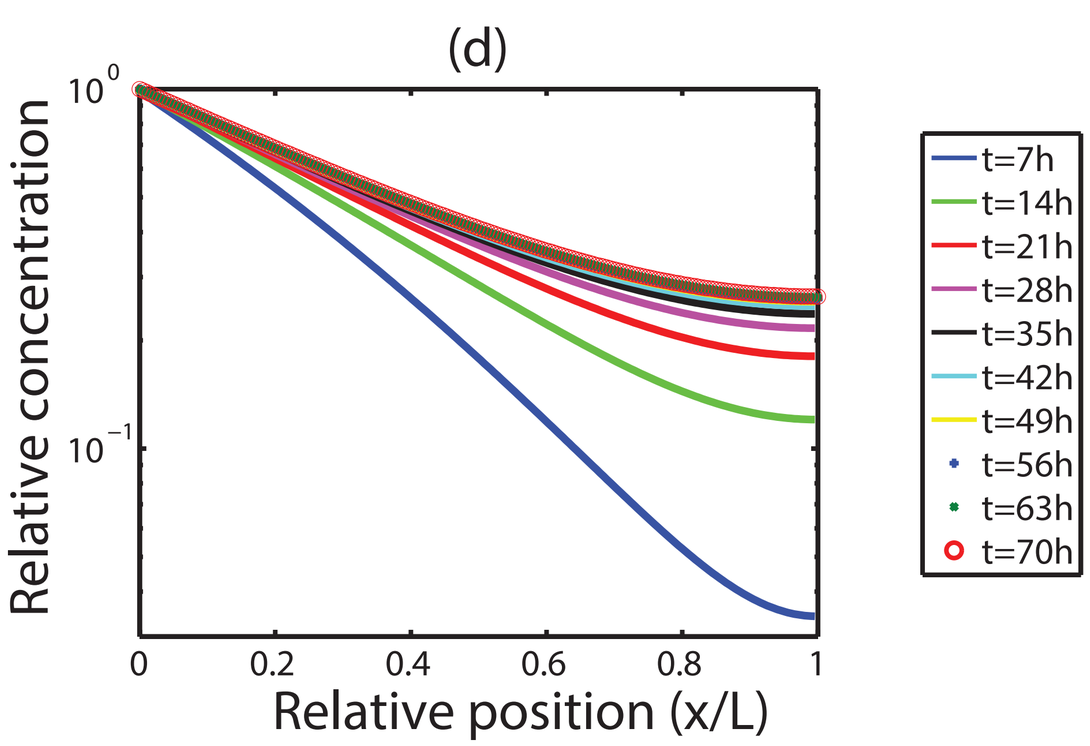
(d)
Relative concentration
10^0
10^{-1}
0
0.2
0.4
0.6
0.8
1
Relative position (x/L)
t=7h
t=14h
t=21h
t=28h
t=35h
t=42h
t=49h
t=56h
t=63h
t=70h

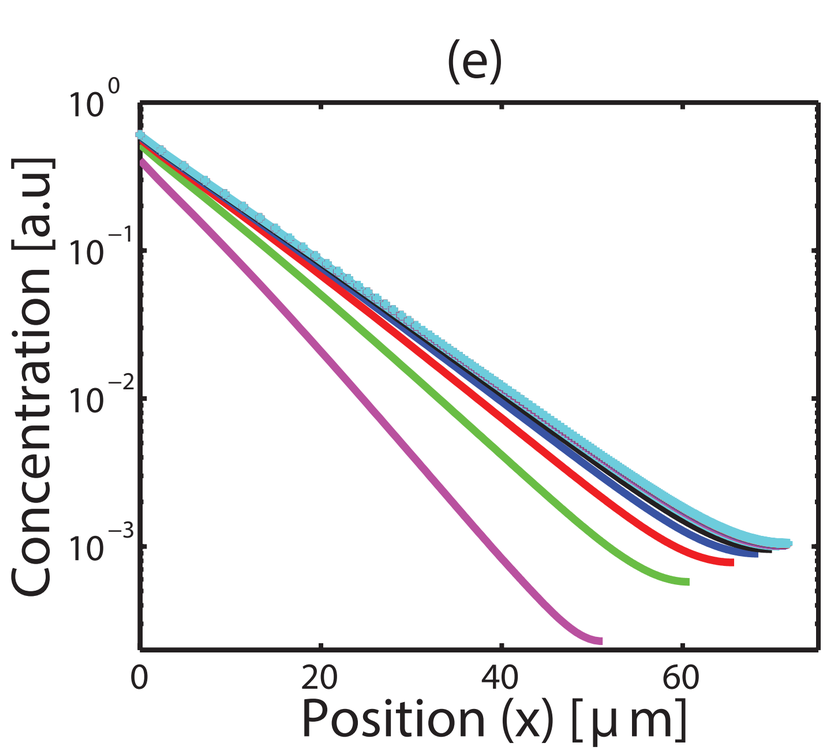
(e)
Concentration [a.u]
10^0
10^{-1}
10^{-2}
10^{-3}
0
20
40
60
Position (x) [μm]

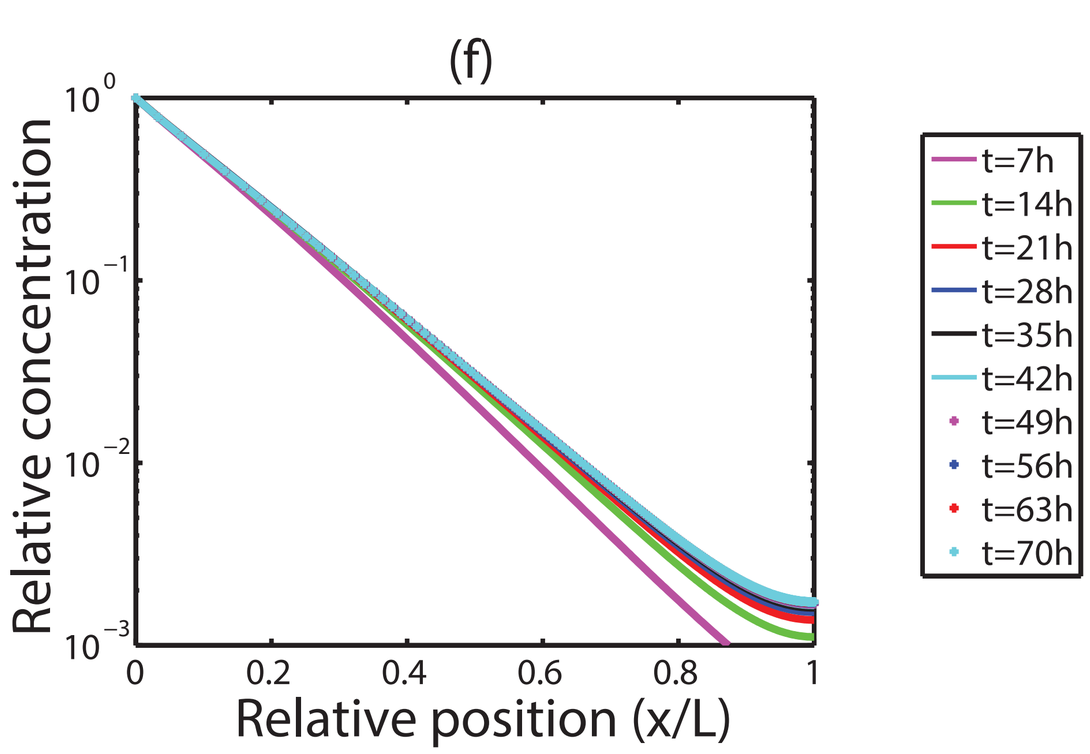
(f)
Relative concentration
10^0
10^{-1}
10^{-2}
10^{-3}
0
0.2
0.4
0.6
0.8
1
Relative position (x/L)
t=7h
t=14h
t=21h
t=28h
t=35h
t=42h
t=49h
t=56h
t=63h
t=70h

Fig. S15

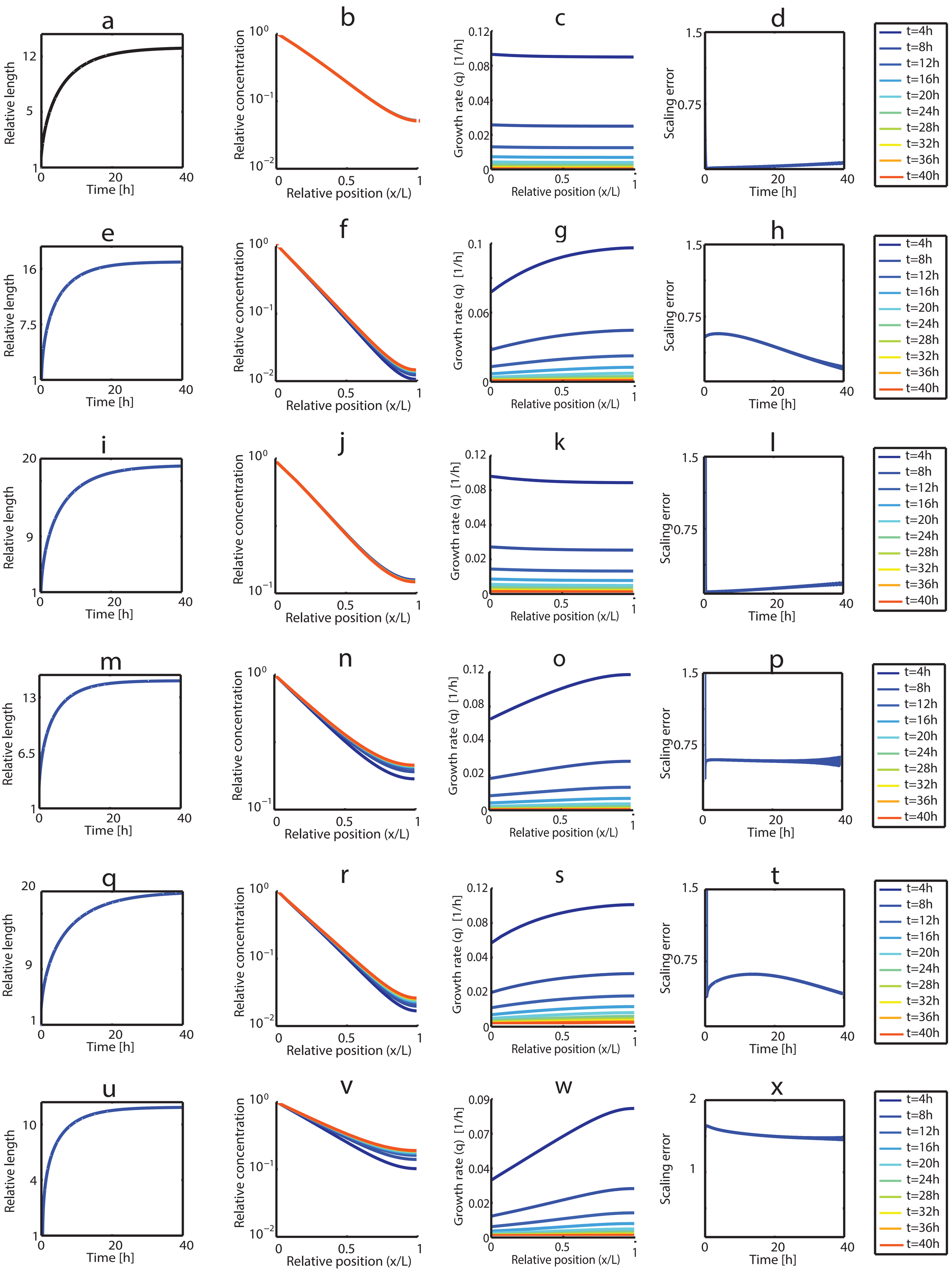
a
Relative length
Time [h]
b
Relative concentration
Relative position (x/L)
c
Growth rate (q) [1/h]
Relative position (x/L)
d
Scaling error
Time [h]
t=4h
t=8h
t=12h
t=16h
t=20h
t=24h
t=28h
t=32h
t=36h
t=40h
e
f
g
h
i
j
k
l
m
n
o
p
q
r
s
t
u
v
w
x

Table S1. Scaling and uniform growth percentages for various simulation scenarios

A

Increasing morphogen flux	MDDR with ExR
Final size	100%
Scaling	100%
Uniform growth	98%
Scaling and Uniform growth	98%

B

Increasing morphogen flux	MDDR
Final size	100%
Scaling	100%
Uniform growth	100%
Scaling and Uniform growth	100%

C

Absorbing B.C for morphogen	MDDR with ExR
Final size	100%
Scaling	100%
Uniform growth	100%
Scaling and Uniform growth	100%

D

Absorbing B.C for morphogen	MDDR
Final size	100%
Scaling	87%
Uniform growth	100%
Scaling and Uniform growth	87%

E

Nonlinear morphogen degradation	MDDR with ExR
Final size	100%
Scaling	100%
Uniform growth	43%
Scaling and Uniform growth	43%

F

Nonlinear morphogen degradation	MDDR
Final size	100%
Scaling	91%
Uniform growth	47%
Scaling and Uniform growth	47%

G

Nonlinear expander degradation	MDDR with ExR
Final size	100%
Scaling	96%
Uniform growth	84%
Scaling and Uniform growth	84%

H

Different forms of h(M) and α(E)	MDDR with ExR
Final size	100%
Scaling	100%
Uniform growth	72%
Scaling and Uniform growth	72%